Ann. Geophys., 31, 909–956, 2013
www.ann-geophys.net/31/909/2013/
doi:10.5194/angeo-31-909-2013

Annales Geophysicae
Open Access

Analysis and parameterisation of ionic reactions affecting middle atmospheric HO_x and NO_y during solar proton events

P. T. Verronen[1] **and R. Lehmann**[2]

[1]Finnish Meteorological Institute, Helsinki, Finland
[2]Alfred Wegener Institute for Polar and Marine Research, Potsdam, Germany

Correspondence to: P. T. Verronen (pekka.verronen@fmi.fi)

Received: 14 December 2012 – Revised: 25 April 2013 – Accepted: 26 April 2013 – Published: 23 May 2013

Abstract. In the polar regions, precipitation of solar high-energy protons and electrons affects the neutral composition of the middle atmosphere. Here we use the Sodankylä Ion and Neutral Chemistry model to calculate ionic production and loss rates of neutral HO_x and NO_y species, imposed by particle precipitation, for a range of atmospheric conditions and levels of ionization. We also analyse in detail the ionic reaction sequences leading to the HO_x and NO_y changes. Our results show that particle impact ionization and positive ion chemistry cause net production of N, NO, HNO_2, H, and OH from N_2 and H_2O. On the other hand, negative ion chemistry redistributes the NO_y species, without net production or loss, so that NO, NO_2, and N_2O_5 are converted to HNO_3 and NO_3. Based on the model results, we provide tables of so-called P/Q numbers (i.e. production and loss rates of neutral species divided by ionization rates) at altitudes between 20 and 90 km. These numbers can be easily used to parameterise the ion chemistry effects when modelling atmospheric response to particle precipitation. Compared to earlier studies, our work is the first to consider in detail the NO_y effect of negative ion chemistry, and the diurnal and seasonal variability of the P/Q numbers.

Keywords. Atmospheric composition and structure (middle atmosphere – composition and chemistry) – Ionosphere (Ion chemistry and composition; Particle precipitation)

1 Introduction

Energetic particle precipitation affects not only the ion and electron densities but also the neutral composition of the middle atmosphere through particle impact ionization, dissociation, and ion chemistry (see Sinnhuber et al., 2012, for a recent review). Precipitating particles are mostly protons and electrons, which are released from the Sun in, for example, coronal mass ejections and arrive in the near-Earth space with the solar wind. The Earth's magnetic field guides these particles, so that they can only access the atmosphere in the polar regions, sometimes after being temporarily stored inside the magnetosphere (e.g. in the radiation belts). At mesospheric and upper stratospheric altitudes, precipitating protons and electrons are an important, although highly varying forcing factor. During periods of strong particle forcing (e.g. in the case of solar proton events (SPEs)), particle precipitation can exceed the background ionization by extreme ultraviolet solar radiation and galactic cosmic rays by several orders of magnitude.

Considering the neutral atmospheric changes caused by particle precipitation, most of the early studies concentrated on understanding the increases in odd hydrogen (HO_x = H + OH + HO_2) and odd nitrogen (NO_x = N + NO + NO_2) because of their important role in catalytic, ozone-destroying reaction cycles in the upper stratosphere and mesosphere (Crutzen et al., 1975; Porter et al., 1976; Heaps, 1978; Crutzen and Solomon, 1980; Solomon et al., 1981; Rusch et al., 1981). SPEs and their influence on ozone have played a large role in the research due to the profound impact of SPEs and the availability of ozone observations from several satellite-based instruments (Jackman and McPeters, 1985; McPeters and Jackman, 1985; Reid et al., 1991; Jackman et al., 2001; Seppälä et al., 2004; López-Puertas et al., 2005a; Verronen et al., 2006). In recent years, changes in other minor species have received substantial attention after a wealth of satellite observations of the winter polar regions became

Table 1. List of ion–ion recombination reactions in which nitrogen is released from negative ions. X^+ denotes any positive ion, Y^+ any positive ion except $H^+(H_2O)_n$ clusters. X and Y are corresponding neutral species. n is the order of water clustering (i.e. a number between 1 and 8).

#1	$NO_2^- + X^+$	$\rightarrow$	$NO_2 + X$
#2	$NO_2^-(H_2O) + X^+$	$\rightarrow$	$NO_2 + H_2O + X$
#3	$NO_3^- + H^+(H_2O)n$	$\rightarrow$	$HNO_3 + nH_2O$
#4	$NO_3^- + Y^+$	$\rightarrow$	$NO_3 + Y$
#5	$NO_3^-(H_2O) + X^+$	$\rightarrow$	$NO_3 + H_2O + X$
#6	$NO_3^-(H_2O)_2 + X^+$	$\rightarrow$	$NO_3 + 2H_2O + X$
#7	$NO_3^-(HNO_3) + H^+(H_2O)n$	$\rightarrow$	$2HNO_3 + nH_2O$
#8	$NO_3^-(HNO_3) + Y^+$	$\rightarrow$	$NO_3 + HNO_3 + Y$
#9	$NO_3^-(HNO_3)_2 + H^+(H_2O)n$	$\rightarrow$	$3HNO_3 + nH_2O$
#10	$NO_3^-(HNO_3)_2 + Y^+$	$\rightarrow$	$NO_3 + 2HNO_3 + Y$
#11	$NO_3^-(HCl) + X^+$	$\rightarrow$	$NO_3 + HCl + X$

available (López-Puertas et al., 2005b; von Clarmann et al., 2005; Orsolini et al., 2009; Verronen et al., 2008; Funke et al., 2008; Jackman et al., 2008; Winkler et al., 2009; Verronen et al., 2011; Winkler et al., 2011; Funke et al., 2011; Damiani et al., 2012).

In middle atmosphere models, HO_x and NO_x production by particle precipitation is typically included as a simple parameterisation, in which the production rates are calculated from the ionization rates by multiplying by an altitude-dependent scaling factor. These scaling factors, so-called P/Q numbers, give the number of molecules produced per each ion pair, and have been calculated to be 0–2.0 and 1.27–1.6 for HO_x and NO_x, respectively, depending upon, for example, water vapour amount and ionization rate (e.g. Porter et al., 1976; Solomon et al., 1981; Rusch et al., 1981). This kind of parameterisation is very simple and useful, especially in case of HO_x, because numerous ion chemical reactions take place between ionization and HO_x production, such that it would be computationally time-consuming to include ions reaction-by-reaction in the models.

The current, widely used parameterisation of HO_x production is based on the work by Solomon et al. (1981). They describe in detail the positive ion reaction paths leading to production of OH and H from water vapour, and also give a detailed description of the HNO_2 production. However, although the possibility of HNO_3 production through ion–ion recombination is discussed in their paper, it is then neglected by assuming that photodissociation of HNO_3 instantly occurs and releases HO_x. This approach was reasonable at that time considering the relatively low level of negative ion knowledge. Also, this simplification can be justified in the summer solstice conditions, when solar radiation is present all day to dissociate HNO_3. But at the winter pole solar radiation is mostly absent. Without solar light, photodissociation of HNO_3 does not occur and its chemical lifetime is of the order of months. Verronen et al. (2006) have shown that during an SPE, HNO_3 is accumulated at nighttime and then rapidly photodissociated at sunrise. This means that the release of HO_x occurs at the time when atomic oxygen is available for the ozone-depleting catalytic reaction cycles. If the same amount of HO_x was produced at night, a large proportion of it would not last until sunrise because of its short chemical lifetime ($\sim$ hours below 80 km). Therefore, assuming instant HO_x release from HNO_3 can lead to underestimation of ozone depletion. Satellite observations made during SPEs have shown significant enhancements of HNO_3 in the stratopause–lower mesosphere region (Orsolini et al., 2009). These so-called direct HNO_3 enhancements can be reasonably explained by ion chemical production (Verronen et al., 2008, 2011). However, atmospheric models using the parameterisation based on Solomon et al. (1981) significantly underestimate the amount of HNO_3 produced compared to observations (e.g. Jackman et al., 2008; Funke et al., 2011).

In this paper, we present an improved, yet simple parameterisation of ion chemistry that can be used to model atmospheric effects of particle precipitation. Our results are based on model calculations with the Sodankylä Ion and Neutral Chemistry model and the current knowledge of ion chemical reactions. An important part of the work is a detailed analysis of all significant reactions paths involved. The final output of work is the P/Q numbers (i.e. net production rates scaled with ionization rates), which we provide for different ionospheric conditions.

2 Ion and neutral chemistry modelling

2.1 Sodankylä Ion and Neutral Chemistry model

The Sodankylä Ion and Neutral Chemistry model, also known as SIC, is a 1-D tool for ionosphere–neutral atmosphere interaction studies. SIC solves for concentrations of 65 ions, positive and negative, and 16 minor neutral species. The altitude range of SIC is from 20 to 150 km, with 1 km resolution. The model includes a chemical scheme of over 400 reactions and takes into account external forcing due to solar UV and soft X-ray radiation, electron and proton precipitation, and galactic cosmic rays. Recent, detailed descriptions of SIC are given by Verronen et al. (2005), Verronen (2006), and Turunen et al. (2009).

Because of our attempt to improve the current parameterisation of HO_x production, it is worthwhile to briefly explain the main differences in chemistry between SIC and the model used by Solomon et al. (1981). For the positive ion scheme, SIC uses more recent reaction rate coefficients and includes a larger number of positive ions. However, the added ions do not significantly change the reaction sequences of HO_x production. The important improvement is that, in contrast to the Solomon model, SIC includes an extensive negative ion scheme which is important, for example, in understanding

the HNO_3 production. The details of the ionic reactions included in SIC can be found in Verronen (2006).

It should be noted that the SIC model has been compared to satellite-based OH and HNO_3 data in several studies of SPEs (Verronen et al., 2006, 2007, 2008, 2011). The reasonably good agreement between the model results and observations found in those studies gives us a confident starting point to this study, which is based solely on the SIC model results.

2.2 Ion chemistry scheme – major assumptions

Compared to the neutral chemistry, the ionic reactions have more uncertainty in general. Concerning this study especially, there are few laboratory studies describing the products of ion–ion recombination reactions, which means that some assumption has to be made. Table 1 presents the ion–ion recombination reactions, as they are in the SIC model, that are most important to our analysis because they release nitrogen from negative ions. Note that corresponding three-body reactions (not listed) are also included in SIC. The reactions leading to HNO_3 production (#3, #7, and #9) are given by Aikin (1997, and references therein). For the other reactions, the most straightforward approach is adopted; for example NO_2^- and NO_3^- recombination produces NO_2 and NO_3, respectively. All the ion–ion recombination reactions have the same rate coefficient in the SIC model (i.e. $6.0 \times 10^{-8} \times (300/T)^{0.5}\,\mathrm{cm^3\,s^{-1}}$ and $1.25 \times 10^{-25} \times (300/T)^4\,\mathrm{cm^6\,s^{-1}}$ for two-body and three-body reactions, respectively), because there seems to be little dependence upon the species involved (Arijs et al., 1987).

We have excluded positive non-hydrate cluster ions (NHCs, e.g. $H^+(CH_3CN)$) and negative sulfur-based ions (SBIs, e.g. HSO_4^-) from the model and our analysis. Although observations have indicated that these types of ions exist in the stratosphere (e.g. Arijs, 1992), modelling NHCs and SBIs would involve significant additional uncertainty because the global atmospheric distribution of the neutral species they are produced from, acetonitrile (CH_3CN) and sulfuric acid (H_2SO_4), is not well known. Also, in high-ionization conditions, such as during SPEs, the precursors of NHCs and SBIs (e.g. $H^+(H_2O)$ and $NO_3^-(HNO_3)$) will more likely recombine rather than react to produce NHCs and SBIs. Finally, the NHC and SBI reactions would lead to the same net effect as those of their precursor ions (e.g. production of HNO_3 through ion–ion recombination Aikin (1997)). Therefore, their exclusion should have a minor impact on the analysis of neutral HO_x and NO_y changes presented in this paper.

2.3 Set-up of model runs

Table 2 summarises the model runs used in this study. By selecting dates in January and October and then running the model in both northern and southern latitudes, four different seasons of the year were considered. Six modelling latitudes were used in both hemispheres, from 55 to 75° with 5° spacing. This set-up of model runs allows us to contrast the particle effects in different states of background atmosphere and solar illumination.

In order to better represent the seasonal changes, in the modelling we took advantage of Microwave Limb Sounder (MLS/Aura) observations of temperature and water vapour. Data from year 2005 were used; the January and October observations were averaged separately for each latitude. The numbers in Table 2 demonstrate how H_2O and temperature vary with latitude and season of the year in the mesosphere. The MLS temperature and H_2O altitude profiles were kept constant during model runs, so the possible changes in temperature or H_2O caused by SPE forcing were not taken into account.

For each of the 24 combinations of month and location, five 24 h model runs were executed, each with a different, fixed rate of SPE ionization ranging from 10^1 to $10^5\,\mathrm{cm^{-3}\,s^{-1}}$. This range generously covers the ionization rates typical for SPEs. Additional 24 h model runs without any SPE forcing provided reference to aid in quantification of the precipitation-induced changes. Although the model runs were made for the full altitude range of SIC (20–150 km), in the following we analyse altitudes between 20–90 km only. These altitudes correspond to the ionospheric D region, where water cluster ions and negative ions can be formed in significant amounts.

2.4 Calculation of P/Q numbers

The model results, from the simulations described in Sect. 2.3, were used to calculate the P/Q numbers for the species of interest. A P/Q number indicates the net change rate of a species, scaled with the ionization rate Q to provide a dimensionless quantity. First, we calculated the production and loss rates (P and L, respectively) due to ion chemistry at each altitude, time, and latitude separately. Second, we calculated the P/Q numbers as

$$P/Q = \frac{(P_{\mathrm{spe}} - L_{\mathrm{spe}}) - (P_{\mathrm{ref}} - L_{\mathrm{ref}})}{Q}.$$

Here "spe" and "ref" denote the results from the SPE and reference model runs, respectively. Third, we calculated the average P/Q numbers for each season of the year using data from the 6 different latitudes. This was done for each altitude separately, at solar zenith angles (SZAs) between 55 and 125° using 5-degree-wide bins. Finally, we checked that there is a balance in production and loss between the P/Q numbers of H and N containing species. The final result is a P/Q table for each combination of species and season, and each table giving values with respect to SZA, ionization rate, and altitude. These P/Q tables are presented in Appendix A but for daytime (SZA < 90°), twilight (SZA = 95°), and nighttime (SZA > 100°) only instead of all SZAs, because the variations of P/Q during day and during night

Table 2. List of model runs. Solar zenith angles (SZAs) give the range between noon and midnight. H_2O and T values are averages of MLS/Aura observations that were used as input to the model.

Month	Latitude	SZA	H_2O (70 km) 10^9 cm^{-3}	H_2O (80 km) 10^9 cm^{-3}	T (80 km) K
January	75° S	54–85°	23.59	5.18	166.5
January	70° S	49–90°	22.57	4.91	166.8
January	65° S	44–95°	21.48	4.59	167.8
January	60° S	39–100°	20.25	4.17	169.3
January	55° S	34–105°	19.07	3.74	172.6
January	50° S	29–110°	17.96	3.36	176.0
January	50° N	70–151°	7.42	0.70	209.7
January	55° N	75–146°	6.64	0.64	210.2
January	60° N	80–141°	5.93	0.61	210.1
January	65° N	85–136°	5.23	0.55	209.9
January	70° N	90–131°	4.67	0.52	209.8
January	75° N	95–126°	4.30	0.51	209.7
October	75° N	88–119°	6.10	0.57	208.7
October	70° N	83–124°	6.45	0.60	207.4
October	65° N	78–129°	6.89	0.66	206.4
October	60° N	73–134°	7.42	0.71	205.0
October	55° N	68–139°	8.02	0.77	204.3
October	50° N	63–144°	8.72	0.86	203.4
October	50° S	36–117°	10.79	0.82	197.1
October	55° S	41–112°	11.42	0.85	197.7
October	60° S	46–107°	12.22	0.95	197.4
October	65° S	51–102°	12.98	1.08	196.5
October	70° S	56–97°	13.57	1.23	195.4
October	75° S	61–92°	13.95	1.38	193.9

are small. A denser SZA grid could in principle be used during the sunset/sunrise transition period. However, the finer P/Q details during the twilight are of secondary importance compared to the day–night differences. Note that to assure that only the effect of protons is considered in P/Qs, the net change in the reference run ($P_{\mathrm{ref}} - L_{\mathrm{ref}}$) was subtracted from that of the SPE run before ionization rate scaling. However, in most cases the reference net change is negligible compared to the SPE-induced net change.

2.5 Reaction pathway analysis

The P/Q numbers, calculated as described in Sect. 2.4, represent the gross effect of the ionization processes. However, they do not reveal the detailed reaction pathways leading from the ionization to the production or destruction of a species of interest. In order to determine such pathways, we applied the algorithm developed by Lehmann (2004).

This algorithm forms pathways step by step, starting from the individual reactions in the system: for every chemical species each pathway producing it is connected with each pathway consuming it. If a newly formed pathway contains sub-pathways (e.g. zero cycles), it is split into these simpler pathways. Rates proportional to "branching probabilities" are calculated. Pathways with a rate that is smaller than a prescribed threshold are deleted, in order to avoid a too large number of (minor) pathways ("numerical explosion").

So far, the algorithm has been applied to the determination of catalytic ozone destruction cycles and methane oxidation pathways in the stratosphere (Lehmann, 2004), ozone production and loss cycles in the stratosphere and mesosphere (Grenfell et al., 2006), pathways of HNO_3 production by ion chemistry in the mesosphere (Verronen et al., 2011), and CO_2 formation pathways in the atmosphere of Mars (Stock et al., 2012a,b).

In this study, the SIC model results, which are produced with a combination of the positive ion, negative ion, minor neutral reactions, provided the input to the pathway analysis. We then analysed the positive and negative ion schemes separately, which simplifies the analysis and is possible because the only direct connection process between the two schemes is ion–ion recombination. All the important pathways of production and loss were identified for the species of interest. In the following sections, the P/Q number discussions are supported by examples of typical reaction sequences, based on results of the pathway analysis.

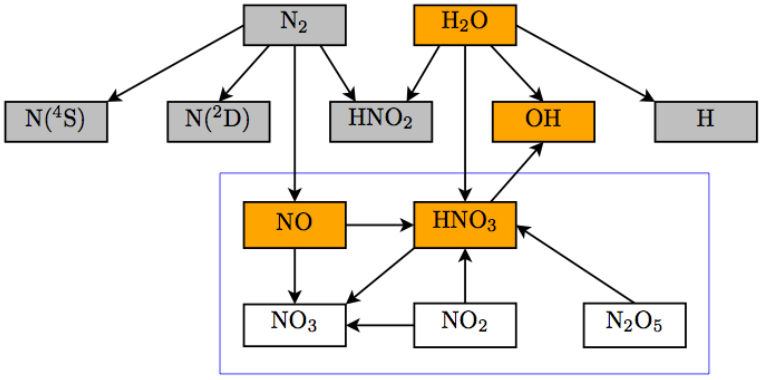

Fig. 1. A diagram of hydrogen and nitrogen conversions due to ionic reactions. The species in the grey boxes are produced by positive ion chemistry, while NO_y redistribution by negative ion chemistry affects the species inside the blue box. NO, HNO_3, OH, and H_2O are directly affected by both positive and negative ion chemistry (orange boxes). Note that the effects of neutral reactions (e.g. production of NO from $N(^2D)$) are not included in the diagram.

3 Results

In this section we demonstrate with examples how the P/Q numbers vary with respect to altitude, SZA, ionization rate, and seasons of year. We also describe, again with examples, the ionic reaction sequences leading to changes in HO_x and NO_y (i.e. N, NO, NO_2, NO_3, N_2O_5, HNO_2, and HNO_3) species during SPEs.

Figure 1 presents a schematic view of the ionic effects on nitrogen and hydrogen species. Positive ion chemistry leads to dissociation of N_2 and H_2O, which ends with production of NO_y and HO_x, respectively. A portion of nitrogen and hydrogen species is combined through ion chemistry, resulting in HNO_2 and HNO_3 production. The main effect of negative ion chemistry is then a redistribution of NO_y species without net production or loss of NO_y. In general, the net effect is that NO, NO_2, and N_2O_5 are converted to HNO_3 and NO_3. As a side effect, negative chemistry consumes H_2O in N_2O_5-to-HNO_3 conversion and releases OH in HNO_3-to-NO_3 conversion.

In the following, Sects. 3.1 and 3.2 consider the HO_x, HNO_2, HNO_3 production by positive ion chemistry, while Sects. 3.3 and 3.4 discuss the NO_y production by positive ion chemistry and NO_y redistribution by negative ion chemistry. Note, however, that there is some overlap between the sections because HNO_2 and HNO_3 production requires ion chemistry related to both HO_x and NO_y changes.

3.1 OH and HNO_2 production

Figures 2a and 2b present the OH and HNO_2 P/Q numbers for the case of January, Northern Hemisphere, and $Q = 100\,\mathrm{cm^{-3}\,s^{-1}}$. OH and HNO_2 are produced when H_2O is dissociated by positive ion chemistry. Formation of O_2^+, directly by proton/secondary electron impact or by ion chemical reactions, leads to production of OH through reaction sequences such as

$$N_2 + p^+(E) \rightarrow N_2^+ + e^- + p^+(E - \Delta E) \quad \text{(R1)}$$
$$N_2^+ + O_2 \rightarrow O_2^+ + N_2 \quad \text{(R2)}$$
$$O_2^+ + O_2 + M \rightarrow O_4^+ + M \quad \text{(R3)}$$
$$O_4^+ + H_2O \rightarrow O_2^+(H_2O) + O_2 \quad \text{(R4)}$$
$$O_2^+(H_2O) + N_2 + M \rightarrow O_2^+(H_2O)N_2 + M \quad \text{(R5)}$$
$$O_2^+(H_2O)N_2 + CO_2 \rightarrow O_2^+(H_2O)CO_2 + N_2 \quad \text{(R6)}$$
$$O_2^+(H_2O)CO_2 + H_2O \rightarrow O_2^+(H_2O)_2 + CO_2 \quad \text{(R7)}$$
$$O_2^+(H_2O)_2 + H_2O \rightarrow H_3O^+(OH)H_2O + O_2 \quad \text{(R8)}$$
$$H_3O^+(OH)H_2O + H_2O \rightarrow H^+(H_2O)_3 + OH \quad \text{(R9)}$$
$$H^+(H_2O)_3 + H_2O + M \rightarrow H^+(H_2O)_4 + M \quad \text{(R10)}$$
$$H^+(H_2O)_4 + e^- \rightarrow H + 4H_2O \quad \text{(R11)}$$
$$\text{Net}: \; H_2O \rightarrow OH + H. \quad \text{(R12)}$$

Here Reaction (R1) marks impact ionization of N_2 by precipitating primary protons, which lose some of their energy in the process. In this pathway, and in a number of similar pathways, the route from O_2^+ always leads to O_4^+ and subsequently to production of water cluster ions $H^+(H_2O)_n$ and neutral OH through reactions like Reaction (R9) above. When NO^+ is created instead O_2^+, HNO_2 can be produced instead of OH. An example of such reaction sequence is

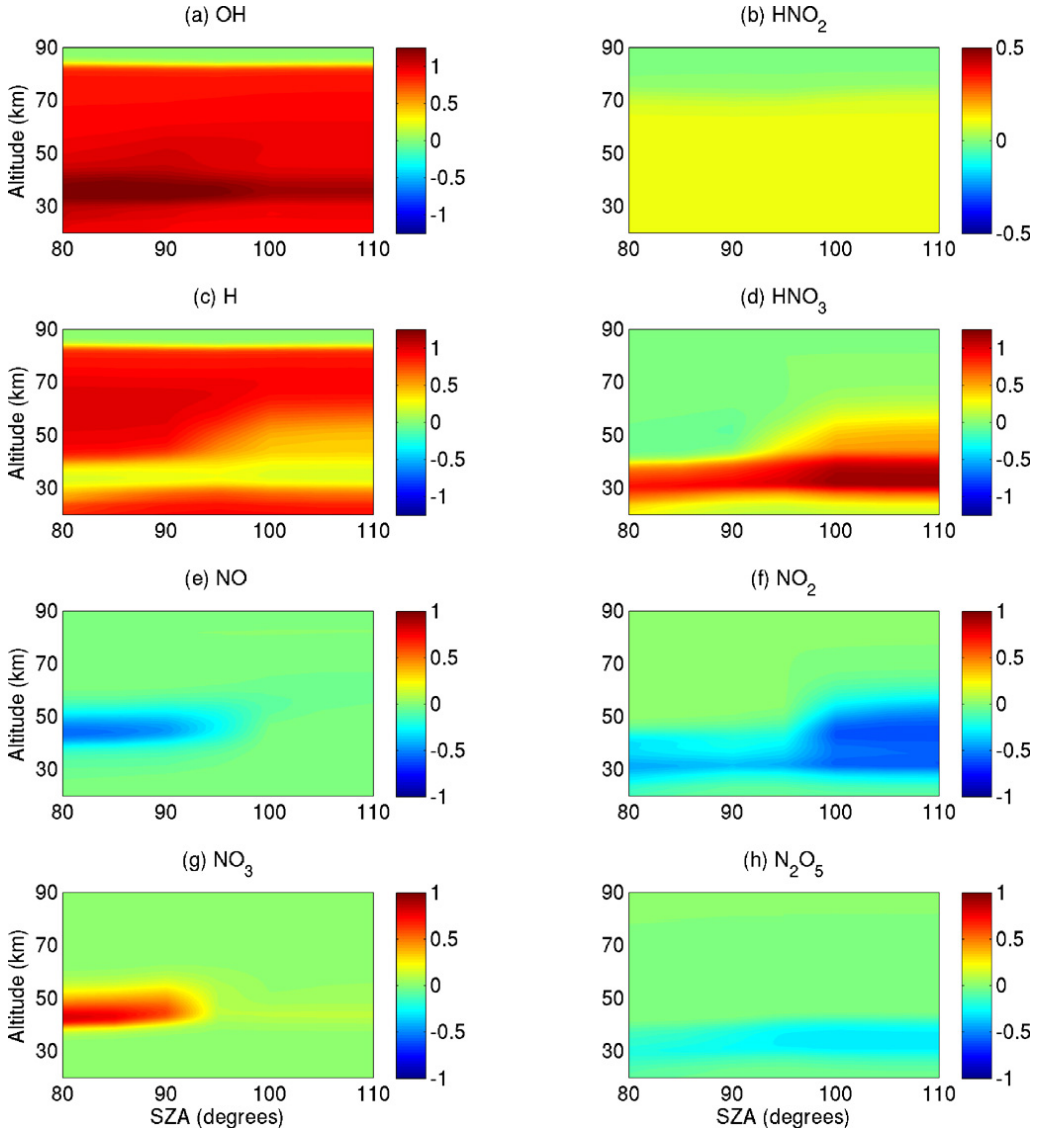

Fig. 2. P/Q numbers for January, Northern Hemisphere, and $Q = 100\,\mathrm{cm^{-3}\,s^{-1}}$. Note that the colour scales of the panels differ.

$$N_2 + p^+(E) \rightarrow N^+ + N(^4S) + e^- + p^+(E - \Delta E) \quad \text{(R13)}$$

$$N^+ + O_2 \rightarrow NO^+ + O \quad \text{(R14)}$$

$$NO^+ + N_2 + M \rightarrow NO^+(N_2) + M \quad \text{(R15)}$$

$$NO^+(N_2) + CO_2 \rightarrow NO^+(CO_2) + N_2 \quad \text{(R16)}$$

$$NO^+(CO_2) + H_2O \rightarrow NO^+(H_2O) + CO_2 \quad \text{(R17)}$$

$$NO^+(H_2O) + H_2O + M \rightarrow NO^+(H_2O)_2 + M \quad \text{(R18)}$$

$$NO^+(H_2O)_2 + H_2O + M \rightarrow NO^+(H_2O)_3 + M \quad \text{(R19)}$$

$$NO^+(H_2O)_3 + H_2O \rightarrow H^+(H_2O)_3 + HNO_2 \quad \text{(R20)}$$

$$H^+(H_2O)_3 + H_2O + M \rightarrow H^+(H_2O)_4 + M \quad \text{(R21)}$$

$$H^+(H_2O)_4 + e^- \rightarrow H + 4H_2O \quad \text{(R22)}$$

$$\text{Net}: \; N_2 + O_2 + H_2O \rightarrow HNO_2 + O + N(^4S) + H \quad \text{(R23)}$$

There are again a number of similar pathways, but in all of them $NO^+(H_2O)_3$ is formed after which $H^+(H_2O)_n$ and HNO_2 are produced. Note that the OH and HNO_2 P/Q numbers in Figs. 2a and 2b show relatively little dependence upon the SZA because the reactions leading to their production (e.g. sequences R1–R9 and R13–R20 above) involve species with weak diurnal variability (N_2, O_2, H_2O, CO_2).

Figures 2a and 2b show that OH production is much larger than HNO_2 production, which is due to most of the initial ionization by protons being directed by ion chemistry to O_2^+ rather than to NO^+ (e.g. the rate of Reaction R1 is larger than that of Reaction R13). Considering the altitude behaviour of the P/Q numbers, H_2O decreases with increasing altitude, and above 70 km its abundance gradually becomes the limiting factor for water cluster ion formation. Also, many of the intermediate reactions require a third body (e.g. Reactions R3

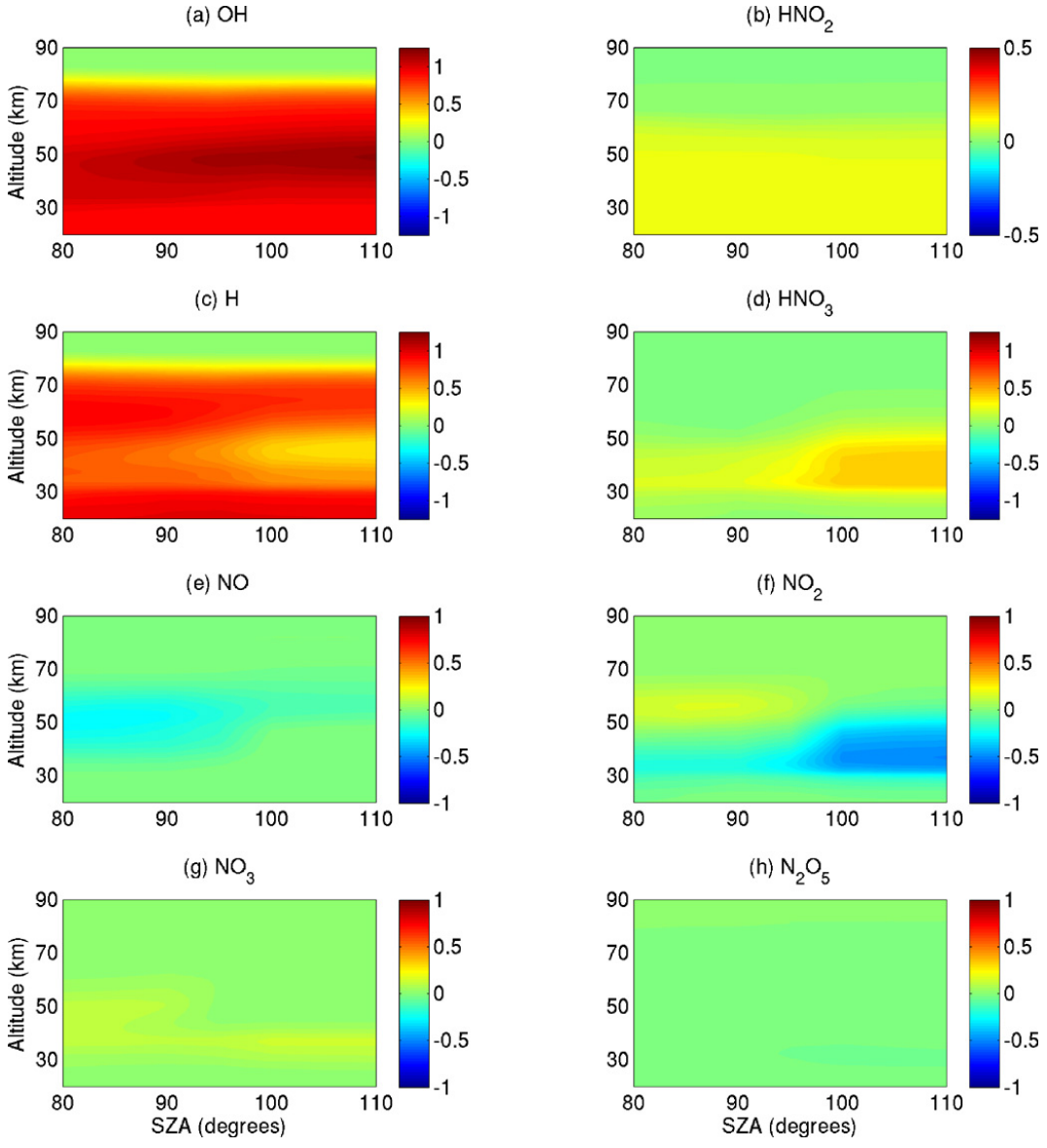

Fig. 3. As Fig. 2, but $Q = 100\,000\,\mathrm{cm}^{-3}\,\mathrm{s}^{-1}$.

and R15), which means their rates are decreasing with altitude. Thus the production of OH and HNO_2 effectively has an upper altitude limit. The OH production displays a maximum at about 35 km, which is due to negative ion chemistry converting HNO_3 to NO_3 and releasing OH. We will discuss this in more detail in Sect. 3.4.

Comparison of Figs. 2a–b with Figs. 3a–b (January, Northern Hemisphere (NH), $Q = 100\,000\,\mathrm{cm}^{-3}\,\mathrm{s}^{-1}$) and Figs. 4a–b (January, Southern Hemisphere (SH), $Q = 100\,\mathrm{cm}^{-3}\,\mathrm{s}^{-1}$) demonstrates how the P/Q numbers change with increasing ionization and water vapour, respectively. When ionization increases, the electron concentration increases, and the probability of recombination of all the intermediate positive ions created in Reactions (R1)–(R8) and (R13)–(R19) increases. For example, recombination of $O_2^+(H_2O)$,

$$O_2^+(H_2O) + e^- \rightarrow O_2 + H_2O, \qquad \text{(R24)}$$

becomes a stronger competitor for Reaction (R5). The increased recombination probability lowers the upper altitude limit of OH and HNO_2 production. The effect is just the opposite, when H_2O is increased. The upper altitude limits of OH and HNO_2 production are elevated when there is more H_2O available in the upper mesosphere for water cluster ion formation.

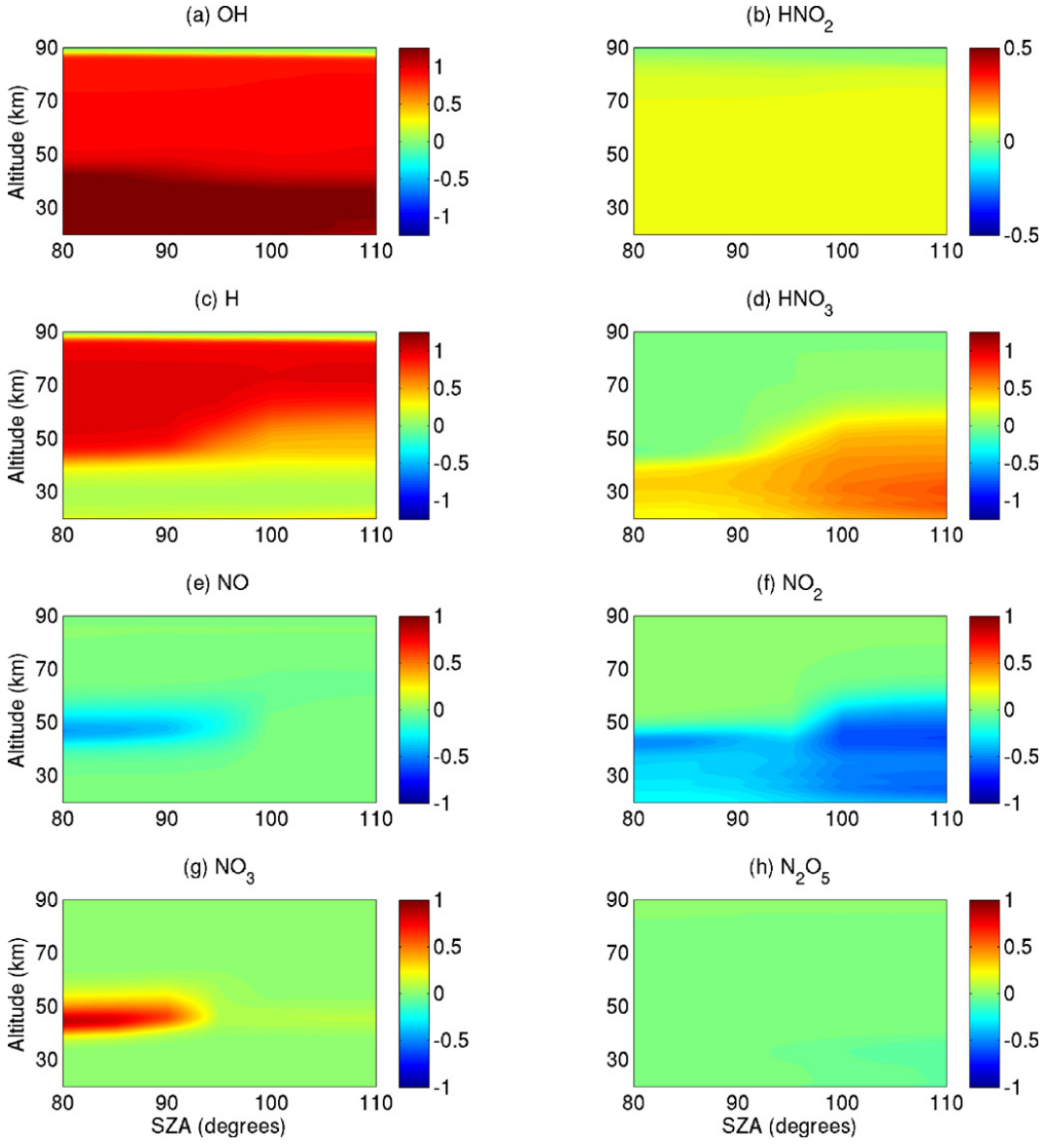

Fig. 4. As Fig. 2, but Southern Hemisphere.

3.2 H and HNO_3 production

While OH and HNO_2 production results from the ionic break-up of H_2O, as shown in the previous section, recombination of the water cluster ions carrying the hydrogen remaining from the H_2O break-up leads subsequently to production of H and HNO_3. Figures 2c and 2d present the H and HNO_3 P/Q numbers for the case of January, Northern Hemisphere, and $Q = 100\,\mathrm{cm}^{-3}\,\mathrm{s}^{-1}$. Atomic hydrogen production takes place when the water cluster ions $H^+(H_2O)_n$, created in reaction sequences such as Reactions (R1)–(R9) and (R13)–(R20), recombine with electrons or negative ions other than $NO_3^-(HNO_3)_n$ (e.g. Reaction R22). HNO_3 is produced when $H^+(H_2O)_n$ recombines with $NO_3^-(HNO_3)_n$ clusters. For example,

$$H^+(H_2O)_n + NO_3^- \rightarrow HNO_3 + nH_2O \qquad \text{(R25)}$$

can replace Reactions (R11) and (R22) in the above reaction sequences. The balance between H and HNO_3 production is therefore determined by the abundance of NO_3^- type ions, and we will discuss their production in Sect. 3.4.

As shown in Figs. 2c and 2d, significant HNO_3 production takes place below 40 km and 60 km during daytime and nighttime, respectively, while atomic hydrogen production dominates in general. The balance between H and HNO_3 production shows relatively little SZA dependence below 40 km where ion–ion recombination prevails over electron–ion recombination at all SZAs. However, there is a clear day–night

Table 3. NO_y P/Q net production numbers for January, NH, $Q = 100\,cm^{-3}\,s^{-1}$.

	30 km	60 km	80 km
$N(^2D)$	0.64	0.64	0.64
$N(^4S)$	0.47	0.47	0.53
HNO_2	0.10	0.10	0.00
NO	0.01	0.01	0.05
Sum	1.22	1.22	1.22

variation at 40–60 km, which is due to the diurnal variation in the electron–negative-ion balance. At daytime, there are significant amounts of electrons available for the ion–electron recombination, which leads to production of H (e.g. Reaction R11). All electrons are rapidly converted to negative ions, so the ion–ion recombination is dominant at night and produces HNO_3 through reactions like Reaction (R25).

When the ionization rate increases (Figs. 3c and 3d, $Q = 100\,000\,cm^{-3}\,s^{-1}$), it increases H production and decreases HNO_3 production relative to the ionization rate. Also, the altitude range of HNO_3 production becomes more limited. Higher ionization increases electron and positive ion concentrations, so the probability of electron–ion recombination increases over electron attachments reactions such as

$$O_2 + O_2 + e^- \rightarrow O_2^- + O_2, \quad \text{(R26)}$$

which initialise the negative ion sequences leading to formation of $NO_3^-(HNO_3)_n$ and HNO_3 (negative ion chemistry is discussed in Sect. 3.4). Figures 4c–d show the P/Q numbers for summer conditions. Compared to winter conditions (Figs. 2c–d), the proportion of HNO_3 production increases below 30 km and decreases at 30–40 km. These differences will be discussed in more detail in Sect. 3.4 together with NO_y redistribution.

3.3 NO_y production

As shown schematically in Fig. 1, proton precipitation leads to NO_y production. A fraction of the NO_y production, which always involves N_2 dissociation, is due to positive ion reaction sequences, such as Reactions (R13)–(R20). In this example, N_2 is converted to $N(^4S)$ and HNO_2. According to the pathway analysis, in other reaction sequences also $N(^2D)$ and NO (in very small amounts) can be produced. The combined P/Q production number for the four species is 0.42, with no significant variability with respect to SZA. Above 80 km there is increase with increasing altitude, but at lower altitudes the total number does not change. However, as shown in Fig. 2b, HNO_2 is produced only at altitudes below ~ 70 km. Note that this altitude limit varies with rate of ionization and amount of water vapour (Figs. 3b and 4b).

Most of the NO_y production is a result of N_2 dissociation by energetic secondary electrons, which are produced in impact ionization by protons (e.g. Reactions R1 and R13). For example, in

$$N_2 + e_s^-(E) \rightarrow N(^4S) + N(^2D) + e_s^-(E - \Delta E) \quad \text{(R27)}$$

the secondary electron e_s^- collides with N_2, loses some of its energy, and produces atomic nitrogen. In the SIC model, Reaction (R27) is parameterised; i.e. the atomic nitrogen production rate from dissociation of N_2 is taken to be $0.8 \times Q$ (Rusch et al., 1981), and the $N(^4S)/N(^2D)$ branching is fixed to 0.4/0.6 (Zipf et al., 1980). Therefore, the P/Q numbers of this process, calculated from the SIC results, are fixed.

Combining the dissociation by secondary electrons and the ion reaction sequences from SIC, the sum of P/Qs of $N(^4S)$, $N(^2D)$, NO, and HNO_2 is 1.22. Of this total, the tables in Appendix A only account for the production of HNO_2. As an example, Table 3 presents NO_y net production numbers for the case of January, NH, $Q = 100\,cm^{-3}\,s^{-1}$. Compared to the lower altitudes, the change at 80 km is that $N(^4S)$ and NO are produced instead of HNO_2 through

$$NO^+ + e^- \rightarrow N(^4S) + O \quad \text{(R28)}$$

and

$$NO^+(H_2O) + e^- \rightarrow NO + H_2O, \quad \text{(R29)}$$

because the decreasing H_2O concentration makes reaction sequences like Reactions (R15)–(R19) less probable compared to more direct ion–electron recombination (e.g. Reactions R28 and R29), which is also enhanced by the increasing electron concentration.

3.4 NO_y redistribution

SPE ionization leads to redistribution of NO_y species through negative ion reaction sequences, as shown in Fig. 1. Some species are produced, like NO_3, or lost, like N_2O_5, while others, like HNO_3, can be both produced and lost in different reaction chains. It should be noted that negative ion chemistry does not change the total NO_y amount. The net NO_y production during particle precipitation is by positive ion chemistry (as described in Sect. 3.3). HNO_3 is a special species here, because its production is a combination of ionic HO_x and NO_y production. In Sect. 3.2, we already discussed the HNO_3 production from the positive ion and hydrogen point of view, and showed how it is produced when positive $H^+(H_2O)_n$ water cluster ions recombine with $NO_3^-(HNO_3)_n$ type negative ions (e.g. Reaction R25). In this section, we investigate the HNO_3 production from the point of view of negative ion and nitrogen chemistry, together with the ionic redistribution of other NO_y species.

The P/Q numbers of the NO_y species are shown in Figs. 2d–h for January, Northern Hemisphere, and $Q = 100\,cm^{-3}\,s^{-1}$. Clearly, significant production of HNO_3 and NO_3 takes place, balanced by loss of NO, NO_2, and N_2O_5. Most of the HNO_3 production pathways involve loss of NO_2,

for example, in the sequence

$$O_2 + O_2 + e^- \rightarrow O_2^- + O_2 \quad (R30)$$
$$O_2^- + O_3 \rightarrow O_3^- + O_2 \quad (R31)$$
$$O_3^- + CO_2 \rightarrow CO_3^- + O_2 \quad (R32)$$
$$CO_3^- + NO_2 \rightarrow NO_3^- + CO_2 \quad (R33)$$
$$NO_3^- + H^+(H_2O)n \rightarrow HNO_3 + nH_2O \quad (R34)$$
$$--- \qquad ---$$
$$\text{Net: } e^- + H^+(H_2O)n + O_3 + NO_2 \rightarrow HNO_3 + O_2 + nH_2O \quad (R35)$$

and other similar sequences with the same net effect. When Reactions (R30)–(R33) are followed by, for example,

$$NO_3^- + H_2O + M \rightarrow NO_3^-(H_2O) + M \quad (R36)$$
$$NO_3^-(H_2O) + N_2O_5 \rightarrow NO_3^-(HNO_3) + HNO_3 \quad (R37)$$
$$NO_3^-(HNO_3) + H^+(H_2O)n \rightarrow HNO_3 + HNO_3 + nH_2O \quad (R38)$$
$$--- \qquad ---$$
$$\text{Net: } e^- + H^+(H_2O)n + H_2O + O_3 + NO_2 + N_2O_5 \rightarrow 3HNO_3 + O_2 + nH_2O \quad (R39)$$

consuming N_2O_5, the net result (Reactions R30–R33 followed by Reactions R36–R38) is production of multiple HNO_3 molecules (Reaction R39). This and other similar sequences have their largest impact around 30 km at night. Note that the N_2O_5-to-HNO_3 conversion by negative ion reaction sequences consumes also water vapour, thus adding to H_2O losses (and eventually to HO_x production) caused by positive ion chemistry. At daytime, also NO can be converted to HNO_3. As an example, Reactions (R30)–(R32) can be followed by

$$CO_3^- + NO \rightarrow NO_2^- + CO_2 \quad (R40)$$
$$NO_2^- + O_3 \rightarrow NO_3^- + O_2 \quad (R41)$$
$$NO_3^- + H^+(H_2O)n \rightarrow HNO_3 + nH_2O \quad (R42)$$
$$--- \qquad ---$$
$$\text{Net: } e^- + H^+(H_2O)n + NO + 2O_3 \rightarrow HNO_3 + 2O_2 + nH_2O \quad (R43)$$

completing the sequence (net Reaction R43 is for sequence of Reactions R30–R32 + R40–R42). Note, however, that most of the daytime NO loss leads to production of NO_3 instead of HNO_3, through pathways such as

$$2O_2 + e^- \rightarrow O_2^- + O_2 \quad (R44)$$
$$O_2^- + O_3 \rightarrow O_3^- + O_2 \quad (R45)$$
$$O_3^- + CO_2 \rightarrow CO_3^- + O_2 \quad (R46)$$
$$CO_3^- + NO \rightarrow NO_2^- + CO_2 \quad (R47)$$
$$NO_2^- + O_3 \rightarrow NO_3^- + O_2 \quad (R48)$$
$$NO_3^- + h\nu \rightarrow NO_3 + e^- \quad (R49)$$
$$--- \qquad ---$$
$$\text{Net: } NO + 2O_3 \rightarrow 2O_2 + NO_3. \quad (R50)$$

These, and other similar pathways leading to NO-to-NO_3 conversion, are only important at daytime because (1) solar UV radiation is required for Reaction (R49), and (2) below about 60 km there is almost no NO available at night, because the neutral chemistry converts it to NO_2.

Net loss of HNO_3 can also occur, for example, at daytime around 45 km, because there are reaction sequences like

$$O_2 + O_2 + e^- \rightarrow O_2^- + O_2 \quad (R51)$$
$$O_2^- + O_3 \rightarrow O_3^- + O_2 \quad (R52)$$
$$O_3^- + CO_2 \rightarrow CO_3^- + O_2 \quad (R53)$$
$$CO_3^- + HNO_3 \rightarrow NO_3^- + CO_2 + OH \quad (R54)$$
$$NO_3^- + h\nu \rightarrow NO_3 + e^- \quad (R55)$$
$$--- \qquad ---$$
$$\text{Net: } HNO_3 + O_3 \rightarrow O_2 + OH + NO_3 \quad (R56)$$

which convert HNO_3 to other NO_y species and release HO_x. This example pathway requires solar light for the photodetachment of electrons (Reaction R55), and thus only functions at daytime. However, there are similar reaction sequences with the same net effect in operation at night; in these the photodetachment reaction is replaced by ion–ion recombination. Although in Fig. 2d net production of HNO_3 is seen at almost all altitudes and SZAs, the rates of the HNO_3 loss pathways can be comparable to those of HNO_3 production, and it is important to take them into account when the net effect is calculated. Also, a significant amount of odd hydrogen is released by these HNO_3 loss sequences. This explains, for example, the maximum in OH P/Q numbers seen in Fig. 2a around 35 km, where the negative ion chemistry adds to the nearly constant 0.9 P/Q by positive ion chemistry.

Figures 3d–h show the NO_y P/Q numbers for a case with increased ionization (January, NH, $Q = 100\,000\,\mathrm{cm^{-3}\,s^{-1}}$). NO_y redistribution is clearly diminished relatively; all the P/Q numbers are smaller than those shown in Figs. 2d–h. As discussed already in Sect. 3.2, the increase in electron and ion (both positive and negative) concentrations makes the recombination processes more probable compared to other ionic reactions which involve neutral species. This means that longer reaction sequences become less probable. Thus, the production of more complex cluster ions such as $H^+(H_2O)_n$ and

$NO_3^-(HNO_3)_n$, and subsequently the HNO_3 production, is relatively smaller. For example, the conversion of N_2O_5 to HNO_3 practically stops (Fig. 3h). At 50–60 km (daytime), a larger proportion of NO is converted to NO_2 rather than to NO_3, because ozone decrease (by extreme ionization and HO_x production) limits the production of NO_3^- through Reaction (R48).

Figures 4d–h present the NO_y P/Q numbers for summer pole conditions (January, SH, $Q = 100\,cm^{-3}\,s^{-1}$). Compared to the winter pole (i.e. Figs. 2d–h), the HNO_3 P/Q increases below 30 km and decreases at 30–40 km (as we mentioned already in Sect. 3.2). The decrease around 35 km is caused by relatively small amounts of N_2O_5 being converted to HNO_3. At the summer pole, N_2O_5 concentrations are smaller than those at the winter pole, because there are less nighttime hours for its production and build-up from NO_2 and NO_3 (at daytime its photodissociation is fast). At lower altitudes, there is more NO_2-to-HNO_3 conversion in the summer because of higher amounts of NO_2 available. At these altitudes, the main source of NO_x production is $N_2O+O(^1D) \rightarrow 2NO$, which is enhanced in the summer due to more solar radiation being available. The enhanced NO (or NO_x) amounts favour NO_3^- type ions, which are needed for ionic production of HNO_3.

4 Comparison with Solomon et al. (1981)

Because the HO_x production numbers from Solomon et al. (1981, Fig. 2) have been used in many modelling studies, it is interesting to compare our results with them. It should be noted that while Solomon et al. (1981) analysed the HO_x production in quite detail (e.g. taking into account the dependency on H_2O and a few other atmospheric parameters), the widely used parameterisation based on their Fig. 2 is much simplified and considers variability with respect to altitude and ionization rate only. We selected the SIC case of January NH, in which the H_2O background was similar to that in Solomon et al. (1981, Fig. 2), and compared their total HO_x P/Q numbers with our P/Q sum of (1) OH and H, i.e. direct HO_x production by positive ion chemistry only, (2) OH, H, HNO_2, and HNO_3 but excluding N_2O_5-to-HNO_3 conversion by negative ion chemistry, and (3) OH, H, HNO_2, and HNO_3 including N_2O_5-to-HNO_3 conversion. Of these, Case #2 corresponds to the assumptions made by Solomon et al. (1981), i.e. instant HO_x release from HNO_2 and HNO_3, and exclusion of negative ion chemistry.

Figures 5a–c show the results for Cases 1–3, respectively. Although not shown, the Solomon et al. (1981) P/Q number is 2 below 40 km. It is evident that the P/Q numbers of Solomon et al. (1981) overestimate the direct HO_x production, especially at altitudes below 70 km where both HNO_2 and HNO_3 production takes place. With the lowest ionization rates, the overestimation reaches 100 % at 35 km (Fig. 5a). For Case #2, corresponding to the Solomon et al. (1981) assumptions, the agreement is very good, although above 70 km our results show a somewhat larger variability with

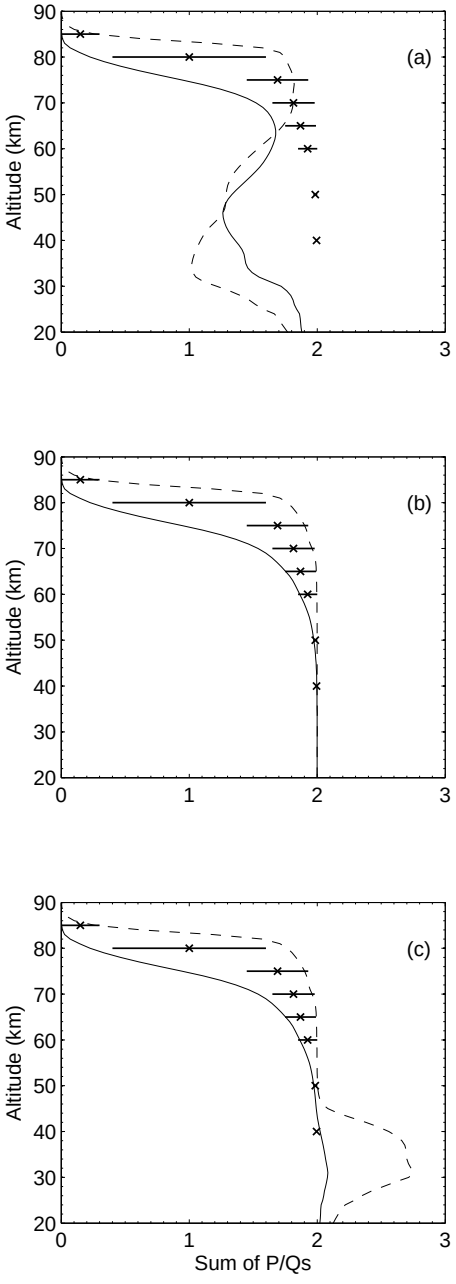

Fig. 5. Comparison of P/Q numbers: SIC results (January NH and SZA = 105°) versus Solomon et al. (1981, Fig. 2). The Solomon et al. data for $Q = 10^3\,cm^{-3}\,s^{-1}$ are marked with X, and the corresponding horizontal lines indicate the variability with respect to $Q = 10^1$–$10^5\,cm^{-3}\,s^{-1}$. The same data are shown in all three panels. SIC results: **(a)** OH and H production only; **(b)** OH, H, HNO_2, and HNO_3 production, excluding N_2O_5-to-HNO_3 conversion; and **(c)** OH, H, HNO_2, and HNO_3 production, including N_2O_5-to-HNO_3 conversion. The dashed and solid lines indicate results for $Q = 10^1$ and $10^5\,cm^{-3}\,s^{-1}$, respectively.

respect to the ionization rate (Fig. 5b). And when N_2O_5-to-HNO_3 conversion is considered, it adds to the total below 50 km through HNO_3 production, so that the Solomon et al. (1981) values now underestimate the P/Q number by up to 25 % at 30–40 km (Fig. 5c), although at very high ionization rates this difference becomes small.

As we showed in Figs. 2 and 4, there are significant differences between winter and summer conditions. For example, the upper altitude limit of HO_x production is elevated in the summer. Thus, the comparison in Fig. 5, for similar atmospheric conditions, shows the "best" match between ours and the Solomon et al. (1981) P/Q numbers, while for other seasons there are larger differences.

5 Discussion

In this section, we discuss briefly the uncertainties of the mean P/Q numbers in order to provide a rough estimate of their accuracy, provide some information on the ionic changes in H_2O and O_3 for which P/Q tables are not provided, and discuss the ionic effects in comparison to standard neutral chemistry. Finally, we point out that our results are also applicable to electron precipitation, and discuss the improvements in the new P/Q numbers and possible future work on chlorine species.

The mean P/Q numbers given in Appendix A have statistical uncertainty, which we estimate using their standard deviations (STDs). This approach takes into account the variability of P/Q numbers with respect to the changes in the background atmosphere (neutral species, temperature), while uncertainties in reaction rate coefficients are not included. A part of the variability in the background atmosphere comes from the latitudinal dependence, but for some species the changes caused by the SPE forcing can be much more important. For example, NO_x species are produced during SPE forcing, and at some altitudes their concentration can increase by an order of magnitude during a 1-day high-ionization model run. This causes variability in the ion composition (e.g. the balance between NO_3^- and CO_3^-) and subsequently in the P/Q numbers of the NO_y species. We calculated STD for all the mean P/Q numbers, and then took an all-SZA all-altitude median for each species. The results indicate that for OH and HNO_2 the median STD is small (≤ 3 %), although the H_2O variability can have a stronger effect (up to tens of percent) at the upper altitude limit where H_2O becomes a limiting factor for HNO_2 and OH production. For NO_y and atomic hydrogen, STDs are larger because the P/Q numbers of these species are sensitive to the SPE-driven changes. The median STD is 0.03–0.06 (6–24 %) depending on species.

Comparison between Figs. 2 and 4 gives information on the variability of the P/Q numbers between winter and summer, as we discussed it in Sect. 3. Generally speaking, the season affects the HO_x production at the upper altitudes, while NO_y distribution is most affected at the lower altitudes. In order to compare the seasonal effects to those related to latitudinal averaging (see previous paragraph), we calculated the median difference between the values given in Appendix A for the January NH and January SH cases (Tables A1–A16). Large seasonal differences in OH and HNO_2 P/Q numbers, up to hundreds of percent, are found near the upper altitude boundary of production at 70–85 km caused by differences in H_2O background. Also, OH is significantly affected by changes in its release from HNO_3 by negative ion chemistry below 30 km, with P/Q variability up to 40 %. However, the median P/Q differences for OH and HNO_2 are again small (< 5 %). In the case of H and NO_y, the median difference between winter and summer P/Q numbers is 0.04–0.16 (18–87 %) depending on species. The seasonal difference is especially large for N_2O_5, because in the summer its concentration, and thus its conversion to HNO_3, is small compared to winter.

We do not provide P/Q tables for the consumption of N_2 and H_2O, or consider changes in oxygen species such as ozone. Clearly, N_2 concentrations in the mesosphere are much too high (e.g. $\sim 10^{15}$ cm^{-3} at 70 km) to be affected by SPEs. In the case of H_2O loss, P/Q numbers can be easily calculated as the sum of hydrogen production numbers (i.e. OH, HNO_2, H, and HNO_3), divided by two. As follows from Fig. 5c, this number is 1–1.4 up to ≈ 50 km, and then gradually decreases to zero between 50 and 90 km. Considering that the H_2O concentration at 70 km is about 10^9 cm^{-3}, and assuming $P/Q = -1$ and ionization rate = 10^3 cm^{-3} s^{-1}, the daily loss of H_2O would be about 8 %, which is not negligible. However, the produced HO_x is converted back to H_2O through relatively fast (HO_x lifetime is $\sim$ hours below 80 km) self-destructive neutral reactions such as

$$OH + HO_2 \rightarrow H_2O + O_2, \quad \text{(R57)}$$

so the net effect on H_2O should be much smaller. Note that at lower altitudes the relative effect on H_2O becomes negligible because of the increasing water vapour concentration. A recent model study on water vapour changes during the January 2005 SPE indicates a decrease in H_2O at altitudes 75–90 km, but this effect has not been seen in satellite observations (Winkler et al., 2012).

Ozone is consumed in net reactions such as Reactions (R35), (R39), (R43), (R50), and (R56). However, the direct effect of ion chemistry on ozone is small compared to catalytic cycles that are enhanced by HO_x and NO_x production. As an interesting detail, the pathway analysis identifies several catalytic cycles of negative ion chemistry which convert ozone to O_2. During night the dominant O_3 loss cycles (by ion chemistry) are of the following form:

$$2O_2 + e^- \rightarrow O_2^- + O_2 \quad \text{(R58)}$$
$$O_2^- + O_2 + M \rightarrow O_4^- + M \quad \text{(R59)}$$
$$O_4^- + CO_2 \rightarrow CO_4^- + O_2 \quad \text{(R60)}$$
$$CO_4^- + O_3 \rightarrow O_3^- + O_2 + CO_2 \quad \text{(R61)}$$
$$O_3^- + O_3 \rightarrow 3O_2 + e^- \quad \text{(R62)}$$
$$--- \quad ---$$
$$\text{Net}: 2O_3 \rightarrow 3O_2. \quad \text{(R63)}$$

However, the ozone loss rates due to these cycles are low, and insignificant compared to those of the daytime HO_x neutral chemistry. On the other hand, when the neutral gas-phase chemistry combines with the NO_y redistribution by ion chemistry, this affects also ozone. For example, the NO-to-NO_2 conversion seen in Fig. 3e–f (daytime, 55 km) proceeds without loss of ozone. The subsequent NO_2 photolysis produces O_3:

$$NO_2 + h\nu \rightarrow NO + O \quad \text{(R64)}$$
$$O + O_2 + M \rightarrow O_3 + M. \quad \text{(R65)}$$

So, both processes together yield a net ozone production. However, the corresponding rates are again too small to compete with the standard ozone production and destruction cycles.

The presented P/Q numbers indicate the pure effect of ion chemistry without consideration of its importance in contrast to the neutral gas-phase chemistry. Obviously, the significance of ion chemistry causing net production of NO_y (or NO_x) and HO_x has been known for a long time, and there is observational evidence indicating substantial increase in these neutral species during particle precipitation events (e.g. Seppälä et al., 2004; Verronen et al., 2006). Also, the magnitude of the nighttime NO_y redistribution by negative ion chemistry is large enough to be detected by satellite-based observations of, for example, HNO_3 (López-Puertas et al., 2005b; Verronen et al., 2011; Funke et al., 2011). However, the daytime ionic NO_y redistribution effect is counteracted at the upper altitudes by solar radiation through photochemical reactions, which drive rapid NO_y changes. For example, it has been shown that photodissociation of HNO_3 is much faster than its ionic production at altitudes near and above the stratopause, even during strong SPEs (Verronen et al., 2008). The situation is similar for NO_3.

Particle precipitation can also affect chlorine species. For example, Winkler et al. (2009) have studied the conversion of HCl to active chlorine species by negative ion chemistry in the stratopause region during SPEs. In the current paper we do not analyse these effects. The SIC model does include the relevant ion chemical reactions, but to date SIC has not been used in studies of chlorine species, so the model predictions have not been validated by, for example, satellite observations. In the future, if such a model-versus-observations study is first conducted, it might be possible to extend the current analysis to include also the chlorine species.

Although we are studying the effects of proton forcing in this paper, the calculated P/Q numbers can be applied for electron precipitation too. In the SIC model, the total particle ionization is divided between N_2, O_2, and O according to relative concentrations and impact cross sections of these species. This partitioning is only slightly different for electrons compared to protons; in both cases the proportion of N_2 and O_2 ionization below 90 km is about 78 % and 22 % of the total, respectively. Further, the partitioning between processes of ionization and dissociative ionization and their products (e.g. production of N_2^+ and N^+ through N_2 ionization) is identical for protons and electrons. Therefore, the same P/Q numbers can be used for both proton and electron precipitation.

The comparisons presented in Figs. 5a–c demonstrate clearly how our results can significantly improve the modelling of ion chemistry and its effects on neutral minor species through a simple parameterisation. For example, understanding the HNO_3 observations during SPEs is not possible without consideration of negative ion chemistry. The diurnal and seasonal variability, which has not been considered before, is also an improvement. For example, the HO_x production upper limit and and NO_y redistribution show significant variability with season, which can potentially affect the ozone chemistry.

6 Summary

We have presented an analysis of D region ion chemistry and its effects on neutral HO_x and NO_y during SPEs. We showed that while positive ion chemistry leads to production of H, OH, HNO_2, N, and NO from water vapour and N_2, the main effect of negative ion chemistry is to redistribute NO_y species, without a net change, by converting NO, NO_2, and N_2O_5 to HNO_3 and NO_3.

Based on the results from the Sodankylä Ion and Neutral Chemistry model, we have calculated tables of so-called P/Q numbers (i.e. production/loss rates divided by ionization rate) for the relevant HO_x and NO_y species. These numbers are provided for different atmospheric conditions taking into account diurnal and seasonal variabilities. The P/Q numbers allow for an easy-to-use parameterisation of ion chemistry for atmospheric modelling of particle precipitation.

The new P/Q parameterisation presented in this paper improves the currently used methods by considering the diurnal and seasonal variability. However, the main improvement is the consideration of negative ion chemistry effects, which was previously neglected but is essential for the modelling and understanding of NO_y changes induced by particle precipitation.

Appendix A

Tables of P/Q numbers

Here we present the P/Q numbers as a function of altitude, solar zenith angle, and ionization rate. The numbers were calculated from SIC model results as described in Sect. 2.4. The tables are given for four different seasons, January Southern Hemisphere/Northern Hemisphere (SH/NH) and October SH/NH, and for eight constituents (H, OH, HNO_2, HNO_3, NO, NO_2, NO_3, and N_2O_5). The figures below the tables present the same data. Note that the numbers in these tables do not include NO_y net production, except for HNO_2, but only redistribution (see Section 3.3 for more details). The tables are available in electronic format from the corresponding author.

Table A1. P_{OH}/Q for January SH.

Q	10^1	10^2	10^3	10^4	10^5	10^1	10^2	10^3	10^4	10^5	10^1	10^2	10^3	10^4	10^5
km		SZA	$\leq$	90°			SZA	$=$	95°			SZA	$\geq$	100°	
90	+0.05	+0.02	+0.01	+0.00	+0.00	+0.03	+0.01	+0.00	+0.00	+0.00	+0.04	+0.02	+0.00	+0.00	+0.00
85	+0.89	+0.88	+0.84	+0.67	+0.29	+0.89	+0.87	+0.82	+0.63	+0.24	+0.89	+0.87	+0.80	+0.57	+0.19
80	+0.90	+0.89	+0.88	+0.84	+0.70	+0.90	+0.90	+0.88	+0.84	+0.66	+0.90	+0.90	+0.89	+0.86	+0.65
75	+0.89	+0.90	+0.89	+0.88	+0.83	+0.90	+0.90	+0.89	+0.88	+0.84	+0.90	+0.90	+0.91	+0.90	+0.84
70	+0.90	+0.90	+0.90	+0.90	+0.89	+0.90	+0.90	+0.91	+0.90	+0.89	+0.90	+0.91	+0.91	+0.93	+0.92
65	+0.90	+0.90	+0.90	+0.90	+0.90	+0.90	+0.90	+0.91	+0.94	+0.93	+0.91	+0.91	+0.92	+0.97	+1.00
60	+0.91	+0.90	+0.92	+0.93	+0.96	+0.91	+0.92	+0.94	+1.00	+1.04	+0.92	+0.92	+0.95	+1.05	+1.09
55	+0.93	+0.92	+0.93	+0.98	+1.05	+0.92	+0.93	+0.96	+1.05	+1.13	+0.92	+0.94	+0.98	+1.07	+1.16
50	+0.99	+0.95	+0.95	+1.01	+1.09	+0.94	+0.95	+0.98	+1.07	+1.17	+0.91	+0.93	+1.00	+1.09	+1.16
45	+1.25	+1.11	+1.02	+1.05	+1.12	+1.03	+1.00	+1.00	+1.07	+1.15	+0.95	+0.97	+1.00	+1.07	+1.13
40	+1.35	+1.28	+1.12	+1.07	+1.13	+1.20	+1.14	+1.07	+1.07	+1.14	+1.14	+1.11	+1.04	+1.06	+1.10
35	+1.41	+1.36	+1.26	+1.10	+1.12	+1.35	+1.31	+1.22	+1.08	+1.11	+1.29	+1.25	+1.19	+1.07	+1.09
30	+1.47	+1.46	+1.37	+1.20	+1.13	+1.39	+1.36	+1.31	+1.15	+1.09	+1.29	+1.27	+1.21	+1.09	+1.07
25	+1.48	+1.46	+1.39	+1.22	+1.11	+1.39	+1.36	+1.29	+1.13	+1.04	+1.24	+1.24	+1.17	+1.06	+1.00
20	+1.43	+1.40	+1.29	+1.12	+1.02	+1.32	+1.30	+1.19	+1.05	+0.97	+1.18	+1.16	+1.07	+0.98	+0.93

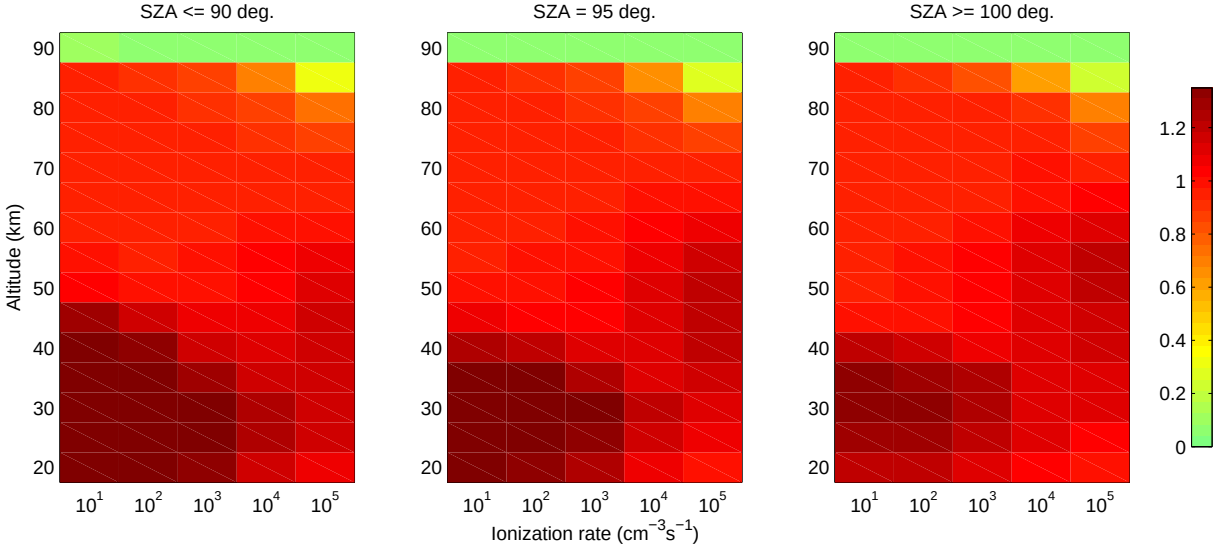

Fig. A1. P_{OH}/Q for January SH.

Table A2. P_{HNO_2}/Q for January SH.

Q	10^1	10^2	10^3	10^4	10^5	10^1	10^2	10^3	10^4	10^5	10^1	10^2	10^3	10^4	10^5
km		SZA	$\leq$	90°			SZA	=	95°			SZA	$\geq$	100°	
90	−0.00	−0.00	−0.00	−0.00	−0.00	−0.00	−0.00	−0.00	−0.00	−0.00	−0.00	−0.00	−0.00	−0.00	−0.00
85	+0.07	+0.04	+0.01	+0.00	+0.00	+0.06	+0.03	+0.01	+0.00	+0.00	+0.04	+0.02	+0.00	+0.00	+0.00
80	+0.09	+0.08	+0.05	+0.02	+0.00	+0.09	+0.07	+0.04	+0.01	+0.00	+0.09	+0.08	+0.05	+0.01	+0.00
75	+0.10	+0.09	+0.07	+0.04	+0.01	+0.10	+0.09	+0.07	+0.04	+0.01	+0.10	+0.09	+0.08	+0.05	+0.01
70	+0.10	+0.09	+0.08	+0.06	+0.03	+0.10	+0.10	+0.09	+0.07	+0.04	+0.10	+0.10	+0.09	+0.07	+0.04
65	+0.10	+0.10	+0.09	+0.09	+0.07	+0.10	+0.10	+0.10	+0.09	+0.07	+0.10	+0.10	+0.10	+0.09	+0.07
60	+0.10	+0.10	+0.10	+0.10	+0.10	+0.10	+0.10	+0.10	+0.10	+0.09	+0.10	+0.10	+0.10	+0.09	+0.08
55	+0.10	+0.10	+0.10	+0.10	+0.10	+0.10	+0.10	+0.10	+0.10	+0.10	+0.10	+0.10	+0.10	+0.10	+0.09
50	+0.10	+0.10	+0.10	+0.10	+0.10	+0.10	+0.10	+0.10	+0.10	+0.10	+0.10	+0.10	+0.10	+0.10	+0.10
45	+0.10	+0.10	+0.10	+0.10	+0.10	+0.10	+0.10	+0.10	+0.10	+0.10	+0.10	+0.10	+0.10	+0.10	+0.10
40	+0.10	+0.10	+0.10	+0.10	+0.10	+0.10	+0.10	+0.10	+0.10	+0.10	+0.10	+0.10	+0.10	+0.10	+0.10
35	+0.10	+0.10	+0.10	+0.10	+0.10	+0.10	+0.10	+0.10	+0.10	+0.10	+0.10	+0.10	+0.10	+0.10	+0.10
30	+0.10	+0.10	+0.10	+0.10	+0.10	+0.10	+0.10	+0.10	+0.10	+0.10	+0.10	+0.10	+0.10	+0.10	+0.10
25	+0.10	+0.10	+0.10	+0.10	+0.10	+0.10	+0.10	+0.10	+0.10	+0.10	+0.10	+0.10	+0.10	+0.10	+0.10
20	+0.10	+0.10	+0.10	+0.10	+0.10	+0.10	+0.10	+0.10	+0.10	+0.10	+0.10	+0.10	+0.10	+0.10	+0.10

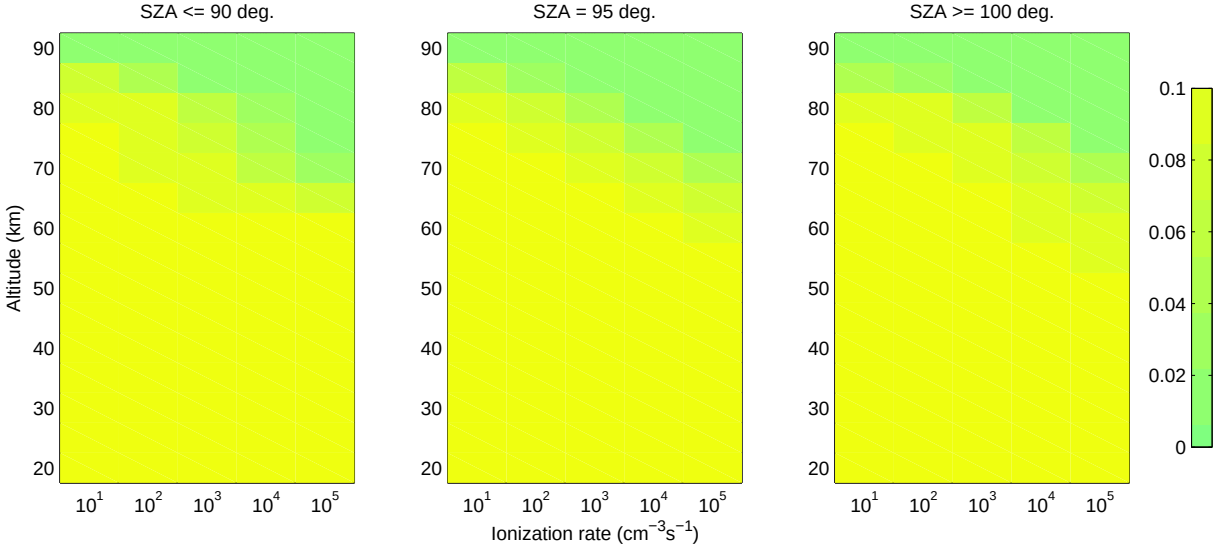

Fig. A2. P_{HNO_2}/Q for January SH.

Table A3. P_H/Q for January SH.

Q	10^1	10^2	10^3	10^4	10^5	10^1	10^2	10^3	10^4	10^5	10^1	10^2	10^3	10^4	10^5
km		SZA	$\leq$	90°			SZA	$=$	95°			SZA	$\geq$	100°	
90	+0.05	+0.02	+0.01	+0.00	+0.00	+0.03	+0.01	+0.00	+0.00	+0.00	+0.04	+0.02	+0.00	+0.00	+0.00
85	+0.96	+0.92	+0.85	+0.67	+0.29	+0.95	+0.90	+0.83	+0.63	+0.24	+0.93	+0.89	+0.80	+0.57	+0.19
80	+0.99	+0.97	+0.93	+0.86	+0.69	+0.99	+0.97	+0.92	+0.85	+0.65	+0.99	+0.97	+0.93	+0.85	+0.62
75	+0.99	+0.99	+0.96	+0.92	+0.83	+1.00	+0.99	+0.96	+0.92	+0.82	+1.00	+0.98	+0.96	+0.90	+0.81
70	+1.00	+0.99	+0.98	+0.96	+0.89	+1.00	+1.00	+0.98	+0.95	+0.88	+0.97	+0.97	+0.94	+0.90	+0.84
65	+1.00	+1.00	+0.99	+0.97	+0.91	+0.98	+0.99	+0.96	+0.91	+0.87	+0.83	+0.89	+0.84	+0.78	+0.78
60	+1.00	+1.00	+0.99	+0.95	+0.85	+0.91	+0.94	+0.92	+0.80	+0.74	+0.60	+0.75	+0.75	+0.61	+0.62
55	+0.99	+0.99	+0.98	+0.90	+0.71	+0.78	+0.83	+0.84	+0.70	+0.56	+0.44	+0.58	+0.65	+0.49	+0.42
50	+0.97	+0.97	+0.95	+0.84	+0.60	+0.61	+0.67	+0.73	+0.62	+0.44	+0.42	+0.48	+0.56	+0.46	+0.30
45	+0.77	+0.83	+0.85	+0.73	+0.50	+0.37	+0.50	+0.61	+0.56	+0.40	+0.30	+0.41	+0.50	+0.45	+0.29
40	+0.28	+0.39	+0.59	+0.61	+0.43	+0.19	+0.29	+0.48	+0.53	+0.38	+0.16	+0.26	+0.44	+0.48	+0.34
35	+0.11	+0.17	+0.32	+0.53	+0.45	+0.11	+0.16	+0.31	+0.51	+0.42	+0.10	+0.15	+0.29	+0.48	+0.39
30	+0.06	+0.10	+0.21	+0.42	+0.47	+0.06	+0.10	+0.21	+0.42	+0.46	+0.06	+0.09	+0.21	+0.41	+0.44
25	+0.08	+0.12	+0.25	+0.47	+0.57	+0.08	+0.13	+0.27	+0.50	+0.59	+0.08	+0.13	+0.29	+0.53	+0.61
20	+0.17	+0.23	+0.41	+0.64	+0.75	+0.21	+0.28	+0.48	+0.70	+0.79	+0.27	+0.36	+0.58	+0.79	+0.85

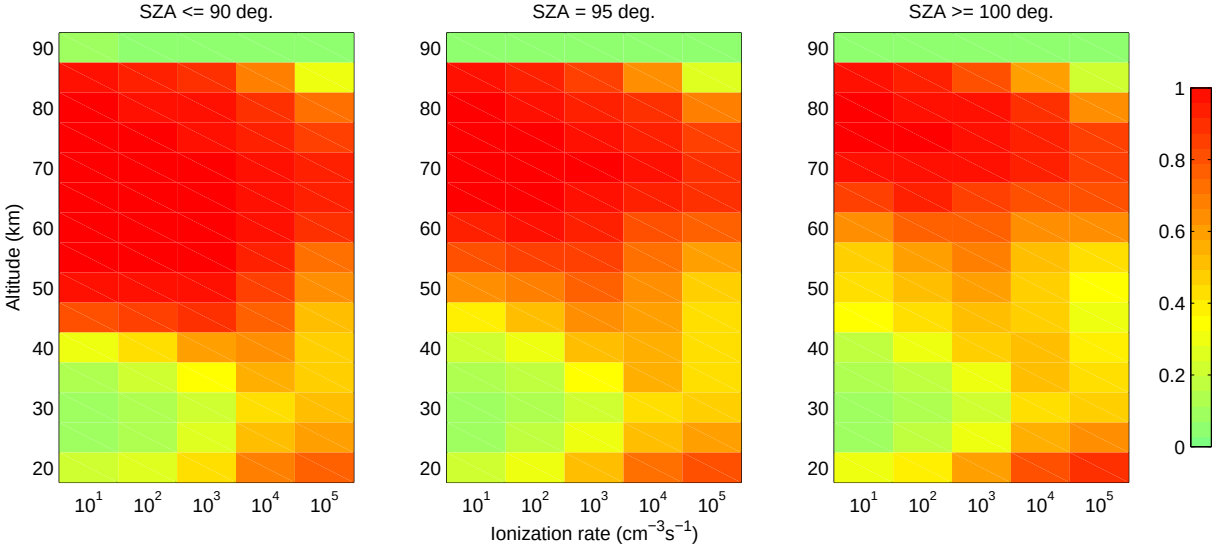

Fig. A3. P_H/Q for January SH.

Table A4. P_{HNO_3}/Q for January SH.

Q	10^1	10^2	10^3	10^4	10^5	10^1	10^2	10^3	10^4	10^5	10^1	10^2	10^3	10^4	10^5
km		SZA	$\leq$	90°			SZA	=	95°			SZA	$\geq$	100°	
90	−0.00	−0.00	−0.00	−0.00	−0.00	−0.00	−0.00	−0.00	−0.00	−0.00	−0.00	−0.00	−0.00	−0.00	−0.00
85	+0.00	+0.00	+0.00	+0.00	+0.00	+0.00	+0.00	+0.00	+0.00	+0.00	+0.00	+0.00	+0.00	+0.00	+0.00
80	+0.00	+0.00	+0.00	+0.00	−0.01	+0.00	+0.00	+0.00	+0.00	−0.01	+0.00	+0.01	+0.01	−0.00	−0.01
75	−0.00	−0.00	−0.00	−0.00	−0.01	−0.00	−0.00	−0.00	−0.00	−0.01	+0.00	+0.01	+0.01	+0.01	−0.00
70	−0.00	−0.00	−0.00	−0.00	−0.01	+0.00	+0.00	+0.00	−0.00	−0.01	+0.03	+0.02	+0.04	+0.04	+0.02
65	−0.00	−0.00	−0.00	−0.00	−0.00	+0.02	+0.01	+0.01	+0.02	+0.01	+0.16	+0.10	+0.12	+0.12	+0.05
60	−0.01	−0.00	−0.01	+0.00	+0.03	+0.08	+0.04	+0.04	+0.08	+0.07	+0.38	+0.23	+0.20	+0.23	+0.15
55	−0.02	−0.01	−0.01	+0.02	+0.10	+0.20	+0.14	+0.10	+0.15	+0.17	+0.54	+0.38	+0.27	+0.32	+0.29
50	−0.06	−0.02	−0.00	+0.05	+0.19	+0.35	+0.28	+0.19	+0.21	+0.27	+0.57	+0.49	+0.34	+0.35	+0.42
45	−0.12	−0.04	+0.03	+0.12	+0.28	+0.50	+0.40	+0.29	+0.27	+0.35	+0.65	+0.52	+0.40	+0.38	+0.48
40	+0.27	+0.23	+0.19	+0.22	+0.34	+0.55	+0.49	+0.37	+0.32	+0.40	+0.66	+0.59	+0.46	+0.40	+0.50
35	+0.42	+0.39	+0.34	+0.29	+0.35	+0.52	+0.49	+0.43	+0.37	+0.41	+0.67	+0.64	+0.56	+0.49	+0.54
30	+0.41	+0.38	+0.34	+0.30	+0.32	+0.53	+0.50	+0.44	+0.37	+0.39	+0.71	+0.68	+0.60	+0.50	+0.49
25	+0.36	+0.34	+0.28	+0.23	+0.24	+0.49	+0.47	+0.38	+0.29	+0.29	+0.70	+0.65	+0.54	+0.37	+0.35
20	+0.34	+0.31	+0.22	+0.16	+0.15	+0.43	+0.38	+0.27	+0.17	+0.16	+0.59	+0.50	+0.33	+0.17	+0.16

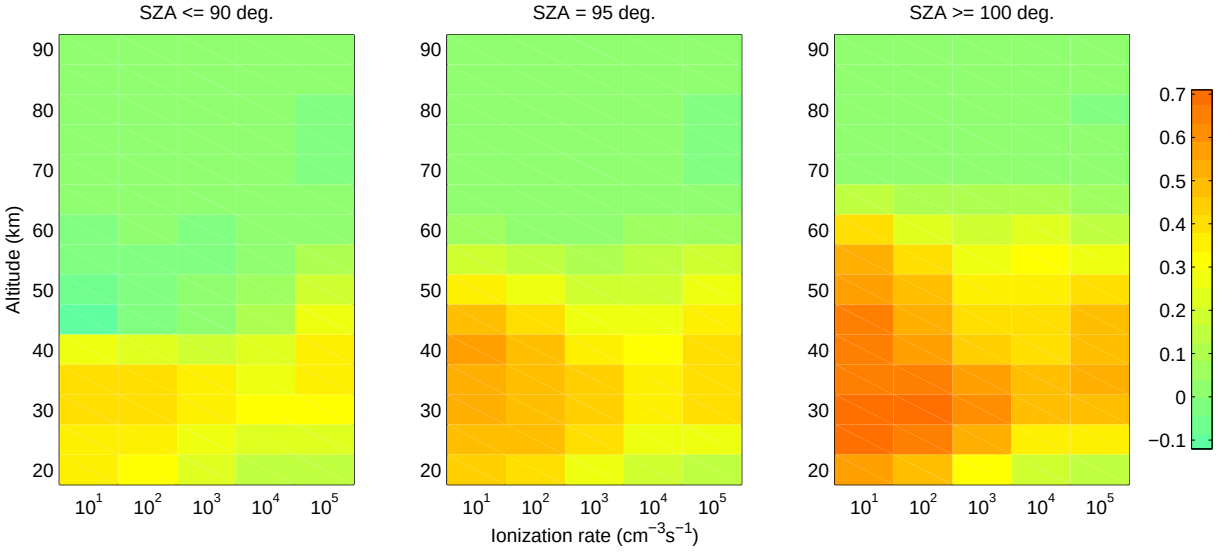

Fig. A4. P_{HNO_3}/Q for January SH.

Table A5. P_{NO}/Q for January SH.

Q	10^1	10^2	10^3	10^4	10^5	10^1	10^2	10^3	10^4	10^5	10^1	10^2	10^3	10^4	10^5
km		SZA	$\leq$	90°			SZA	$=$	95°			SZA	$\geq$	100°	
90	+0.00	+0.00	+0.00	+0.00	+0.00	+0.00	+0.00	+0.00	+0.00	+0.00	+0.00	+0.00	+0.00	+0.00	+0.00
85	+0.00	+0.00	+0.00	+0.00	+0.00	+0.00	+0.00	+0.00	+0.00	+0.00	+0.00	+0.00	+0.00	+0.00	+0.00
80	−0.00	−0.00	−0.00	−0.00	−0.00	−0.00	−0.00	−0.00	−0.00	−0.00	−0.01	−0.01	−0.01	−0.01	−0.00
75	+0.00	+0.00	+0.00	−0.01	−0.02	+0.00	+0.00	+0.00	−0.02	−0.02	−0.01	−0.01	−0.02	−0.02	−0.02
70	−0.01	−0.01	−0.01	−0.04	−0.09	−0.01	−0.01	−0.02	−0.06	−0.09	−0.04	−0.02	−0.04	−0.05	−0.05
65	−0.03	−0.02	−0.04	−0.13	−0.25	−0.06	−0.04	−0.05	−0.13	−0.21	−0.07	−0.04	−0.06	−0.09	−0.09
60	−0.13	−0.08	−0.08	−0.21	−0.42	−0.20	−0.10	−0.09	−0.16	−0.30	−0.06	−0.04	−0.03	−0.07	−0.12
55	−0.37	−0.20	−0.14	−0.25	−0.46	−0.35	−0.18	−0.12	−0.17	−0.31	−0.01	−0.01	−0.01	−0.02	−0.11
50	−0.72	−0.38	−0.21	−0.24	−0.38	−0.36	−0.23	−0.14	−0.15	−0.25	−0.00	−0.00	−0.00	−0.00	−0.02
45	−0.68	−0.41	−0.22	−0.17	−0.26	−0.23	−0.18	−0.12	−0.11	−0.18	+0.00	−0.00	−0.00	−0.00	−0.00
40	−0.19	−0.17	−0.12	−0.10	−0.13	−0.10	−0.09	−0.08	−0.07	−0.08	−0.00	−0.00	−0.00	−0.00	−0.00
35	−0.06	−0.06	−0.06	−0.05	−0.06	−0.04	−0.04	−0.04	−0.04	−0.04	−0.00	−0.00	−0.00	−0.00	−0.00
30	−0.03	−0.03	−0.03	−0.03	−0.03	−0.02	−0.02	−0.02	−0.02	−0.02	−0.00	−0.00	−0.00	−0.00	−0.00
25	−0.02	−0.02	−0.02	−0.01	−0.02	−0.01	−0.01	−0.01	−0.01	−0.01	−0.00	−0.00	−0.00	−0.00	−0.00
20	−0.01	−0.01	−0.01	−0.01	−0.01	−0.01	−0.01	−0.00	−0.00	−0.00	−0.00	−0.00	−0.00	−0.00	−0.00

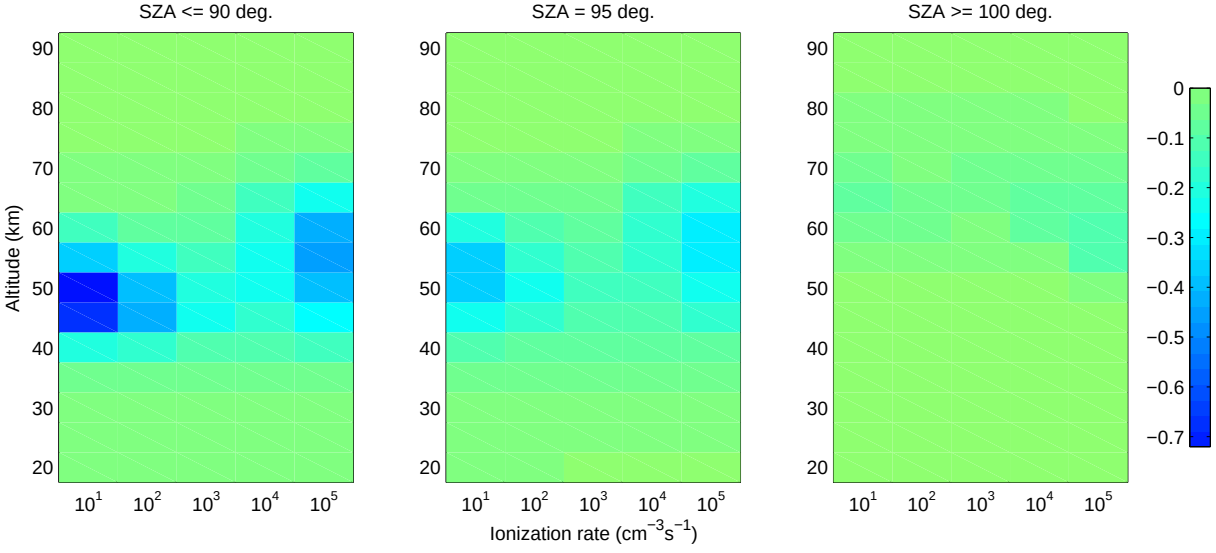

Fig. A5. P_{NO}/Q for January SH.

Table A6. P_{NO_2}/Q for January SH.

Q	10^1	10^2	10^3	10^4	10^5	10^1	10^2	10^3	10^4	10^5	10^1	10^2	10^3	10^4	10^5
km		SZA	$\leq$	90°			SZA	=	95°			SZA	$\geq$	100°	
90	+0.00	+0.00	+0.00	+0.00	+0.00	+0.00	+0.00	+0.00	+0.00	+0.00	+0.00	+0.00	+0.00	+0.00	+0.00
85	+0.00	+0.00	+0.00	+0.00	+0.00	+0.00	+0.00	+0.00	+0.00	+0.00	+0.00	+0.00	+0.00	+0.00	+0.00
80	+0.00	+0.00	+0.00	+0.00	+0.00	+0.00	+0.00	+0.00	+0.00	+0.00	+0.00	+0.00	+0.00	+0.00	−0.00
75	+0.00	+0.00	+0.00	+0.01	+0.02	+0.00	+0.00	+0.00	+0.01	+0.02	−0.00	−0.00	−0.00	−0.00	+0.00
70	+0.00	+0.00	+0.00	+0.03	+0.08	+0.00	+0.00	+0.01	+0.05	+0.08	−0.02	−0.02	−0.02	−0.01	+0.01
65	+0.01	+0.01	+0.02	+0.08	+0.20	+0.01	+0.01	+0.01	+0.07	+0.17	−0.11	−0.07	−0.07	−0.05	+0.01
60	+0.04	+0.02	+0.03	+0.09	+0.28	+0.01	+0.01	+0.01	+0.04	+0.19	−0.35	−0.20	−0.18	−0.17	−0.05
55	+0.03	+0.02	+0.02	+0.04	+0.20	−0.03	−0.02	−0.01	−0.00	+0.12	−0.60	−0.39	−0.27	−0.31	−0.19
50	−0.14	−0.07	−0.04	−0.03	+0.03	−0.18	−0.12	−0.07	−0.07	−0.03	−0.71	−0.54	−0.36	−0.36	−0.41
45	−0.65	−0.40	−0.20	−0.16	−0.13	−0.35	−0.30	−0.21	−0.18	−0.18	−0.74	−0.62	−0.44	−0.40	−0.49
40	−0.53	−0.46	−0.35	−0.27	−0.28	−0.42	−0.41	−0.32	−0.27	−0.33	−0.62	−0.57	−0.48	−0.40	−0.49
35	−0.36	−0.36	−0.32	−0.31	−0.33	−0.41	−0.40	−0.36	−0.34	−0.39	−0.52	−0.51	−0.45	−0.42	−0.48
30	−0.34	−0.32	−0.31	−0.29	−0.32	−0.43	−0.43	−0.38	−0.35	−0.38	−0.55	−0.55	−0.50	−0.44	−0.45
25	−0.32	−0.30	−0.25	−0.22	−0.23	−0.42	−0.40	−0.34	−0.28	−0.29	−0.58	−0.54	−0.45	−0.34	−0.33
20	−0.29	−0.26	−0.20	−0.14	−0.14	−0.36	−0.32	−0.24	−0.16	−0.16	−0.45	−0.39	−0.26	−0.15	−0.14

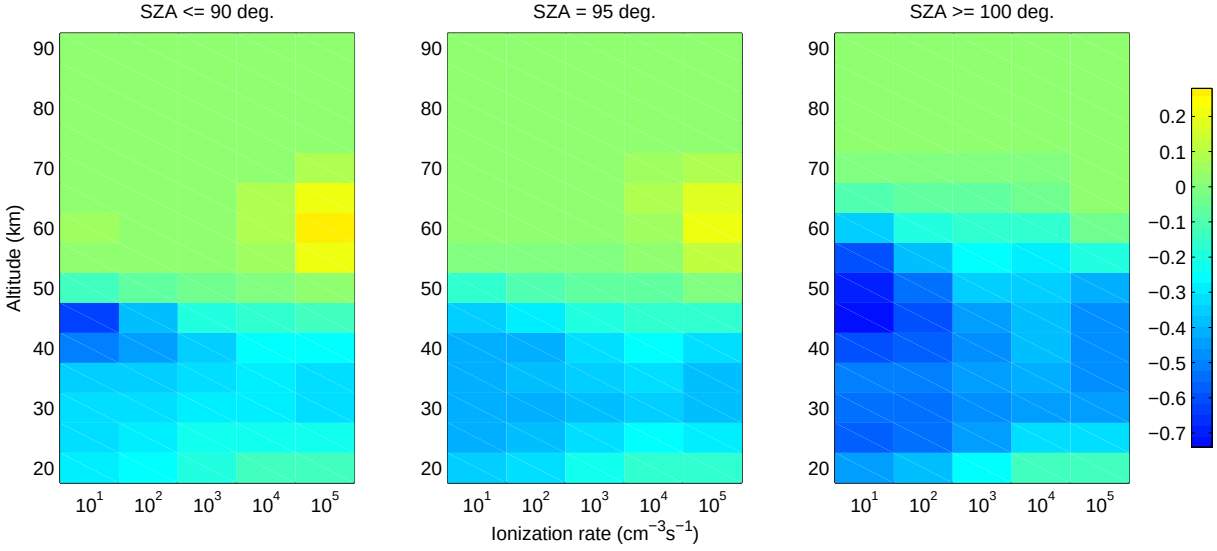

Fig. A6. P_{NO_2}/Q for January SH.

Table A7. P_{NO_3}/Q for January SH.

Q	10^1	10^2	10^3	10^4	10^5	10^1	10^2	10^3	10^4	10^5	10^1	10^2	10^3	10^4	10^5
km		SZA	$\leq$	90°			SZA	$=$	95°			SZA	$\geq$	100°	
90	+0.00	+0.00	+0.00	+0.00	+0.00	+0.00	+0.00	+0.00	+0.00	+0.00	+0.00	+0.00	+0.00	+0.00	+0.00
85	+0.00	+0.00	+0.00	+0.00	+0.00	+0.00	+0.00	+0.00	+0.00	+0.00	+0.00	+0.00	+0.00	+0.00	+0.00
80	+0.00	+0.00	+0.00	+0.00	+0.01	+0.00	+0.00	+0.00	+0.00	+0.01	+0.01	+0.00	+0.00	+0.01	+0.01
75	+0.00	+0.00	+0.00	+0.00	+0.01	+0.00	+0.00	+0.00	+0.01	+0.01	+0.01	+0.00	+0.01	+0.01	+0.02
70	+0.01	+0.01	+0.01	+0.01	+0.02	+0.01	+0.01	+0.01	+0.01	+0.02	+0.03	+0.02	+0.02	+0.02	+0.02
65	+0.02	+0.01	+0.02	+0.05	+0.05	+0.03	+0.02	+0.03	+0.04	+0.03	+0.02	+0.01	+0.01	+0.02	+0.03
60	+0.10	+0.06	+0.06	+0.12	+0.11	+0.11	+0.05	+0.04	+0.04	+0.04	+0.03	+0.01	+0.01	+0.01	+0.02
55	+0.36	+0.19	+0.13	+0.19	+0.16	+0.18	+0.06	+0.03	+0.02	+0.02	+0.07	+0.02	+0.01	+0.01	+0.01
50	+0.92	+0.47	+0.25	+0.22	+0.16	+0.19	+0.07	+0.02	+0.01	+0.01	+0.14	+0.05	+0.02	+0.01	+0.01
45	+1.45	+0.85	+0.39	+0.21	+0.11	+0.08	+0.08	+0.04	+0.02	+0.01	+0.09	+0.10	+0.04	+0.02	+0.01
40	+0.45	+0.40	+0.28	+0.15	+0.07	+0.01	+0.03	+0.05	+0.04	+0.03	+0.02	+0.04	+0.06	+0.04	+0.03
35	+0.04	+0.05	+0.06	+0.09	+0.06	+0.01	+0.01	+0.03	+0.07	+0.06	+0.01	+0.01	+0.03	+0.07	+0.06
30	+0.00	+0.01	+0.02	+0.04	+0.05	+0.00	+0.01	+0.02	+0.04	+0.05	+0.00	+0.01	+0.02	+0.04	+0.06
25	+0.00	+0.00	+0.01	+0.02	+0.03	+0.00	+0.00	+0.01	+0.02	+0.03	+0.00	+0.01	+0.01	+0.03	+0.04
20	+0.00	+0.00	+0.01	+0.01	+0.02	+0.00	+0.01	+0.01	+0.01	+0.02	+0.00	+0.01	+0.01	+0.02	+0.02

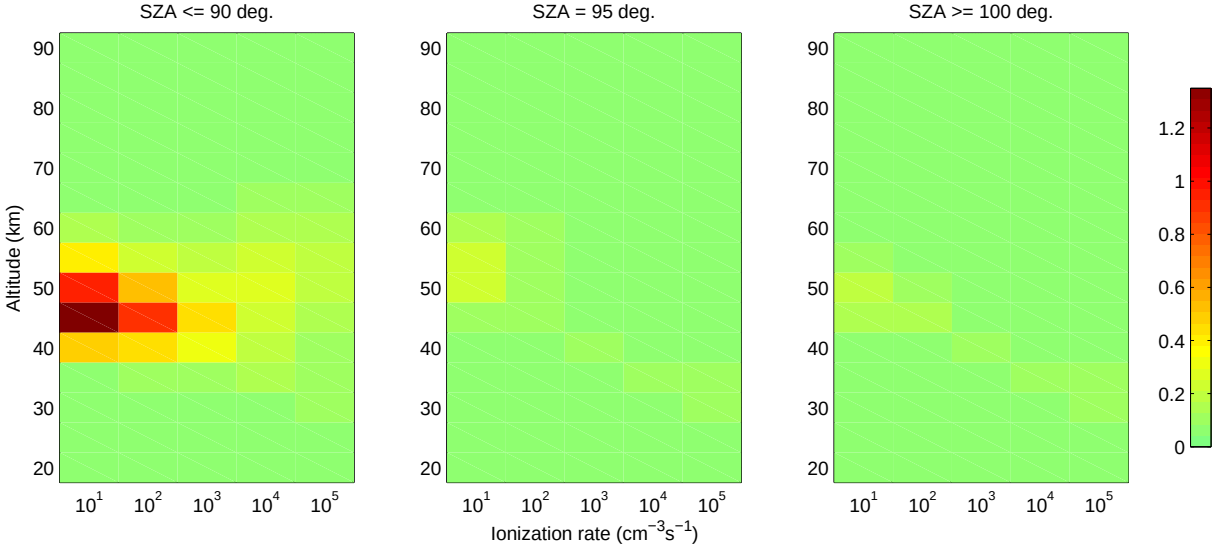

Fig. A7. P_{NO_3}/Q for January SH.

Table A8. $P_{N_2O_5}/Q$ for January SH.

Q	10^1	10^2	10^3	10^4	10^5	10^1	10^2	10^3	10^4	10^5	10^1	10^2	10^3	10^4	10^5
km		SZA	$\leq$	90°			SZA	$=$	95°			SZA	$\geq$	100°	
90	+0.00	−0.00	−0.00	−0.00	−0.00	+0.00	−0.00	−0.00	−0.00	−0.00	−0.00	−0.00	−0.00	−0.00	−0.00
85	−0.00	−0.00	−0.00	−0.00	−0.00	−0.00	−0.00	−0.00	−0.00	−0.00	−0.00	−0.00	−0.00	−0.00	−0.00
80	−0.00	−0.00	−0.00	−0.00	−0.00	−0.00	−0.00	−0.00	−0.00	−0.00	−0.00	−0.00	−0.00	−0.00	−0.00
75	−0.00	−0.00	−0.00	−0.00	−0.00	−0.00	−0.00	−0.00	−0.00	−0.00	−0.00	−0.00	−0.00	−0.00	−0.00
70	−0.00	−0.00	−0.00	−0.00	−0.00	−0.00	−0.00	−0.00	−0.00	−0.00	−0.00	−0.00	−0.00	−0.00	−0.00
65	−0.00	−0.00	−0.00	−0.00	−0.00	−0.00	−0.00	−0.00	−0.00	−0.00	−0.00	−0.00	−0.00	−0.00	−0.00
60	−0.00	−0.00	−0.00	−0.00	−0.00	−0.00	−0.00	−0.00	−0.00	−0.00	−0.00	−0.00	−0.00	−0.00	−0.00
55	−0.00	−0.00	−0.00	−0.00	−0.00	−0.00	−0.00	−0.00	−0.00	−0.00	−0.00	−0.00	−0.00	−0.00	−0.00
50	−0.00	−0.00	−0.00	−0.00	−0.00	−0.00	−0.00	−0.00	−0.00	−0.00	−0.00	−0.00	−0.00	−0.00	−0.00
45	−0.00	−0.00	−0.00	−0.00	−0.00	−0.00	−0.00	−0.00	−0.00	−0.00	−0.00	−0.00	−0.00	−0.00	−0.00
40	−0.00	−0.00	−0.00	−0.00	−0.00	−0.02	−0.01	−0.01	−0.01	−0.01	−0.03	−0.03	−0.02	−0.02	−0.02
35	−0.02	−0.01	−0.01	−0.01	−0.01	−0.04	−0.03	−0.03	−0.03	−0.02	−0.08	−0.07	−0.07	−0.07	−0.06
30	−0.02	−0.02	−0.01	−0.01	−0.01	−0.04	−0.03	−0.03	−0.02	−0.02	−0.08	−0.07	−0.06	−0.05	−0.05
25	−0.01	−0.01	−0.01	−0.01	−0.01	−0.03	−0.03	−0.02	−0.01	−0.01	−0.06	−0.06	−0.05	−0.03	−0.03
20	−0.02	−0.02	−0.01	−0.01	−0.01	−0.03	−0.03	−0.02	−0.01	−0.01	−0.07	−0.06	−0.04	−0.02	−0.02

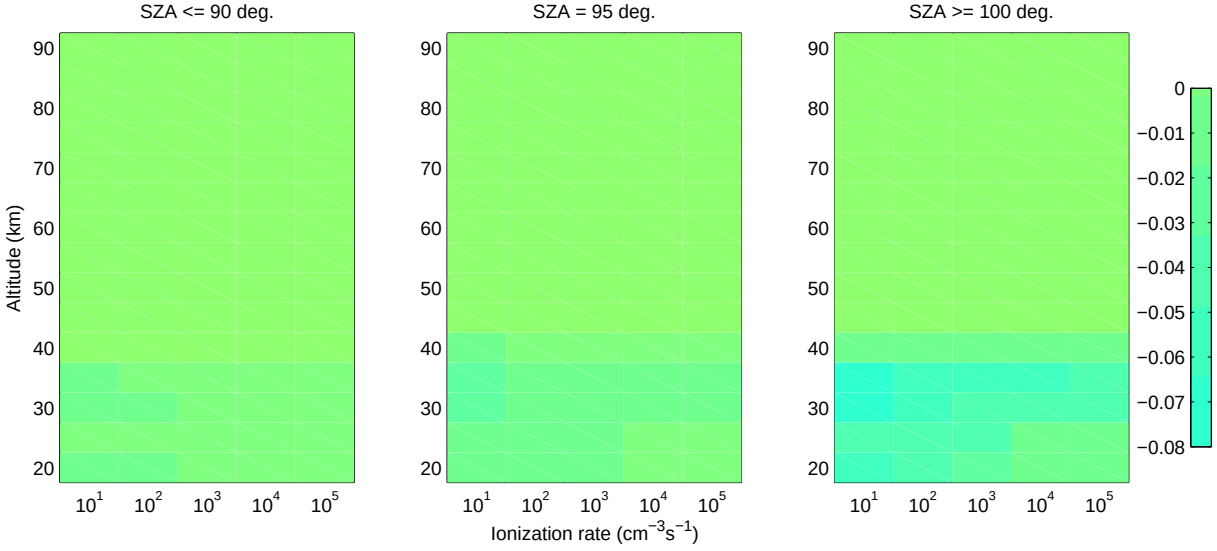

Fig. A8. $P_{N_2O_5}/Q$ for January SH.

Table A9. P_{OH}/Q for January NH.

Q	10^1	10^2	10^3	10^4	10^5	10^1	10^2	10^3	10^4	10^5	10^1	10^2	10^3	10^4	10^5
km		SZA	$\leq$	90°			SZA	$=$	95°			SZA	$\geq$	100°	
90	+0.00	+0.00	+0.00	+0.00	+0.00	+0.00	+0.00	+0.00	+0.00	+0.00	+0.00	+0.00	+0.00	+0.00	+0.00
85	+0.20	+0.14	+0.06	+0.02	+0.00	+0.10	+0.07	+0.04	+0.01	+0.00	+0.13	+0.10	+0.05	+0.01	+0.00
80	+0.87	+0.85	+0.74	+0.47	+0.15	+0.87	+0.84	+0.73	+0.44	+0.12	+0.87	+0.86	+0.76	+0.48	+0.11
75	+0.89	+0.88	+0.87	+0.78	+0.51	+0.90	+0.89	+0.86	+0.75	+0.45	+0.90	+0.88	+0.89	+0.80	+0.48
70	+0.90	+0.89	+0.89	+0.87	+0.79	+0.89	+0.90	+0.89	+0.87	+0.75	+0.91	+0.91	+0.90	+0.89	+0.78
65	+0.90	+0.90	+0.91	+0.90	+0.88	+0.92	+0.92	+0.92	+0.92	+0.87	+0.92	+0.93	+0.94	+0.94	+0.90
60	+0.91	+0.92	+0.91	+0.92	+0.91	+0.94	+0.95	+0.97	+0.99	+0.96	+0.93	+0.95	+0.98	+1.00	+0.99
55	+0.93	+0.95	+0.95	+0.97	+0.95	+0.95	+0.99	+1.02	+1.07	+1.05	+0.94	+0.98	+1.02	+1.07	+1.09
50	+0.96	+0.97	+1.00	+1.02	+1.02	+0.95	+1.00	+1.05	+1.10	+1.16	+0.92	+0.98	+1.04	+1.10	+1.17
45	+1.07	+1.04	+1.03	+1.03	+1.05	+1.02	+1.02	+1.03	+1.07	+1.13	+0.94	+0.98	+1.04	+1.09	+1.13
40	+1.29	+1.20	+1.10	+1.03	+1.03	+1.18	+1.14	+1.10	+1.07	+1.05	+1.08	+1.07	+1.06	+1.04	+1.05
35	+1.31	+1.23	+1.16	+1.05	+1.02	+1.30	+1.24	+1.14	+1.05	+1.01	+1.17	+1.15	+1.09	+1.01	+0.99
30	+1.15	+1.12	+1.04	+0.97	+0.96	+1.03	+0.99	+0.96	+0.92	+0.93	+0.98	+0.96	+0.92	+0.93	+0.92
25	+1.08	+1.04	+0.98	+0.93	+0.92	+0.96	+0.94	+0.93	+0.91	+0.92	+0.95	+0.95	+0.92	+0.92	+0.90
20	+0.98	+0.95	+0.93	+0.92	+0.90	+0.93	+0.92	+0.92	+0.91	+0.92	+0.92	+0.94	+0.91	+0.90	+0.91

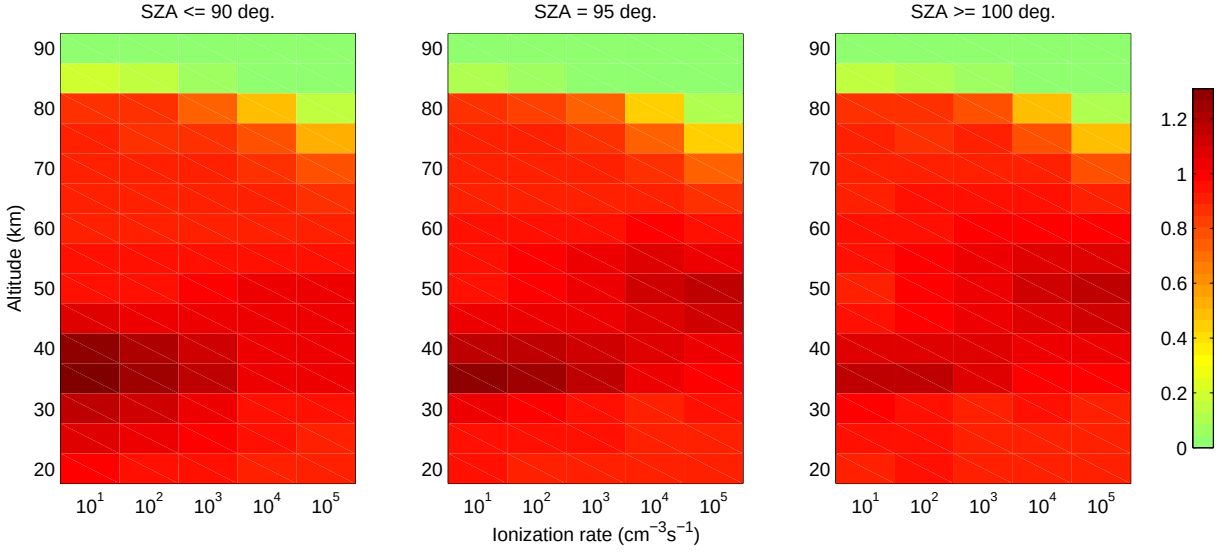

Fig. A9. P_{OH}/Q for January NH.

Table A10. P_{HNO_2}/Q for January NH.

Q	10^1	10^2	10^3	10^4	10^5	10^1	10^2	10^3	10^4	10^5	10^1	10^2	10^3	10^4	10^5
km		SZA	$\leq$	90°			SZA	$=$	95°			SZA	$\geq$	100°	
90	−0.00	−0.00	−0.00	−0.00	−0.00	−0.00	−0.00	−0.00	−0.00	−0.00	−0.00	−0.00	−0.00	−0.00	−0.00
85	−0.00	−0.00	−0.00	−0.00	−0.00	−0.00	−0.00	−0.00	−0.00	−0.00	−0.00	−0.00	−0.00	−0.00	−0.00
80	−0.00	−0.00	−0.00	−0.00	−0.00	+0.00	−0.00	−0.00	−0.00	−0.00	+0.01	+0.00	−0.00	−0.00	−0.00
75	+0.05	+0.02	+0.00	+0.00	+0.00	+0.04	+0.01	+0.00	+0.00	+0.00	+0.06	+0.03	+0.00	+0.00	+0.00
70	+0.09	+0.07	+0.03	+0.01	+0.00	+0.09	+0.06	+0.03	+0.01	+0.00	+0.09	+0.08	+0.05	+0.01	+0.00
65	+0.10	+0.09	+0.08	+0.06	+0.03	+0.10	+0.09	+0.08	+0.05	+0.02	+0.10	+0.09	+0.08	+0.06	+0.02
60	+0.10	+0.10	+0.10	+0.09	+0.07	+0.10	+0.10	+0.09	+0.08	+0.05	+0.10	+0.10	+0.09	+0.08	+0.06
55	+0.10	+0.10	+0.10	+0.10	+0.09	+0.10	+0.10	+0.10	+0.09	+0.08	+0.10	+0.10	+0.10	+0.09	+0.08
50	+0.10	+0.10	+0.10	+0.10	+0.10	+0.10	+0.10	+0.10	+0.10	+0.09	+0.10	+0.10	+0.10	+0.10	+0.09
45	+0.10	+0.10	+0.10	+0.10	+0.10	+0.10	+0.10	+0.10	+0.10	+0.10	+0.10	+0.10	+0.10	+0.10	+0.10
40	+0.10	+0.10	+0.10	+0.10	+0.10	+0.10	+0.10	+0.10	+0.10	+0.10	+0.10	+0.10	+0.10	+0.10	+0.10
35	+0.10	+0.10	+0.10	+0.10	+0.10	+0.10	+0.10	+0.10	+0.10	+0.10	+0.10	+0.10	+0.10	+0.10	+0.10
30	+0.10	+0.10	+0.10	+0.10	+0.10	+0.10	+0.10	+0.10	+0.10	+0.10	+0.10	+0.10	+0.10	+0.10	+0.10
25	+0.10	+0.10	+0.10	+0.10	+0.10	+0.10	+0.10	+0.10	+0.10	+0.10	+0.10	+0.10	+0.10	+0.10	+0.10
20	+0.10	+0.10	+0.10	+0.10	+0.10	+0.10	+0.10	+0.10	+0.10	+0.10	+0.10	+0.10	+0.10	+0.10	+0.10

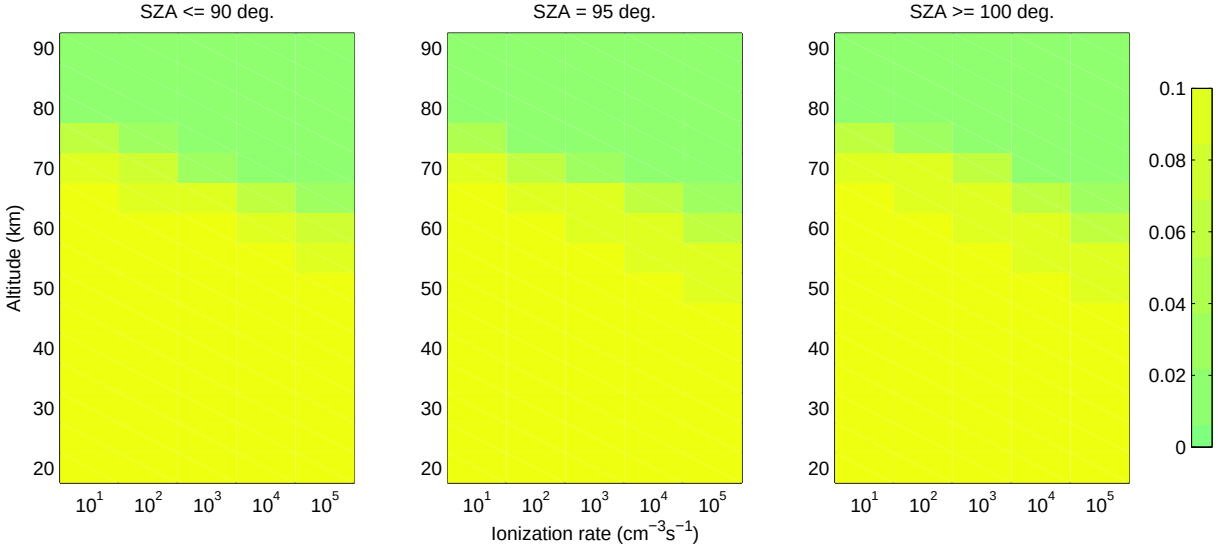

Fig. A10. P_{HNO_2}/Q for January NH.

Table A11. P_H/Q for January NH.

Q	10^1	10^2	10^3	10^4	10^5	10^1	10^2	10^3	10^4	10^5	10^1	10^2	10^3	10^4	10^5
km		SZA	$\leq$	90°			SZA	$=$	95°			SZA	$\geq$	100°	
90	+0.00	+0.00	+0.00	+0.00	+0.00	+0.00	+0.00	+0.00	+0.00	+0.00	+0.00	+0.00	+0.00	+0.00	+0.00
85	+0.20	+0.14	+0.06	+0.02	+0.00	+0.10	+0.07	+0.04	+0.01	+0.00	+0.13	+0.10	+0.05	+0.01	+0.00
80	+0.87	+0.85	+0.74	+0.47	+0.15	+0.87	+0.84	+0.73	+0.44	+0.12	+0.87	+0.84	+0.76	+0.48	+0.11
75	+0.94	+0.90	+0.87	+0.78	+0.51	+0.93	+0.90	+0.86	+0.75	+0.45	+0.92	+0.90	+0.87	+0.78	+0.47
70	+0.99	+0.96	+0.92	+0.88	+0.78	+0.98	+0.96	+0.91	+0.87	+0.74	+0.93	+0.94	+0.90	+0.85	+0.76
65	+1.00	+0.99	+0.98	+0.95	+0.88	+0.98	+0.97	+0.95	+0.90	+0.84	+0.84	+0.89	+0.88	+0.84	+0.81
60	+1.00	+1.00	+0.99	+0.97	+0.93	+0.92	+0.94	+0.92	+0.87	+0.85	+0.64	+0.77	+0.78	+0.75	+0.76
55	+1.00	+0.99	+0.99	+0.94	+0.91	+0.80	+0.84	+0.84	+0.78	+0.77	+0.46	+0.59	+0.67	+0.61	+0.63
50	+0.99	+0.98	+0.96	+0.89	+0.80	+0.66	+0.70	+0.73	+0.68	+0.62	+0.39	+0.45	+0.55	+0.51	+0.44
45	+0.93	+0.92	+0.90	+0.83	+0.72	+0.50	+0.58	+0.65	+0.64	+0.55	+0.34	+0.41	+0.50	+0.48	+0.37
40	+0.45	+0.58	+0.72	+0.76	+0.70	+0.27	+0.39	+0.56	+0.65	+0.60	+0.19	+0.30	+0.46	+0.54	+0.46
35	+0.14	+0.24	+0.44	+0.65	+0.70	+0.16	+0.27	+0.47	+0.63	+0.65	+0.12	+0.21	+0.39	+0.54	+0.54
30	+0.20	+0.35	+0.61	+0.80	+0.84	+0.39	+0.56	+0.75	+0.86	+0.87	+0.32	+0.47	+0.68	+0.80	+0.82
25	+0.46	+0.61	+0.80	+0.91	+0.93	+0.75	+0.82	+0.91	+0.95	+0.96	+0.68	+0.76	+0.88	+0.93	+0.94
20	+0.74	+0.82	+0.91	+0.96	+0.97	+0.90	+0.93	+0.96	+0.98	+0.98	+0.87	+0.90	+0.95	+0.98	+0.98

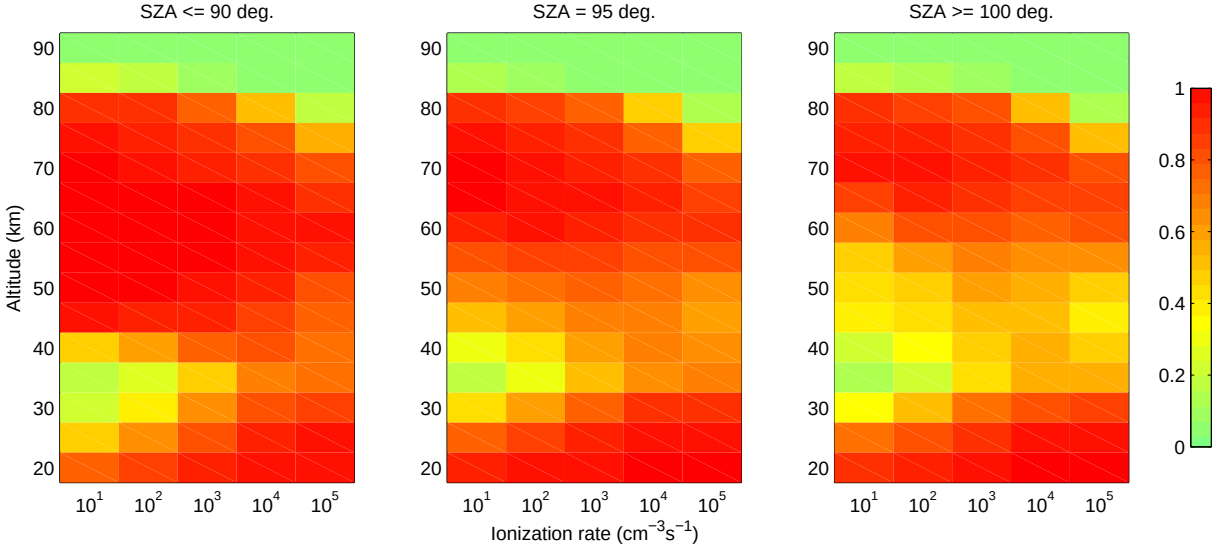

Fig. A11. P_H/Q for January NH.

Table A12. P_{HNO_3}/Q for January NH.

Q	10^1	10^2	10^3	10^4	10^5	10^1	10^2	10^3	10^4	10^5	10^1	10^2	10^3	10^4	10^5
km		SZA	$\leq$	90°			SZA	=	95°			SZA	$\geq$	100°	
90	−0.00	−0.00	−0.00	−0.00	−0.00	−0.00	−0.00	−0.00	−0.00	−0.00	−0.00	−0.00	−0.00	−0.00	−0.00
85	−0.00	−0.00	−0.00	−0.00	−0.00	−0.00	−0.00	−0.00	−0.00	−0.00	−0.00	−0.00	−0.00	−0.00	−0.00
80	+0.00	+0.00	+0.00	+0.00	+0.00	+0.00	−0.00	+0.00	+0.00	+0.00	+0.01	+0.00	−0.00	+0.00	+0.00
75	+0.00	+0.00	+0.00	+0.00	+0.00	−0.01	−0.00	−0.00	−0.00	+0.00	+0.02	+0.01	+0.00	−0.00	−0.01
70	−0.00	−0.00	+0.00	−0.00	−0.01	−0.00	−0.00	−0.01	−0.01	−0.01	+0.05	+0.03	+0.03	+0.01	−0.00
65	−0.00	−0.00	−0.01	−0.01	−0.01	+0.00	−0.00	−0.01	−0.01	−0.01	+0.14	+0.07	+0.06	+0.04	+0.01
60	−0.01	−0.02	−0.02	−0.02	−0.01	+0.04	+0.01	+0.00	+0.00	−0.00	+0.33	+0.18	+0.13	+0.11	+0.05
55	−0.03	−0.04	−0.04	−0.03	+0.01	+0.15	+0.07	+0.04	+0.04	+0.04	+0.50	+0.33	+0.21	+0.21	+0.14
50	−0.05	−0.05	−0.06	−0.01	+0.06	+0.29	+0.20	+0.12	+0.12	+0.11	+0.59	+0.47	+0.31	+0.29	+0.28
45	−0.10	−0.06	−0.03	+0.04	+0.13	+0.46	+0.34	+0.22	+0.19	+0.22	+0.70	+0.55	+0.38	+0.33	+0.40
40	+0.32	+0.24	+0.14	+0.13	+0.17	+0.99	+0.77	+0.44	+0.26	+0.27	+1.19	+0.97	+0.60	+0.40	+0.41
35	+0.81	+0.73	+0.50	+0.28	+0.20	+1.14	+0.97	+0.65	+0.38	+0.30	+1.31	+1.14	+0.82	+0.53	+0.43
30	+1.07	+0.85	+0.49	+0.23	+0.14	+1.14	+0.81	+0.43	+0.24	+0.16	+1.32	+0.99	+0.58	+0.33	+0.24
25	+0.74	+0.53	+0.26	+0.12	+0.09	+0.43	+0.30	+0.14	+0.08	+0.06	+0.57	+0.39	+0.20	+0.11	+0.10
20	+0.40	+0.29	+0.14	+0.06	+0.05	+0.17	+0.13	+0.06	+0.03	+0.02	+0.23	+0.16	+0.08	+0.04	+0.03

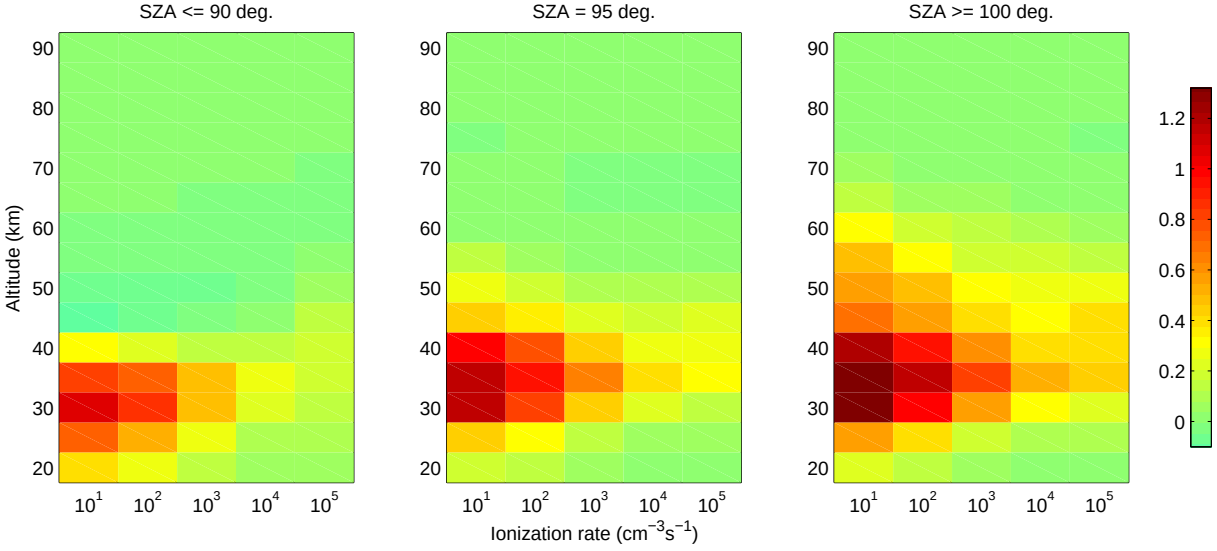

Fig. A12. P_{HNO_3}/Q for January NH.

Table A13. P_{NO}/Q for January NH.

Q	10^1	10^2	10^3	10^4	10^5	10^1	10^2	10^3	10^4	10^5	10^1	10^2	10^3	10^4	10^5
km		SZA	$\leq$	90°			SZA	$=$	95°			SZA	$\geq$	100°	
90	+0.00	+0.00	+0.00	+0.00	+0.00	+0.00	+0.00	+0.00	+0.00	+0.00	+0.00	+0.00	+0.00	+0.00	+0.00
85	+0.00	+0.00	+0.00	+0.00	+0.00	+0.00	+0.00	+0.00	+0.00	+0.00	+0.00	+0.00	+0.00	+0.00	+0.00
80	+0.00	−0.00	−0.00	−0.00	−0.00	+0.00	+0.00	−0.00	−0.00	−0.00	−0.01	−0.01	+0.00	−0.00	−0.00
75	+0.00	−0.00	−0.00	−0.00	−0.00	−0.00	+0.00	+0.00	+0.00	−0.00	−0.02	−0.01	−0.01	−0.01	+0.00
70	+0.00	+0.00	−0.00	−0.01	−0.01	−0.01	−0.01	+0.00	−0.01	−0.02	−0.04	−0.02	−0.03	−0.03	−0.03
65	−0.01	−0.01	−0.01	−0.03	−0.06	−0.04	−0.02	−0.02	−0.04	−0.06	−0.07	−0.04	−0.04	−0.04	−0.05
60	−0.06	−0.03	−0.04	−0.07	−0.14	−0.13	−0.06	−0.05	−0.07	−0.12	−0.10	−0.05	−0.04	−0.06	−0.07
55	−0.23	−0.13	−0.10	−0.13	−0.22	−0.31	−0.15	−0.09	−0.09	−0.16	−0.07	−0.04	−0.03	−0.04	−0.08
50	−0.60	−0.34	−0.19	−0.19	−0.25	−0.42	−0.25	−0.13	−0.12	−0.15	−0.02	−0.01	−0.01	−0.01	−0.05
45	−0.97	−0.55	−0.26	−0.19	−0.22	−0.32	−0.24	−0.16	−0.13	−0.15	−0.00	−0.00	−0.00	−0.00	−0.01
40	−0.45	−0.35	−0.20	−0.15	−0.16	−0.17	−0.14	−0.10	−0.09	−0.10	−0.00	−0.00	−0.00	−0.00	−0.00
35	−0.13	−0.11	−0.09	−0.07	−0.07	−0.06	−0.05	−0.04	−0.03	−0.04	−0.00	−0.00	−0.00	−0.00	−0.00
30	−0.07	−0.06	−0.04	−0.02	−0.02	−0.03	−0.02	−0.01	−0.01	−0.01	−0.00	−0.00	−0.00	−0.00	−0.00
25	−0.03	−0.02	−0.01	−0.01	−0.01	−0.01	−0.00	−0.00	−0.00	−0.00	−0.00	−0.00	−0.00	−0.00	−0.00
20	−0.01	−0.01	−0.00	−0.00	−0.00	−0.00	−0.00	−0.00	−0.00	−0.00	−0.00	−0.00	−0.00	−0.00	−0.00

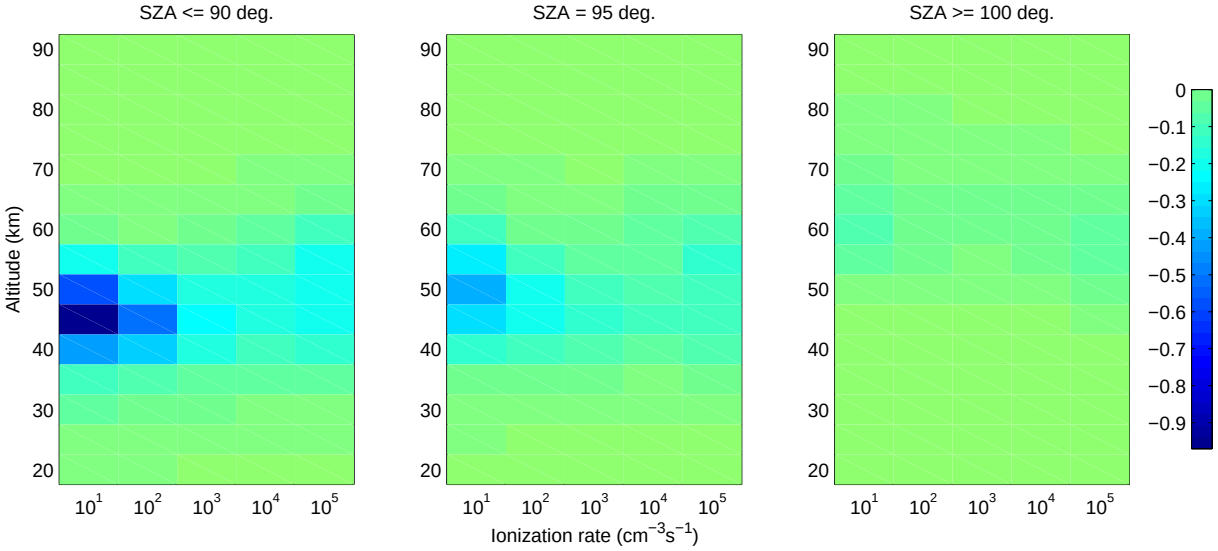

Fig. A13. P_{NO}/Q for January NH.

Table A14. P_{NO_2}/Q for January NH.

Q	10^1	10^2	10^3	10^4	10^5	10^1	10^2	10^3	10^4	10^5	10^1	10^2	10^3	10^4	10^5
km		SZA	$\leq$	90°			SZA	=	95°			SZA	$\geq$	100°	
90	+0.00	+0.00	+0.00	+0.00	+0.00	+0.00	+0.00	+0.00	+0.00	+0.00	+0.00	+0.00	+0.00	+0.00	+0.00
85	+0.00	+0.00	+0.00	+0.00	+0.00	+0.00	+0.00	+0.00	+0.00	+0.00	+0.00	+0.00	+0.00	+0.00	+0.00
80	+0.00	+0.00	+0.00	+0.00	+0.00	+0.00	+0.00	+0.00	+0.00	+0.00	+0.00	+0.00	+0.00	+0.00	+0.00
75	+0.00	+0.00	+0.00	+0.00	+0.00	+0.00	+0.00	+0.00	+0.00	+0.00	−0.00	−0.00	−0.00	+0.00	+0.01
70	+0.00	+0.00	+0.00	+0.01	+0.01	+0.00	+0.00	+0.01	+0.01	+0.02	−0.02	−0.02	−0.01	+0.00	+0.01
65	+0.00	+0.00	+0.01	+0.02	+0.05	+0.01	+0.00	+0.01	+0.03	+0.05	−0.10	−0.05	−0.04	−0.02	+0.01
60	+0.02	+0.01	+0.01	+0.05	+0.12	+0.01	+0.01	+0.01	+0.04	+0.09	−0.27	−0.15	−0.11	−0.07	−0.01
55	+0.05	+0.03	+0.02	+0.05	+0.14	+0.01	+0.01	+0.00	+0.02	+0.09	−0.50	−0.32	−0.20	−0.19	−0.09
50	+0.02	+0.01	+0.01	+0.02	+0.09	−0.07	−0.04	−0.03	−0.02	+0.02	−0.68	−0.51	−0.32	−0.29	−0.25
45	−0.21	−0.12	−0.06	−0.04	−0.02	−0.21	−0.16	−0.10	−0.08	−0.09	−0.74	−0.61	−0.41	−0.36	−0.41
40	−0.43	−0.32	−0.19	−0.12	−0.12	−0.30	−0.28	−0.21	−0.16	−0.22	−0.66	−0.58	−0.46	−0.41	−0.48
35	−0.35	−0.36	−0.27	−0.21	−0.20	−0.39	−0.36	−0.29	−0.25	−0.29	−0.62	−0.56	−0.46	−0.43	−0.49
30	−0.49	−0.39	−0.24	−0.15	−0.13	−0.46	−0.34	−0.20	−0.14	−0.14	−0.61	−0.48	−0.32	−0.21	−0.23
25	−0.34	−0.24	−0.12	−0.07	−0.06	−0.18	−0.14	−0.07	−0.05	−0.04	−0.27	−0.20	−0.11	−0.06	−0.08
20	−0.17	−0.12	−0.06	−0.03	−0.04	−0.07	−0.05	−0.02	−0.01	−0.01	−0.11	−0.06	−0.04	−0.02	−0.02

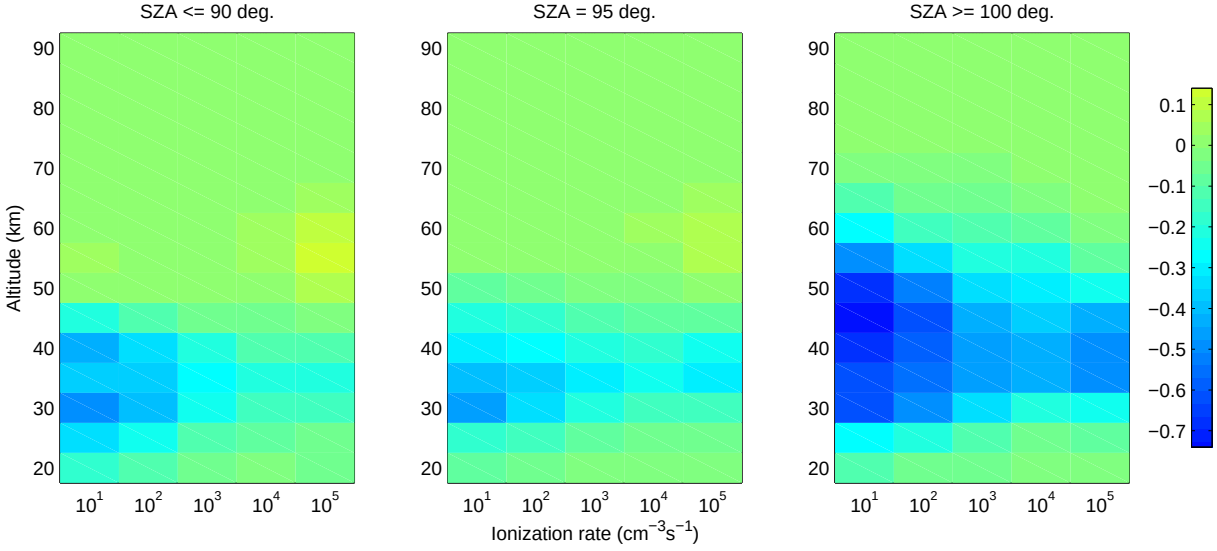

Fig. A14. P_{NO_2}/Q for January NH.

Table A15. P_{NO_3}/Q for January NH.

Q	10^1	10^2	10^3	10^4	10^5	10^1	10^2	10^3	10^4	10^5	10^1	10^2	10^3	10^4	10^5
km		SZA	$\leq$	90°			SZA	=	95°			SZA	$\geq$	100°	
90	+0.00	+0.00	+0.00	+0.00	+0.00	+0.00	+0.00	+0.00	+0.00	+0.00	+0.00	+0.00	+0.00	+0.00	+0.00
85	+0.00	+0.00	+0.00	+0.00	+0.00	+0.00	+0.00	+0.00	+0.00	+0.00	+0.00	+0.00	+0.00	+0.00	+0.00
80	+0.00	+0.00	+0.00	+0.00	+0.00	+0.00	+0.00	+0.00	+0.00	+0.00	+0.00	+0.01	+0.00	+0.00	+0.00
75	+0.00	+0.00	+0.00	+0.00	+0.00	+0.01	+0.00	+0.00	+0.00	+0.00	+0.00	+0.00	+0.01	+0.01	+0.00
70	+0.00	+0.00	+0.00	+0.00	+0.01	+0.01	+0.01	+0.00	+0.01	+0.01	+0.01	+0.01	+0.01	+0.02	+0.02
65	+0.01	+0.01	+0.01	+0.02	+0.02	+0.03	+0.02	+0.02	+0.02	+0.02	+0.03	+0.02	+0.02	+0.02	+0.03
60	+0.05	+0.04	+0.05	+0.04	+0.03	+0.08	+0.04	+0.04	+0.03	+0.03	+0.04	+0.02	+0.02	+0.02	+0.03
55	+0.21	+0.14	+0.12	+0.11	+0.07	+0.15	+0.07	+0.05	+0.03	+0.03	+0.07	+0.03	+0.02	+0.02	+0.03
50	+0.63	+0.38	+0.24	+0.18	+0.10	+0.20	+0.09	+0.04	+0.02	+0.02	+0.11	+0.05	+0.02	+0.01	+0.02
45	+1.28	+0.73	+0.35	+0.19	+0.11	+0.15	+0.10	+0.04	+0.02	+0.02	+0.12	+0.10	+0.05	+0.03	+0.02
40	+0.72	+0.55	+0.31	+0.16	+0.11	+0.02	+0.05	+0.07	+0.07	+0.07	+0.03	+0.05	+0.08	+0.09	+0.09
35	+0.03	+0.04	+0.06	+0.08	+0.09	+0.01	+0.02	+0.04	+0.06	+0.09	+0.01	+0.02	+0.04	+0.08	+0.12
30	+0.01	+0.02	+0.03	+0.04	+0.05	+0.01	+0.01	+0.02	+0.03	+0.05	+0.01	+0.01	+0.02	+0.04	+0.07
25	+0.01	+0.01	+0.01	+0.02	+0.02	+0.00	+0.00	+0.01	+0.01	+0.02	+0.00	+0.01	+0.01	+0.01	+0.02
20	+0.00	+0.00	+0.00	+0.01	+0.01	+0.00	+0.00	+0.00	+0.00	+0.01	+0.00	+0.00	+0.00	+0.00	+0.01

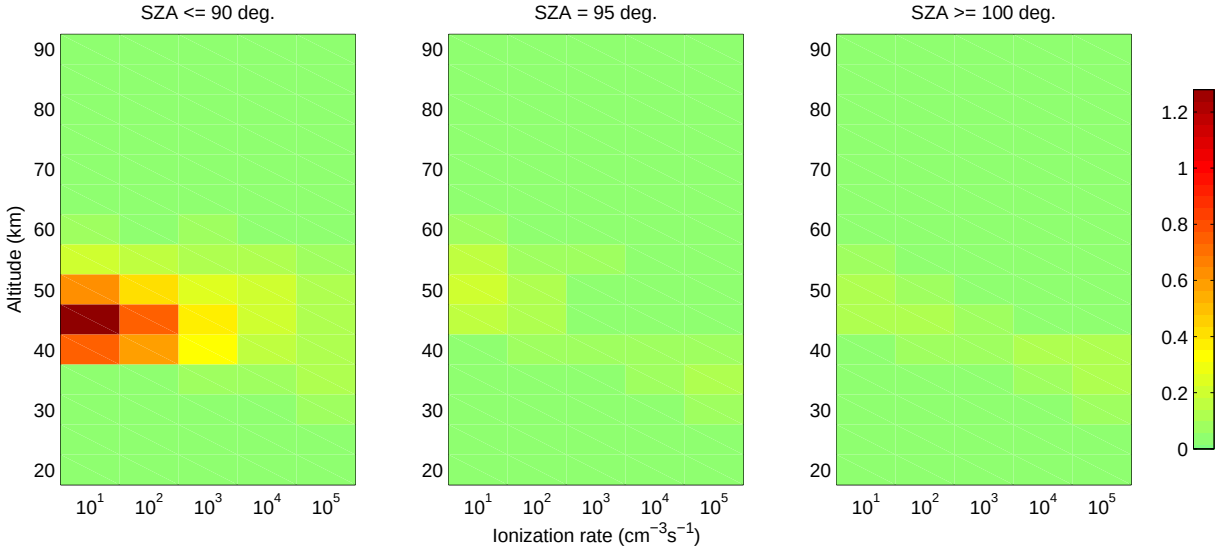

Fig. A15. P_{NO_3}/Q for January NH.

Table A16. $P_{N_2O_5}/Q$ for January NH.

Q	10^1	10^2	10^3	10^4	10^5	10^1	10^2	10^3	10^4	10^5	10^1	10^2	10^3	10^4	10^5
km		SZA	$\leq$	90°			SZA	=	95°			SZA	$\geq$	100°	
90	+0.00	+0.00	−0.00	−0.00	−0.00	+0.00	+0.00	+0.00	−0.00	−0.00	−0.00	+0.00	+0.00	+0.00	−0.00
85	−0.00	−0.00	−0.00	−0.00	−0.00	−0.00	−0.00	−0.00	−0.00	−0.00	−0.00	−0.00	−0.00	−0.00	−0.00
80	−0.00	−0.00	−0.00	−0.00	−0.00	−0.00	−0.00	−0.00	−0.00	−0.00	−0.00	−0.00	−0.00	−0.00	−0.00
75	−0.00	−0.00	−0.00	−0.00	−0.00	−0.00	−0.00	−0.00	−0.00	−0.00	−0.00	−0.00	−0.00	−0.00	−0.00
70	−0.00	−0.00	−0.00	−0.00	−0.00	−0.00	−0.00	−0.00	−0.00	−0.00	−0.00	−0.00	−0.00	−0.00	−0.00
65	−0.00	−0.00	−0.00	−0.00	−0.00	−0.00	−0.00	−0.00	−0.00	−0.00	−0.00	−0.00	−0.00	−0.00	−0.00
60	−0.00	−0.00	−0.00	−0.00	−0.00	−0.00	−0.00	−0.00	−0.00	−0.00	−0.00	−0.00	−0.00	−0.00	−0.00
55	−0.00	−0.00	−0.00	−0.00	−0.00	−0.00	−0.00	−0.00	−0.00	−0.00	−0.00	−0.00	−0.00	−0.00	−0.00
50	−0.00	−0.00	−0.00	−0.00	−0.00	−0.00	−0.00	−0.00	−0.00	−0.00	−0.00	−0.00	−0.00	−0.00	−0.00
45	−0.00	−0.00	−0.00	−0.00	−0.00	−0.04	−0.02	−0.00	−0.00	−0.00	−0.04	−0.02	−0.01	−0.00	−0.00
40	−0.08	−0.06	−0.03	−0.01	−0.00	−0.27	−0.20	−0.10	−0.04	−0.01	−0.28	−0.22	−0.11	−0.04	−0.01
35	−0.18	−0.15	−0.10	−0.04	−0.01	−0.35	−0.29	−0.18	−0.08	−0.03	−0.35	−0.30	−0.20	−0.09	−0.03
30	−0.26	−0.21	−0.12	−0.05	−0.02	−0.33	−0.23	−0.12	−0.06	−0.03	−0.36	−0.26	−0.14	−0.08	−0.04
25	−0.19	−0.14	−0.07	−0.03	−0.02	−0.12	−0.08	−0.04	−0.02	−0.02	−0.15	−0.10	−0.05	−0.03	−0.02
20	−0.11	−0.08	−0.04	−0.02	−0.01	−0.05	−0.04	−0.02	−0.01	−0.01	−0.06	−0.05	−0.02	−0.01	−0.01

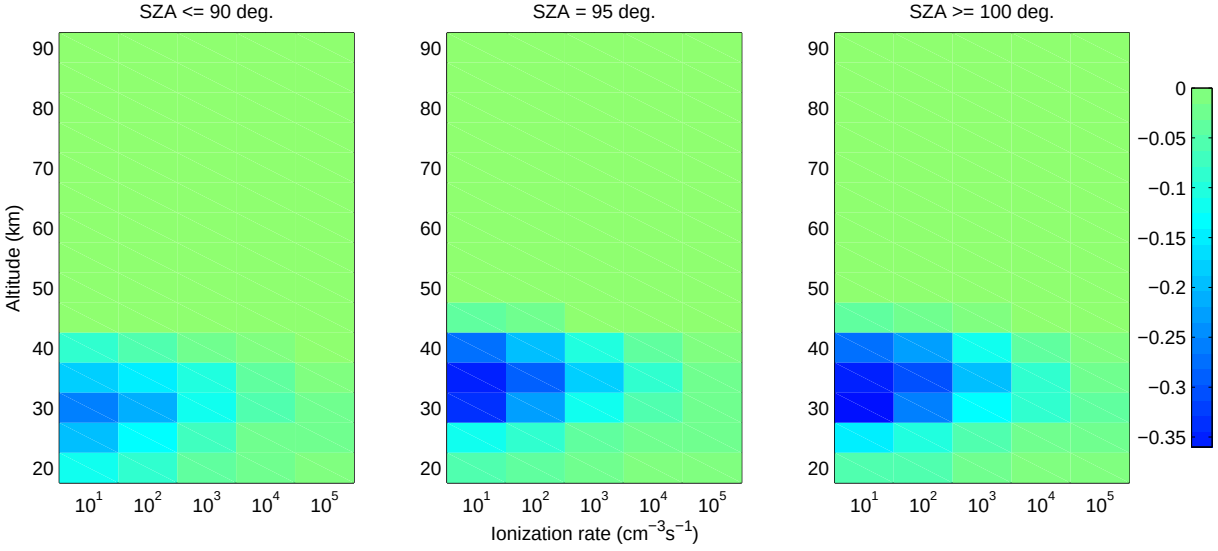

Fig. A16. $P_{N_2O_5}/Q$ for January NH.

Table A17. P_{OH}/Q for October NH.

Q	10^1	10^2	10^3	10^4	10^5	10^1	10^2	10^3	10^4	10^5	10^1	10^2	10^3	10^4	10^5
km		SZA	≤	90°			SZA	=	95°			SZA	≥	100°	
90	+0.00	+0.00	+0.00	+0.00	+0.00	+0.00	+0.00	+0.00	+0.00	+0.00	+0.00	+0.00	+0.00	+0.00	+0.00
85	+0.24	+0.16	+0.07	+0.02	+0.00	+0.21	+0.14	+0.06	+0.02	+0.00	+0.27	+0.19	+0.08	+0.02	+0.00
80	+0.88	+0.86	+0.76	+0.50	+0.17	+0.88	+0.85	+0.76	+0.51	+0.16	+0.89	+0.87	+0.79	+0.57	+0.16
75	+0.89	+0.89	+0.88	+0.80	+0.56	+0.89	+0.89	+0.87	+0.80	+0.54	+0.90	+0.90	+0.90	+0.84	+0.59
70	+0.90	+0.90	+0.89	+0.87	+0.80	+0.90	+0.90	+0.90	+0.89	+0.79	+0.89	+0.90	+0.91	+0.90	+0.82
65	+0.90	+0.90	+0.91	+0.90	+0.88	+0.91	+0.91	+0.93	+0.93	+0.90	+0.92	+0.90	+0.92	+0.95	+0.91
60	+0.91	+0.92	+0.92	+0.94	+0.92	+0.93	+0.94	+0.96	+0.98	+0.96	+0.93	+0.95	+0.98	+1.01	+1.01
55	+0.93	+0.95	+0.96	+0.97	+0.97	+0.93	+0.97	+1.00	+1.04	+1.06	+0.93	+0.96	+1.01	+1.06	+1.09
50	+0.96	+0.97	+1.01	+1.03	+1.03	+0.95	+0.98	+1.03	+1.08	+1.14	+0.92	+0.95	+1.02	+1.09	+1.15
45	+1.12	+1.04	+1.02	+1.02	+1.03	+1.02	+1.01	+1.02	+1.04	+1.08	+0.96	+0.97	+0.99	+1.02	+1.08
40	+1.21	+1.14	+1.05	+1.01	+1.00	+1.10	+1.09	+1.04	+1.00	+1.02	+1.01	+1.00	+1.00	+0.99	+1.00
35	+1.22	+1.17	+1.09	+1.01	+1.02	+1.12	+1.11	+1.05	+0.99	+0.99	+1.03	+1.03	+1.01	+0.97	+0.97
30	+1.15	+1.11	+1.04	+0.96	+0.97	+1.07	+1.03	+1.00	+0.95	+0.93	+1.02	+0.99	+0.96	+0.93	+0.93
25	+1.08	+1.05	+0.96	+0.93	+0.92	+1.02	+1.00	+0.95	+0.92	+0.92	+1.00	+0.99	+0.95	+0.91	+0.90
20	+1.03	+1.00	+0.96	+0.92	+0.91	+1.01	+0.99	+0.94	+0.92	+0.91	+1.01	+1.00	+0.95	+0.91	+0.90

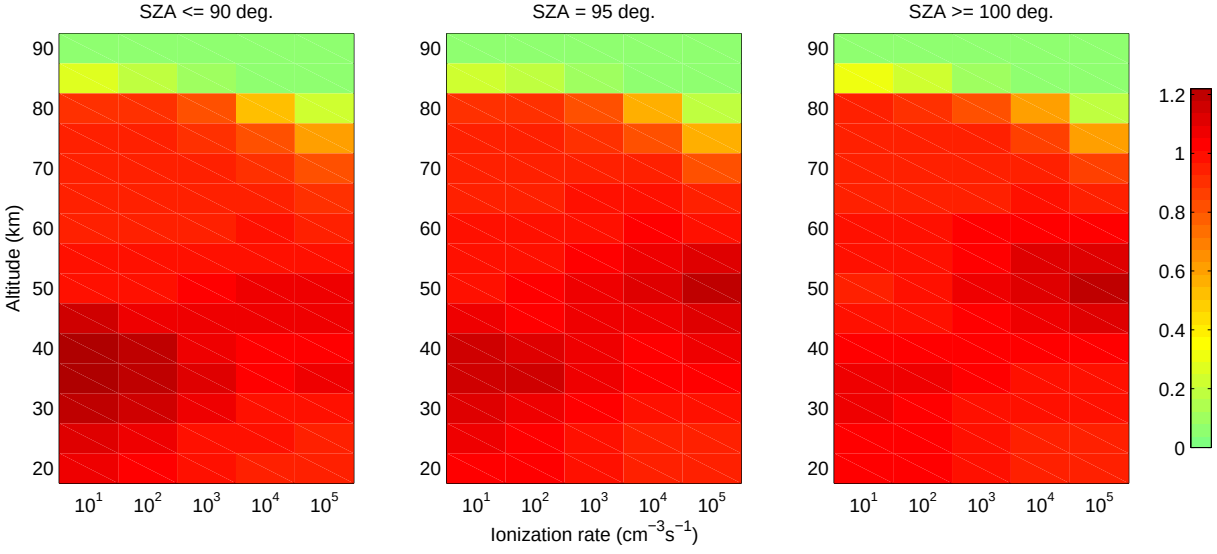

Fig. A17. P_{OH}/Q for October NH.

Table A18. P_{HNO_2}/Q for October NH.

Q	10^1	10^2	10^3	10^4	10^5	10^1	10^2	10^3	10^4	10^5	10^1	10^2	10^3	10^4	10^5
km		SZA	$\leq$	90°			SZA	$=$	95°			SZA	$\geq$	100°	
90	−0.00	−0.00	−0.00	−0.00	−0.00	−0.00	−0.00	−0.00	−0.00	−0.00	−0.00	−0.00	−0.00	−0.00	−0.00
85	−0.00	−0.00	−0.00	−0.00	−0.00	−0.00	−0.00	−0.00	−0.00	−0.00	−0.00	−0.00	−0.00	−0.00	−0.00
80	−0.00	−0.00	−0.00	−0.00	−0.00	+0.01	+0.00	+0.00	−0.00	−0.00	+0.01	+0.00	+0.00	−0.00	−0.00
75	+0.06	+0.02	+0.00	+0.00	+0.00	+0.06	+0.02	+0.00	+0.00	+0.00	+0.07	+0.04	+0.01	+0.00	+0.00
70	+0.09	+0.07	+0.04	+0.01	+0.00	+0.09	+0.07	+0.04	+0.01	+0.00	+0.10	+0.09	+0.06	+0.02	+0.00
65	+0.10	+0.09	+0.08	+0.05	+0.02	+0.10	+0.09	+0.08	+0.06	+0.02	+0.10	+0.10	+0.09	+0.06	+0.03
60	+0.10	+0.10	+0.10	+0.09	+0.07	+0.10	+0.10	+0.10	+0.09	+0.07	+0.10	+0.10	+0.09	+0.09	+0.07
55	+0.10	+0.10	+0.10	+0.10	+0.09	+0.10	+0.10	+0.10	+0.10	+0.09	+0.10	+0.10	+0.10	+0.10	+0.09
50	+0.10	+0.10	+0.10	+0.10	+0.10	+0.10	+0.10	+0.10	+0.10	+0.10	+0.10	+0.10	+0.10	+0.10	+0.09
45	+0.10	+0.10	+0.10	+0.10	+0.10	+0.10	+0.10	+0.10	+0.10	+0.10	+0.10	+0.10	+0.10	+0.10	+0.10
40	+0.10	+0.10	+0.10	+0.10	+0.10	+0.10	+0.10	+0.10	+0.10	+0.10	+0.10	+0.10	+0.10	+0.10	+0.10
35	+0.10	+0.10	+0.10	+0.10	+0.10	+0.10	+0.10	+0.10	+0.10	+0.10	+0.10	+0.10	+0.10	+0.10	+0.10
30	+0.10	+0.10	+0.10	+0.10	+0.10	+0.10	+0.10	+0.10	+0.10	+0.10	+0.10	+0.10	+0.10	+0.10	+0.10
25	+0.10	+0.10	+0.10	+0.10	+0.10	+0.10	+0.10	+0.10	+0.10	+0.10	+0.10	+0.10	+0.10	+0.10	+0.10
20	+0.10	+0.10	+0.10	+0.10	+0.10	+0.10	+0.10	+0.10	+0.10	+0.10	+0.10	+0.10	+0.10	+0.10	+0.10

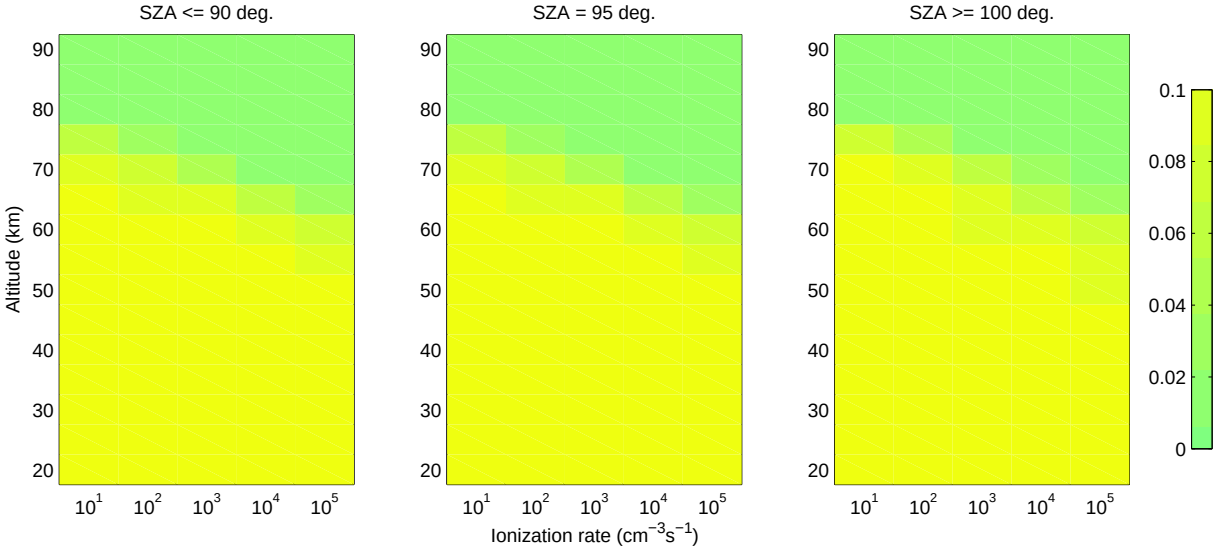

Fig. A18. P_{HNO_2}/Q for October NH.

Table A19. P_H/Q for October NH.

Q	10^1	10^2	10^3	10^4	10^5	10^1	10^2	10^3	10^4	10^5	10^1	10^2	10^3	10^4	10^5
km		SZA	$\leq$	90°			SZA	$=$	95°			SZA	$\geq$	100°	
90	+0.00	+0.00	+0.00	+0.00	+0.00	+0.00	+0.00	+0.00	+0.00	+0.00	+0.00	+0.00	+0.00	+0.00	+0.00
85	+0.24	+0.16	+0.07	+0.02	+0.00	+0.21	+0.14	+0.06	+0.02	+0.00	+0.27	+0.19	+0.08	+0.02	+0.00
80	+0.88	+0.86	+0.76	+0.50	+0.17	+0.89	+0.85	+0.76	+0.51	+0.16	+0.89	+0.86	+0.79	+0.57	+0.16
75	+0.95	+0.91	+0.88	+0.80	+0.56	+0.95	+0.91	+0.87	+0.80	+0.54	+0.95	+0.93	+0.88	+0.82	+0.58
70	+0.99	+0.97	+0.93	+0.88	+0.79	+0.99	+0.97	+0.93	+0.87	+0.78	+0.94	+0.94	+0.90	+0.86	+0.78
65	+1.00	+0.99	+0.98	+0.94	+0.87	+0.98	+0.98	+0.96	+0.92	+0.85	+0.83	+0.89	+0.87	+0.84	+0.82
60	+1.00	+1.00	+0.99	+0.96	+0.92	+0.92	+0.95	+0.92	+0.88	+0.85	+0.64	+0.77	+0.78	+0.74	+0.76
55	+1.00	+0.99	+0.98	+0.94	+0.89	+0.81	+0.85	+0.85	+0.77	+0.76	+0.47	+0.60	+0.68	+0.61	+0.63
50	+0.99	+0.98	+0.95	+0.88	+0.78	+0.66	+0.71	+0.74	+0.68	+0.59	+0.40	+0.47	+0.56	+0.51	+0.43
45	+0.88	+0.90	+0.89	+0.82	+0.74	+0.45	+0.58	+0.70	+0.70	+0.62	+0.29	+0.43	+0.56	+0.56	+0.45
40	+0.32	+0.47	+0.68	+0.77	+0.75	+0.22	+0.36	+0.60	+0.73	+0.70	+0.14	+0.26	+0.48	+0.63	+0.57
35	+0.14	+0.26	+0.49	+0.69	+0.71	+0.14	+0.26	+0.48	+0.68	+0.69	+0.09	+0.18	+0.38	+0.58	+0.59
30	+0.19	+0.33	+0.58	+0.77	+0.80	+0.22	+0.37	+0.61	+0.78	+0.81	+0.16	+0.29	+0.53	+0.72	+0.75
25	+0.42	+0.56	+0.78	+0.90	+0.92	+0.48	+0.61	+0.80	+0.90	+0.91	+0.41	+0.55	+0.76	+0.88	+0.89
20	+0.65	+0.73	+0.87	+0.94	+0.96	+0.68	+0.76	+0.88	+0.94	+0.95	+0.66	+0.74	+0.87	+0.94	+0.95

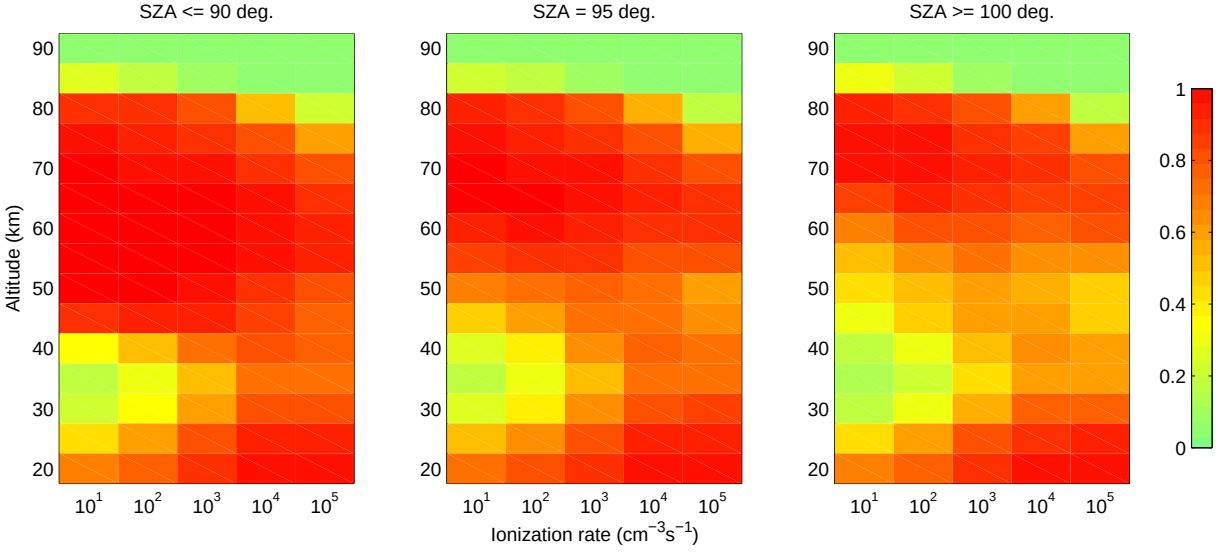

Fig. A19. P_H/Q for October NH.

Table A20. P_{HNO_3}/Q for October NH.

Q	10^1	10^2	10^3	10^4	10^5	10^1	10^2	10^3	10^4	10^5	10^1	10^2	10^3	10^4	10^5
km		SZA	$\leq$	90°			SZA	$=$	95°			SZA	$\geq$	100°	
90	−0.00	−0.00	−0.00	−0.00	−0.00	−0.00	−0.00	−0.00	−0.00	−0.00	−0.00	−0.00	−0.00	−0.00	−0.00
85	−0.00	−0.00	−0.00	−0.00	−0.00	−0.00	−0.00	−0.00	−0.00	−0.00	−0.00	−0.00	−0.00	−0.00	−0.00
80	+0.00	+0.00	+0.00	+0.00	+0.00	+0.00	+0.00	+0.00	+0.00	+0.00	+0.01	+0.01	+0.00	−0.00	+0.00
75	+0.00	+0.00	+0.00	+0.00	+0.00	+0.00	−0.00	+0.00	−0.00	−0.00	+0.02	+0.01	+0.01	+0.00	−0.01
70	−0.00	−0.00	+0.00	−0.00	−0.01	+0.00	−0.00	−0.01	−0.01	−0.01	+0.05	+0.03	+0.03	+0.02	−0.00
65	−0.00	−0.00	−0.01	−0.01	−0.01	+0.01	−0.00	−0.01	−0.01	−0.01	+0.15	+0.09	+0.08	+0.05	+0.02
60	−0.01	−0.02	−0.03	−0.03	−0.01	+0.05	+0.01	+0.00	+0.01	+0.00	+0.33	+0.18	+0.13	+0.12	+0.06
55	−0.03	−0.04	−0.04	−0.03	+0.01	+0.16	+0.08	+0.05	+0.07	+0.05	+0.50	+0.34	+0.21	+0.21	+0.15
50	−0.05	−0.05	−0.06	−0.01	+0.07	+0.29	+0.21	+0.13	+0.14	+0.15	+0.58	+0.48	+0.32	+0.30	+0.31
45	−0.08	−0.04	−0.01	+0.06	+0.13	+0.55	+0.37	+0.20	+0.16	+0.20	+0.79	+0.58	+0.37	+0.32	+0.37
40	+0.59	+0.45	+0.23	+0.14	+0.15	+0.92	+0.71	+0.38	+0.21	+0.20	+1.13	+0.94	+0.58	+0.34	+0.35
35	+0.88	+0.75	+0.48	+0.26	+0.19	+1.14	+0.95	+0.61	+0.33	+0.26	+1.30	+1.15	+0.81	+0.47	+0.38
30	+0.98	+0.80	+0.48	+0.25	+0.17	+1.19	+0.94	+0.55	+0.29	+0.22	+1.34	+1.12	+0.71	+0.39	+0.30
25	+0.74	+0.55	+0.28	+0.13	+0.10	+0.78	+0.57	+0.29	+0.14	+0.13	+0.91	+0.68	+0.35	+0.19	+0.17
20	+0.48	+0.35	+0.17	+0.08	+0.07	+0.45	+0.33	+0.16	+0.08	+0.08	+0.49	+0.36	+0.18	+0.09	+0.09

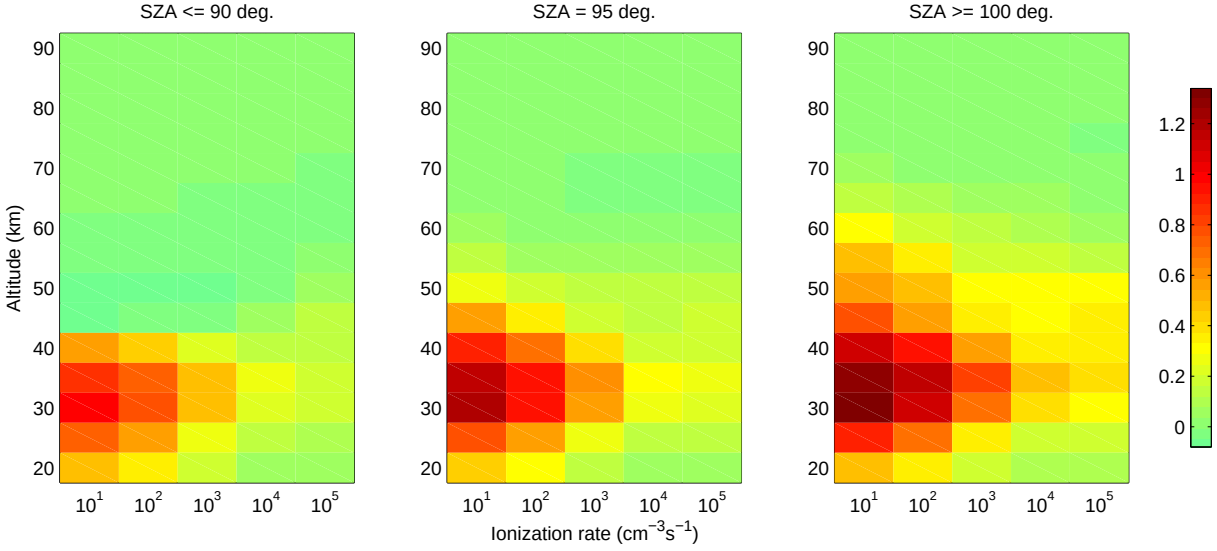

Fig. A20. P_{HNO_3}/Q for October NH.

Table A21. P_{NO}/Q for October NH.

Q	10^1	10^2	10^3	10^4	10^5	10^1	10^2	10^3	10^4	10^5	10^1	10^2	10^3	10^4	10^5
km		SZA	$\leq$	90°			SZA	$=$	95°			SZA	$\geq$	100°	
90	+0.00	+0.00	+0.00	+0.00	+0.00	+0.00	+0.00	+0.00	+0.00	+0.00	+0.00	+0.00	+0.00	+0.00	+0.00
85	+0.00	+0.00	+0.00	+0.00	+0.00	+0.00	+0.00	+0.00	+0.00	+0.00	+0.00	+0.00	+0.00	+0.00	+0.00
80	+0.00	−0.00	−0.00	−0.00	−0.00	−0.01	+0.00	−0.00	−0.00	−0.00	−0.01	−0.01	+0.00	+0.00	−0.00
75	+0.00	−0.00	−0.00	−0.00	−0.00	−0.01	+0.00	−0.00	−0.01	−0.01	−0.02	−0.01	−0.02	−0.01	−0.01
70	+0.00	+0.00	−0.00	−0.01	−0.02	−0.01	−0.01	+0.00	−0.02	−0.02	−0.03	−0.02	−0.03	−0.03	−0.03
65	−0.01	−0.01	−0.01	−0.04	−0.08	−0.05	−0.02	−0.02	−0.06	−0.08	−0.07	−0.04	−0.04	−0.05	−0.05
60	−0.06	−0.03	−0.04	−0.09	−0.18	−0.16	−0.07	−0.05	−0.09	−0.14	−0.10	−0.05	−0.04	−0.07	−0.08
55	−0.23	−0.13	−0.11	−0.15	−0.25	−0.36	−0.17	−0.10	−0.11	−0.18	−0.07	−0.05	−0.03	−0.04	−0.09
50	−0.62	−0.35	−0.19	−0.21	−0.27	−0.45	−0.26	−0.14	−0.13	−0.17	−0.02	−0.01	−0.01	−0.01	−0.04
45	−0.96	−0.55	−0.26	−0.19	−0.22	−0.33	−0.25	−0.15	−0.13	−0.15	−0.00	−0.00	−0.00	−0.00	−0.01
40	−0.33	−0.26	−0.17	−0.12	−0.13	−0.18	−0.15	−0.11	−0.08	−0.09	−0.00	−0.00	−0.00	−0.00	−0.00
35	−0.12	−0.11	−0.08	−0.06	−0.06	−0.08	−0.07	−0.05	−0.04	−0.04	−0.00	−0.00	−0.00	−0.00	−0.00
30	−0.07	−0.05	−0.04	−0.02	−0.02	−0.04	−0.03	−0.02	−0.01	−0.01	−0.00	−0.00	−0.00	−0.00	−0.00
25	−0.03	−0.03	−0.01	−0.01	−0.01	−0.01	−0.01	−0.01	−0.00	−0.00	−0.00	−0.00	−0.00	−0.00	−0.00
20	−0.01	−0.01	−0.00	−0.00	−0.00	−0.00	−0.00	−0.00	−0.00	−0.00	−0.00	−0.00	−0.00	−0.00	−0.00

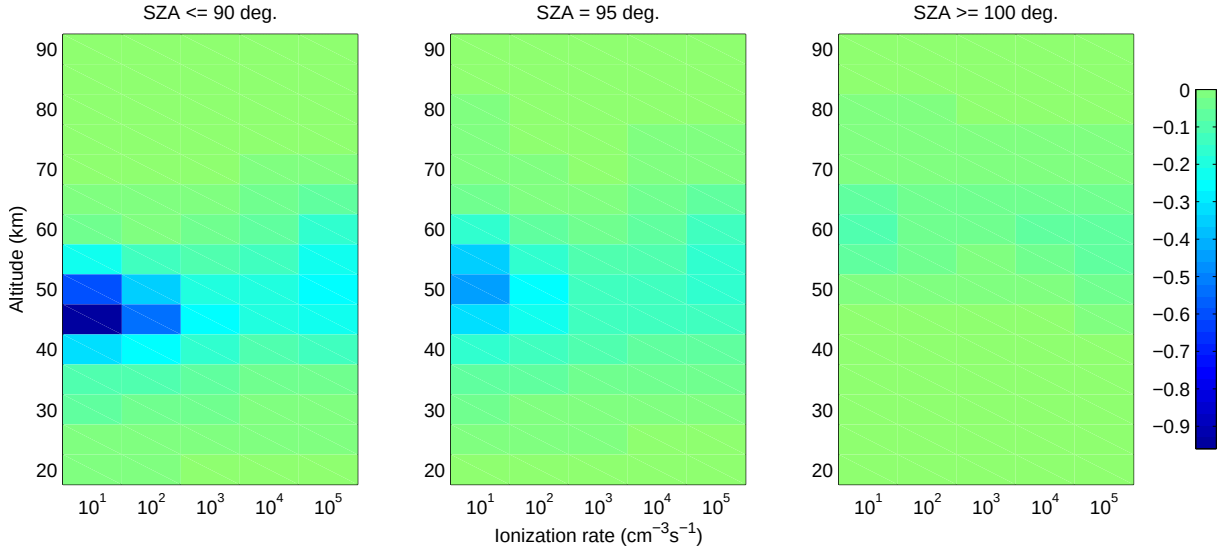

Fig. A21. P_{NO}/Q for October NH.

Table A22. P_{NO_2}/Q for October NH.

Q	10^1	10^2	10^3	10^4	10^5	10^1	10^2	10^3	10^4	10^5	10^1	10^2	10^3	10^4	10^5
km		SZA	$\leq$	90°			SZA	=	95°			SZA	$\geq$	100°	
90	+0.00	+0.00	+0.00	+0.00	+0.00	+0.00	+0.00	+0.00	+0.00	+0.00	+0.00	+0.00	+0.00	+0.00	+0.00
85	+0.00	+0.00	+0.00	+0.00	+0.00	+0.00	+0.00	+0.00	+0.00	+0.00	+0.00	+0.00	+0.00	+0.00	+0.00
80	+0.00	+0.00	+0.00	+0.00	+0.00	+0.00	+0.00	+0.00	+0.00	+0.00	+0.00	+0.00	+0.00	+0.00	+0.00
75	+0.00	+0.00	+0.00	+0.00	+0.00	+0.00	+0.00	+0.00	+0.01	+0.00	−0.00	−0.00	−0.00	+0.01	+0.01
70	+0.00	+0.00	+0.00	+0.01	+0.02	+0.00	+0.00	+0.00	+0.02	+0.02	−0.03	−0.02	−0.01	+0.00	+0.02
65	+0.00	+0.00	+0.01	+0.03	+0.07	+0.01	+0.00	+0.01	+0.05	+0.07	−0.10	−0.06	−0.05	−0.02	+0.01
60	+0.02	+0.01	+0.02	+0.06	+0.15	+0.01	+0.01	+0.01	+0.05	+0.11	−0.27	−0.15	−0.11	−0.07	−0.01
55	+0.05	+0.03	+0.02	+0.05	+0.16	+0.00	+0.00	+0.00	+0.01	+0.10	−0.51	−0.33	−0.21	−0.20	−0.09
50	+0.02	+0.01	+0.01	+0.02	+0.08	−0.09	−0.06	−0.03	−0.03	+0.00	−0.69	−0.53	−0.34	−0.31	−0.29
45	−0.26	−0.14	−0.07	−0.05	−0.03	−0.24	−0.19	−0.12	−0.10	−0.11	−0.77	−0.65	−0.47	−0.41	−0.44
40	−0.38	−0.32	−0.21	−0.14	−0.14	−0.43	−0.36	−0.26	−0.21	−0.22	−0.78	−0.71	−0.56	−0.46	−0.50
35	−0.44	−0.40	−0.30	−0.22	−0.20	−0.57	−0.49	−0.37	−0.27	−0.28	−0.79	−0.72	−0.57	−0.46	−0.48
30	−0.50	−0.43	−0.27	−0.19	−0.16	−0.58	−0.49	−0.30	−0.20	−0.21	−0.73	−0.64	−0.44	−0.31	−0.30
25	−0.38	−0.27	−0.16	−0.08	−0.07	−0.40	−0.29	−0.15	−0.10	−0.10	−0.50	−0.37	−0.21	−0.13	−0.15
20	−0.21	−0.17	−0.08	−0.05	−0.04	−0.21	−0.16	−0.09	−0.05	−0.05	−0.23	−0.17	−0.09	−0.06	−0.07

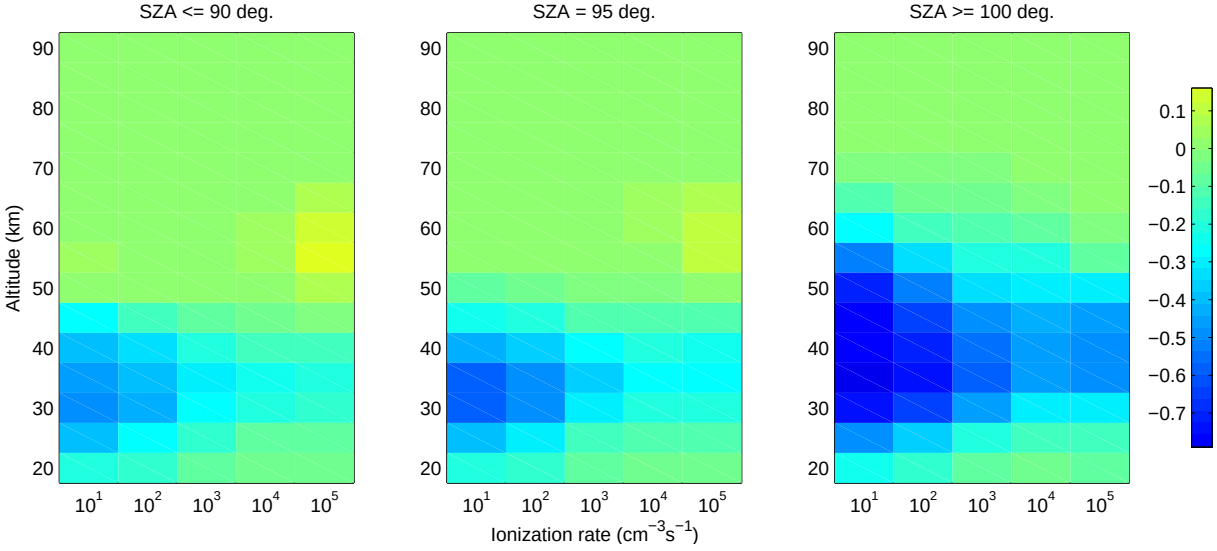

Fig. A22. P_{NO_2}/Q for October NH.

Table A23. P_{NO_3}/Q for October NH.

Q	10^1	10^2	10^3	10^4	10^5	10^1	10^2	10^3	10^4	10^5	10^1	10^2	10^3	10^4	10^5
km		SZA	$\leq$	90°			SZA	=	95°			SZA	$\geq$	100°	
90	+0.00	+0.00	+0.00	+0.00	+0.00	+0.00	+0.00	+0.00	+0.00	+0.00	+0.00	+0.00	+0.00	+0.00	+0.00
85	+0.00	+0.00	+0.00	+0.00	+0.00	+0.00	+0.00	+0.00	+0.00	+0.00	+0.00	+0.00	+0.00	+0.00	+0.00
80	+0.00	+0.00	+0.00	+0.00	+0.00	+0.01	+0.00	+0.00	+0.00	+0.00	+0.00	+0.00	+0.00	+0.00	+0.00
75	+0.00	+0.00	+0.00	+0.00	+0.00	+0.01	+0.00	+0.00	+0.00	+0.01	+0.00	+0.00	+0.01	+0.00	+0.01
70	+0.00	+0.00	+0.00	+0.00	+0.01	+0.01	+0.01	+0.01	+0.01	+0.01	+0.01	+0.01	+0.01	+0.01	+0.01
65	+0.01	+0.01	+0.01	+0.02	+0.02	+0.03	+0.02	+0.02	+0.02	+0.02	+0.02	+0.01	+0.01	+0.02	+0.02
60	+0.05	+0.04	+0.05	+0.06	+0.04	+0.10	+0.05	+0.04	+0.03	+0.03	+0.04	+0.02	+0.02	+0.02	+0.03
55	+0.21	+0.14	+0.13	+0.13	+0.08	+0.20	+0.09	+0.05	+0.03	+0.03	+0.08	+0.04	+0.03	+0.03	+0.03
50	+0.65	+0.39	+0.24	+0.20	+0.12	+0.25	+0.11	+0.04	+0.02	+0.02	+0.13	+0.06	+0.03	+0.02	+0.02
45	+1.32	+0.73	+0.34	+0.18	+0.12	+0.14	+0.13	+0.09	+0.07	+0.06	+0.12	+0.15	+0.12	+0.09	+0.08
40	+0.34	+0.29	+0.21	+0.14	+0.12	+0.03	+0.06	+0.11	+0.12	+0.13	+0.03	+0.07	+0.14	+0.18	+0.17
35	+0.02	+0.04	+0.06	+0.08	+0.09	+0.01	+0.03	+0.05	+0.08	+0.10	+0.01	+0.03	+0.06	+0.11	+0.14
30	+0.01	+0.02	+0.03	+0.04	+0.05	+0.01	+0.02	+0.03	+0.04	+0.06	+0.01	+0.02	+0.03	+0.06	+0.08
25	+0.01	+0.01	+0.01	+0.02	+0.02	+0.01	+0.01	+0.01	+0.02	+0.03	+0.01	+0.01	+0.02	+0.02	+0.04
20	+0.00	+0.01	+0.01	+0.01	+0.01	+0.00	+0.01	+0.01	+0.01	+0.01	+0.00	+0.01	+0.01	+0.01	+0.02

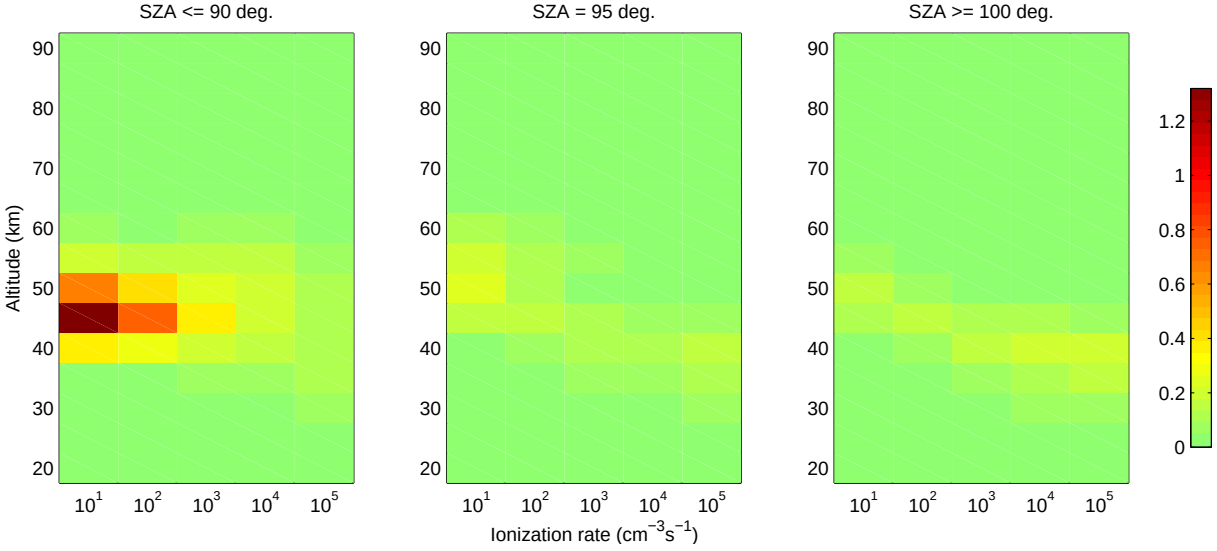

Fig. A23. P_{NO_3}/Q for October NH.

Table A24. $P_{N_2O_5}/Q$ for October NH.

Q	10^1	10^2	10^3	10^4	10^5	10^1	10^2	10^3	10^4	10^5	10^1	10^2	10^3	10^4	10^5
km		SZA	$\leq$	90°			SZA	$=$	95°			SZA	$\geq$	100°	
90	+0.00	−0.00	−0.00	−0.00	−0.00	+0.00	+0.00	−0.00	−0.00	−0.00	−0.00	−0.00	−0.00	−0.00	−0.00
85	−0.00	−0.00	−0.00	−0.00	−0.00	−0.00	−0.00	−0.00	−0.00	−0.00	−0.00	−0.00	−0.00	−0.00	−0.00
80	−0.00	−0.00	−0.00	−0.00	−0.00	−0.00	−0.00	−0.00	−0.00	−0.00	−0.00	−0.00	−0.00	−0.00	−0.00
75	−0.00	−0.00	−0.00	−0.00	−0.00	−0.00	−0.00	−0.00	−0.00	−0.00	−0.00	−0.00	−0.00	−0.00	−0.00
70	−0.00	−0.00	−0.00	−0.00	−0.00	−0.00	−0.00	−0.00	−0.00	−0.00	−0.00	−0.00	−0.00	−0.00	−0.00
65	−0.00	−0.00	−0.00	−0.00	−0.00	−0.00	−0.00	−0.00	−0.00	−0.00	−0.00	−0.00	−0.00	−0.00	−0.00
60	−0.00	−0.00	−0.00	−0.00	−0.00	−0.00	−0.00	−0.00	−0.00	−0.00	−0.00	−0.00	−0.00	−0.00	−0.00
55	−0.00	−0.00	−0.00	−0.00	−0.00	−0.00	−0.00	−0.00	−0.00	−0.00	−0.00	−0.00	−0.00	−0.00	−0.00
50	−0.00	−0.00	−0.00	−0.00	−0.00	−0.00	−0.00	−0.00	−0.00	−0.00	−0.00	−0.00	−0.00	−0.00	−0.00
45	−0.01	−0.00	−0.00	−0.00	−0.00	−0.06	−0.03	−0.01	−0.00	−0.00	−0.07	−0.04	−0.01	−0.00	−0.00
40	−0.11	−0.08	−0.03	−0.01	−0.00	−0.17	−0.13	−0.06	−0.02	−0.01	−0.19	−0.15	−0.08	−0.03	−0.01
35	−0.17	−0.14	−0.08	−0.03	−0.01	−0.25	−0.21	−0.12	−0.05	−0.02	−0.26	−0.23	−0.15	−0.06	−0.02
30	−0.21	−0.17	−0.10	−0.04	−0.02	−0.29	−0.22	−0.13	−0.06	−0.03	−0.31	−0.25	−0.15	−0.07	−0.04
25	−0.17	−0.13	−0.06	−0.03	−0.02	−0.19	−0.14	−0.07	−0.03	−0.03	−0.21	−0.16	−0.08	−0.04	−0.03
20	−0.13	−0.09	−0.05	−0.02	−0.02	−0.12	−0.09	−0.04	−0.02	−0.02	−0.13	−0.10	−0.05	−0.02	−0.02

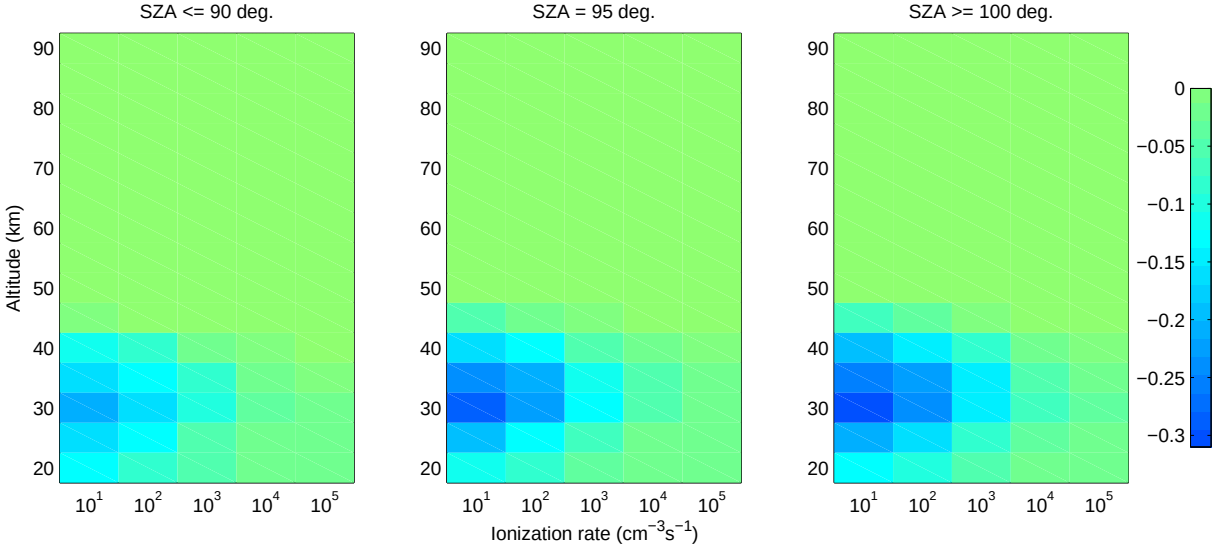

Fig. A24. $P_{N_2O_5}/Q$ for October NH.

Table A25. P_{OH}/Q for October SH.

Q	10^1	10^2	10^3	10^4	10^5	10^1	10^2	10^3	10^4	10^5	10^1	10^2	10^3	10^4	10^5
km		SZA	$\leq$	90°			SZA	$=$	95°			SZA	$\geq$	100°	
90	+0.01	+0.00	+0.00	+0.00	+0.00	+0.01	+0.00	+0.00	+0.00	+0.00	+0.01	+0.01	+0.00	+0.00	+0.00
85	+0.66	+0.47	+0.21	+0.06	+0.01	+0.67	+0.47	+0.21	+0.06	+0.01	+0.62	+0.42	+0.17	+0.05	+0.01
80	+0.89	+0.88	+0.84	+0.70	+0.35	+0.89	+0.88	+0.84	+0.70	+0.35	+0.89	+0.88	+0.86	+0.73	+0.34
75	+0.90	+0.89	+0.89	+0.86	+0.74	+0.89	+0.90	+0.89	+0.86	+0.74	+0.90	+0.91	+0.90	+0.88	+0.77
70	+0.90	+0.90	+0.90	+0.89	+0.86	+0.90	+0.90	+0.90	+0.90	+0.88	+0.90	+0.90	+0.91	+0.93	+0.90
65	+0.90	+0.90	+0.91	+0.91	+0.91	+0.91	+0.91	+0.92	+0.93	+0.92	+0.92	+0.92	+0.93	+0.98	+0.97
60	+0.91	+0.91	+0.92	+0.94	+0.96	+0.90	+0.92	+0.95	+1.00	+1.03	+0.92	+0.93	+0.96	+1.04	+1.06
55	+0.93	+0.93	+0.94	+0.99	+1.04	+0.92	+0.93	+0.97	+1.04	+1.12	+0.92	+0.93	+0.98	+1.07	+1.16
50	+0.97	+0.96	+0.97	+1.03	+1.09	+0.94	+0.95	+0.98	+1.07	+1.16	+0.92	+0.94	+0.99	+1.09	+1.16
45	+1.20	+1.08	+1.03	+1.05	+1.12	+1.02	+1.01	+1.01	+1.07	+1.14	+0.97	+0.96	+0.98	+1.05	+1.11
40	+1.34	+1.24	+1.10	+1.07	+1.12	+1.16	+1.13	+1.06	+1.05	+1.12	+1.11	+1.09	+1.04	+1.02	+1.07
35	+1.36	+1.33	+1.23	+1.09	+1.11	+1.29	+1.27	+1.19	+1.05	+1.10	+1.20	+1.18	+1.12	+1.04	+1.06
30	+1.41	+1.39	+1.31	+1.16	+1.09	+1.34	+1.34	+1.27	+1.12	+1.08	+1.19	+1.18	+1.13	+1.05	+1.02
25	+1.23	+1.20	+1.12	+1.01	+0.96	+1.19	+1.18	+1.10	+1.01	+0.97	+1.14	+1.14	+1.09	+1.01	+0.97
20	+1.01	+1.00	+0.95	+0.93	+0.91	+1.01	+1.00	+0.95	+0.91	+0.91	+1.08	+1.06	+1.01	+0.93	+0.92

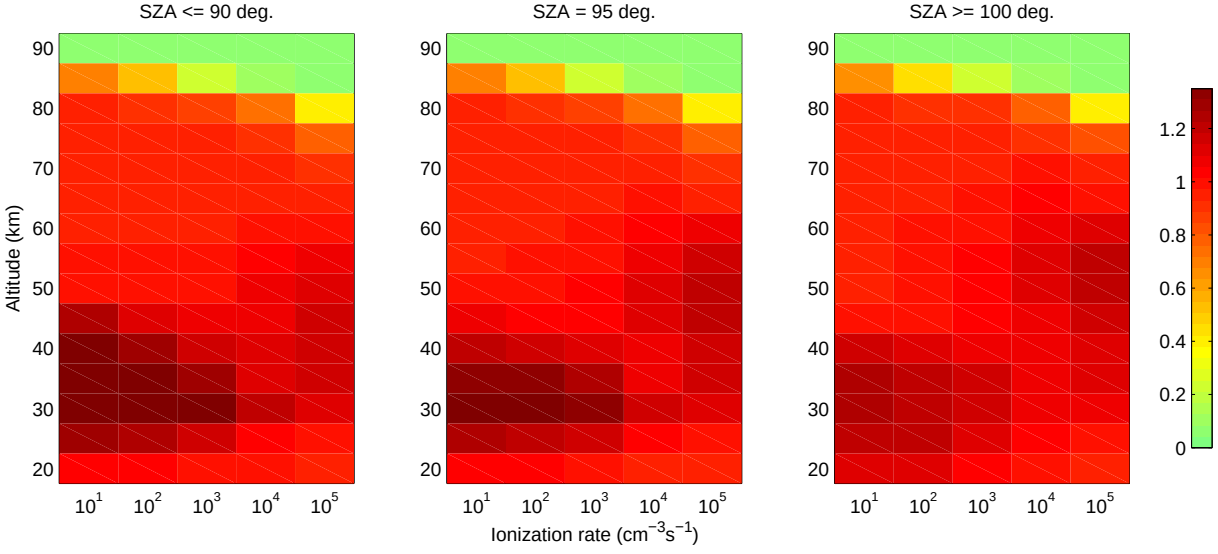

Fig. A25. P_{OH}/Q for October SH.

Table A26. P_{HNO_2}/Q for October SH.

Q	10^1	10^2	10^3	10^4	10^5	10^1	10^2	10^3	10^4	10^5	10^1	10^2	10^3	10^4	10^5
km		SZA	$\leq$	90°			SZA	$=$	95°			SZA	$\geq$	100°	
90	−0.00	−0.00	−0.00	−0.00	−0.00	−0.00	−0.00	−0.00	−0.00	−0.00	−0.00	−0.00	−0.00	−0.00	−0.00
85	−0.00	−0.00	−0.00	−0.00	−0.00	+0.00	+0.00	−0.00	−0.00	−0.00	+0.00	−0.00	−0.00	−0.00	−0.00
80	+0.03	+0.01	+0.00	+0.00	+0.00	+0.03	+0.01	+0.00	+0.00	+0.00	+0.05	+0.02	+0.00	+0.00	+0.00
75	+0.08	+0.06	+0.02	+0.00	+0.00	+0.09	+0.06	+0.03	+0.01	+0.00	+0.09	+0.08	+0.05	+0.01	+0.00
70	+0.10	+0.09	+0.07	+0.04	+0.01	+0.10	+0.09	+0.08	+0.05	+0.02	+0.10	+0.09	+0.08	+0.06	+0.02
65	+0.10	+0.10	+0.09	+0.08	+0.05	+0.10	+0.10	+0.09	+0.08	+0.06	+0.10	+0.10	+0.09	+0.08	+0.06
60	+0.10	+0.10	+0.10	+0.09	+0.08	+0.10	+0.10	+0.10	+0.09	+0.08	+0.10	+0.10	+0.10	+0.09	+0.08
55	+0.10	+0.10	+0.10	+0.10	+0.10	+0.10	+0.10	+0.10	+0.10	+0.10	+0.10	+0.10	+0.10	+0.10	+0.09
50	+0.10	+0.10	+0.10	+0.10	+0.10	+0.10	+0.10	+0.10	+0.10	+0.10	+0.10	+0.10	+0.10	+0.10	+0.10
45	+0.10	+0.10	+0.10	+0.10	+0.10	+0.10	+0.10	+0.10	+0.10	+0.10	+0.10	+0.10	+0.10	+0.10	+0.10
40	+0.10	+0.10	+0.10	+0.10	+0.10	+0.10	+0.10	+0.10	+0.10	+0.10	+0.10	+0.10	+0.10	+0.10	+0.10
35	+0.10	+0.10	+0.10	+0.10	+0.10	+0.10	+0.10	+0.10	+0.10	+0.10	+0.10	+0.10	+0.10	+0.10	+0.10
30	+0.10	+0.10	+0.10	+0.10	+0.10	+0.10	+0.10	+0.10	+0.10	+0.10	+0.10	+0.10	+0.10	+0.10	+0.10
25	+0.10	+0.10	+0.10	+0.10	+0.10	+0.10	+0.10	+0.10	+0.10	+0.10	+0.10	+0.10	+0.10	+0.10	+0.10
20	+0.10	+0.10	+0.10	+0.10	+0.10	+0.10	+0.10	+0.10	+0.10	+0.10	+0.10	+0.10	+0.10	+0.10	+0.10

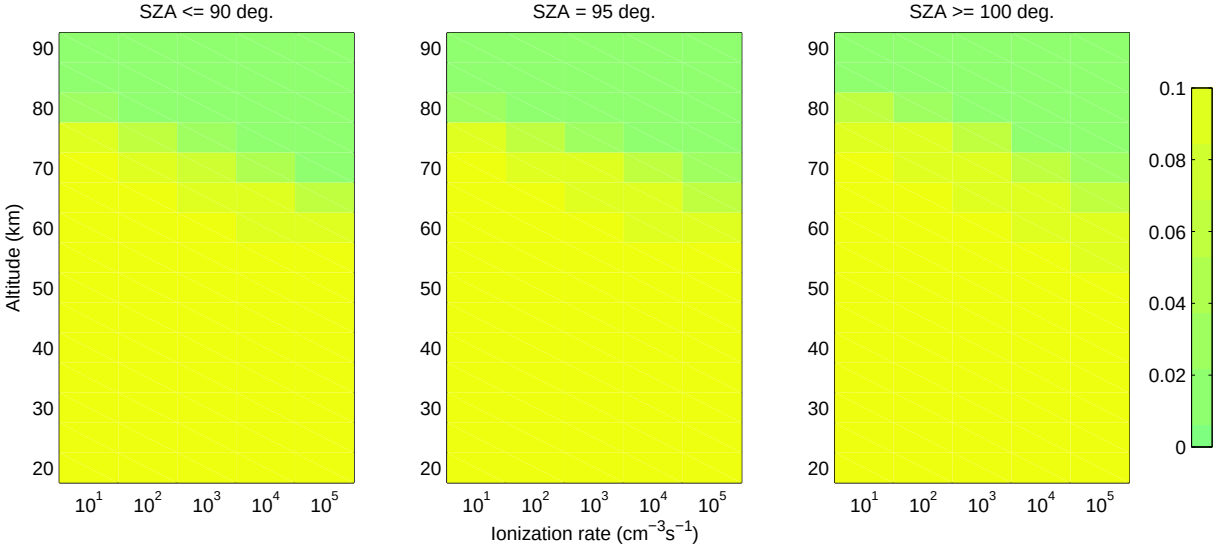

Fig. A26. P_{HNO_2}/Q for October SH.

Table A27. P_H/Q for October SH.

Q	10^1	10^2	10^3	10^4	10^5	10^1	10^2	10^3	10^4	10^5	10^1	10^2	10^3	10^4	10^5
km		SZA	$\leq$	90°			SZA	$=$	95°			SZA	$\geq$	100°	
90	+0.01	+0.00	+0.00	+0.00	+0.00	+0.01	+0.00	+0.00	+0.00	+0.00	+0.01	+0.01	+0.00	+0.00	+0.00
85	+0.66	+0.47	+0.21	+0.06	+0.01	+0.67	+0.47	+0.21	+0.06	+0.01	+0.62	+0.42	+0.17	+0.05	+0.01
80	+0.92	+0.89	+0.84	+0.70	+0.35	+0.92	+0.89	+0.84	+0.70	+0.35	+0.93	+0.89	+0.85	+0.73	+0.33
75	+0.98	+0.95	+0.91	+0.86	+0.73	+0.98	+0.96	+0.92	+0.87	+0.73	+0.98	+0.96	+0.92	+0.86	+0.74
70	+1.00	+0.99	+0.97	+0.93	+0.86	+1.00	+0.99	+0.96	+0.93	+0.85	+0.96	+0.96	+0.93	+0.88	+0.83
65	+1.00	+1.00	+0.99	+0.96	+0.91	+0.97	+0.98	+0.96	+0.91	+0.87	+0.83	+0.89	+0.85	+0.80	+0.79
60	+1.00	+1.00	+0.99	+0.96	+0.89	+0.90	+0.93	+0.91	+0.82	+0.78	+0.62	+0.76	+0.76	+0.65	+0.67
55	+0.99	+0.99	+0.98	+0.90	+0.76	+0.76	+0.82	+0.83	+0.70	+0.60	+0.44	+0.58	+0.65	+0.51	+0.46
50	+0.98	+0.97	+0.95	+0.84	+0.64	+0.61	+0.67	+0.73	+0.63	+0.47	+0.41	+0.47	+0.56	+0.46	+0.32
45	+0.82	+0.86	+0.86	+0.75	+0.55	+0.39	+0.51	+0.62	+0.58	+0.43	+0.29	+0.41	+0.51	+0.47	+0.33
40	+0.31	+0.44	+0.63	+0.65	+0.49	+0.20	+0.30	+0.50	+0.56	+0.42	+0.15	+0.25	+0.45	+0.52	+0.39
35	+0.12	+0.19	+0.35	+0.56	+0.49	+0.11	+0.17	+0.32	+0.53	+0.45	+0.09	+0.15	+0.30	+0.50	+0.44
30	+0.07	+0.11	+0.24	+0.46	+0.52	+0.06	+0.10	+0.23	+0.44	+0.48	+0.06	+0.11	+0.24	+0.45	+0.49
25	+0.18	+0.28	+0.50	+0.73	+0.79	+0.14	+0.22	+0.43	+0.66	+0.72	+0.11	+0.18	+0.37	+0.62	+0.68
20	+0.64	+0.71	+0.85	+0.93	+0.96	+0.56	+0.65	+0.81	+0.92	+0.94	+0.38	+0.48	+0.69	+0.86	+0.90

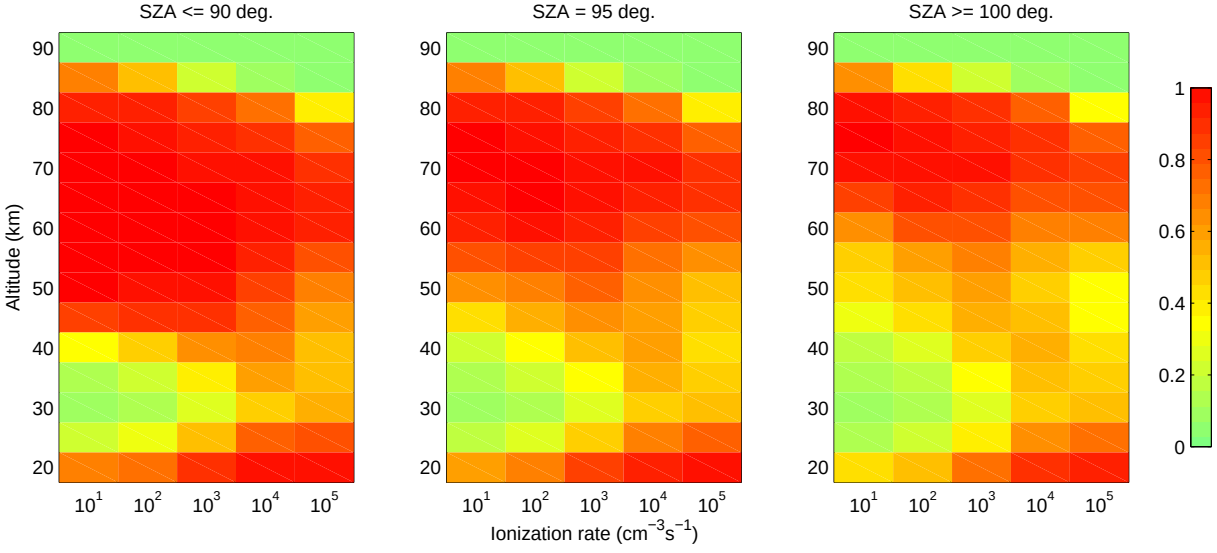

Fig. A27. P_H/Q for October SH.

Table A28. P_{HNO_3}/Q for October SH.

Q	10^1	10^2	10^3	10^4	10^5	10^1	10^2	10^3	10^4	10^5	10^1	10^2	10^3	10^4	10^5
km		SZA	$\leq$	90°			SZA	=	95°			SZA	$\geq$	100°	
90	−0.00	−0.00	−0.00	−0.00	−0.00	−0.00	−0.00	−0.00	−0.00	−0.00	−0.00	−0.00	−0.00	−0.00	−0.00
85	−0.00	−0.00	−0.00	−0.00	−0.00	−0.00	−0.00	−0.00	−0.00	−0.00	−0.00	−0.00	−0.00	−0.00	−0.00
80	+0.00	+0.00	+0.00	+0.00	+0.00	−0.00	−0.00	−0.00	−0.00	+0.00	+0.01	+0.01	+0.01	−0.00	−0.01
75	−0.00	−0.00	−0.00	−0.00	−0.01	−0.00	−0.00	−0.00	−0.00	−0.01	+0.01	+0.01	+0.01	+0.01	−0.01
70	−0.00	−0.00	−0.00	−0.00	−0.01	+0.00	+0.00	+0.00	−0.00	−0.01	+0.04	+0.03	+0.04	+0.03	+0.01
65	−0.00	−0.00	−0.01	−0.01	−0.01	+0.02	+0.01	+0.01	+0.02	+0.01	+0.15	+0.09	+0.11	+0.10	+0.04
60	−0.01	−0.01	−0.01	−0.01	+0.01	+0.10	+0.05	+0.04	+0.07	+0.05	+0.36	+0.21	+0.18	+0.20	+0.13
55	−0.02	−0.02	−0.02	−0.01	+0.06	+0.22	+0.15	+0.10	+0.14	+0.14	+0.54	+0.39	+0.27	+0.30	+0.25
50	−0.05	−0.03	−0.02	+0.03	+0.15	+0.35	+0.28	+0.19	+0.20	+0.25	+0.57	+0.49	+0.35	+0.35	+0.40
45	−0.12	−0.04	+0.01	+0.10	+0.23	+0.51	+0.40	+0.27	+0.25	+0.33	+0.68	+0.55	+0.41	+0.38	+0.46
40	+0.31	+0.26	+0.19	+0.20	+0.31	+0.62	+0.53	+0.38	+0.31	+0.38	+0.80	+0.70	+0.51	+0.42	+0.50
35	+0.50	+0.46	+0.38	+0.29	+0.32	+0.60	+0.56	+0.47	+0.38	+0.41	+0.83	+0.77	+0.64	+0.50	+0.52
30	+0.50	+0.48	+0.41	+0.32	+0.31	+0.60	+0.56	+0.48	+0.40	+0.40	+0.83	+0.79	+0.67	+0.50	+0.47
25	+0.57	+0.50	+0.34	+0.20	+0.17	+0.67	+0.60	+0.43	+0.27	+0.25	+0.81	+0.74	+0.56	+0.35	+0.31
20	+0.35	+0.27	+0.14	+0.06	+0.05	+0.47	+0.37	+0.20	+0.09	+0.07	+0.62	+0.52	+0.30	+0.15	+0.12

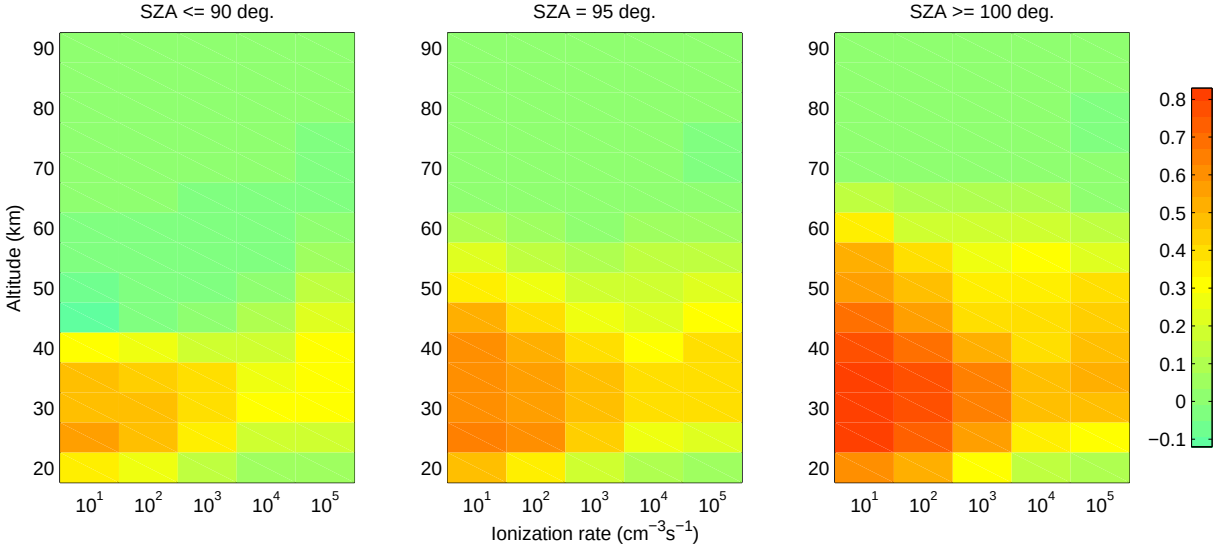

Fig. A28. P_{HNO_3}/Q for October SH.

Table A29. P_{NO}/Q for October SH.

Q	10^1	10^2	10^3	10^4	10^5	10^1	10^2	10^3	10^4	10^5	10^1	10^2	10^3	10^4	10^5
km		SZA	$\leq$	90°			SZA	$=$	95°			SZA	$\geq$	100°	
90	+0.00	+0.00	+0.00	+0.00	+0.00	+0.00	+0.00	+0.00	+0.00	+0.00	+0.00	+0.00	+0.00	+0.00	+0.00
85	+0.00	+0.00	+0.00	+0.00	+0.00	+0.00	+0.00	+0.00	+0.00	+0.00	+0.00	+0.00	+0.00	+0.00	+0.00
80	−0.00	−0.00	−0.00	−0.00	−0.00	+0.00	+0.00	+0.00	+0.00	−0.00	−0.01	−0.01	−0.01	−0.01	−0.00
75	+0.00	+0.00	+0.00	+0.00	−0.01	+0.00	+0.00	+0.00	−0.02	−0.01	−0.02	−0.02	−0.02	−0.02	−0.02
70	+0.00	+0.00	−0.01	−0.03	−0.06	−0.01	−0.01	−0.02	−0.05	−0.07	−0.04	−0.02	−0.04	−0.04	−0.04
65	−0.02	−0.02	−0.02	−0.08	−0.17	−0.06	−0.03	−0.04	−0.11	−0.16	−0.07	−0.04	−0.05	−0.08	−0.08
60	−0.10	−0.06	−0.08	−0.17	−0.31	−0.19	−0.09	−0.08	−0.14	−0.25	−0.07	−0.04	−0.04	−0.07	−0.11
55	−0.34	−0.19	−0.14	−0.22	−0.39	−0.35	−0.19	−0.12	−0.16	−0.27	−0.02	−0.02	−0.01	−0.03	−0.11
50	−0.75	−0.39	−0.21	−0.23	−0.35	−0.38	−0.25	−0.15	−0.16	−0.24	−0.00	−0.00	−0.00	−0.00	−0.02
45	−0.80	−0.48	−0.23	−0.18	−0.25	−0.26	−0.21	−0.13	−0.12	−0.18	−0.00	−0.00	−0.00	−0.00	−0.00
40	−0.25	−0.21	−0.15	−0.11	−0.14	−0.11	−0.10	−0.08	−0.07	−0.09	−0.00	−0.00	−0.00	−0.00	−0.00
35	−0.08	−0.08	−0.07	−0.06	−0.07	−0.05	−0.04	−0.04	−0.04	−0.04	−0.00	−0.00	−0.00	−0.00	−0.00
30	−0.04	−0.04	−0.03	−0.03	−0.03	−0.02	−0.02	−0.02	−0.01	−0.02	−0.00	−0.00	−0.00	−0.00	−0.00
25	−0.03	−0.03	−0.02	−0.01	−0.01	−0.01	−0.01	−0.01	−0.01	−0.01	−0.00	−0.00	−0.00	−0.00	−0.00
20	−0.01	−0.01	−0.01	−0.00	−0.00	−0.00	−0.00	−0.00	−0.00	−0.00	−0.00	−0.00	−0.00	−0.00	−0.00

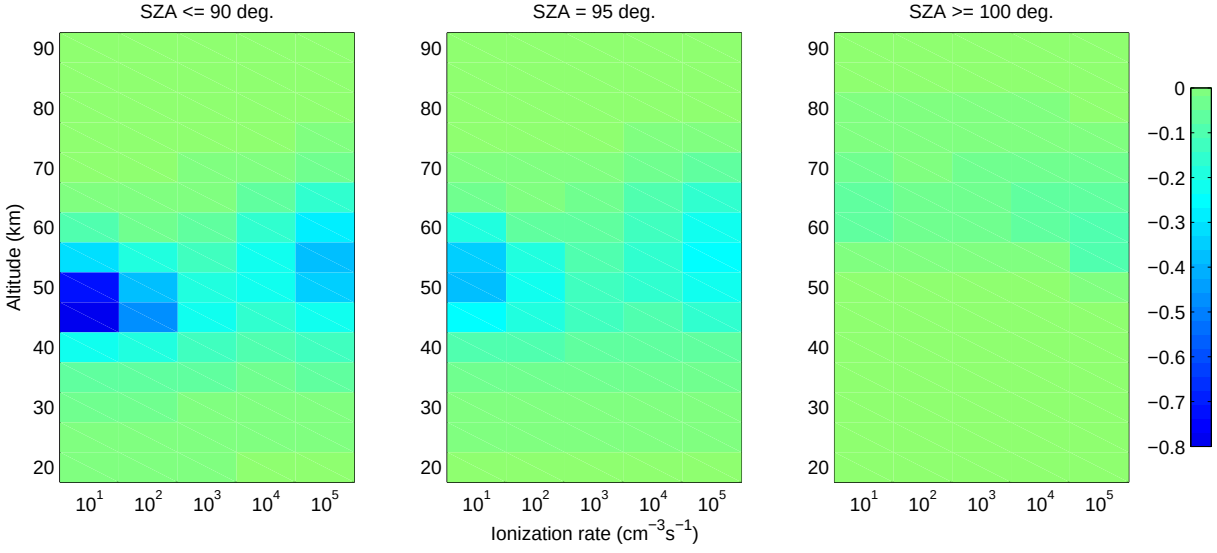

Fig. A29. P_{NO}/Q for October SH.

Table A30. P_{NO_2}/Q for October SH.

Q	10^1	10^2	10^3	10^4	10^5	10^1	10^2	10^3	10^4	10^5	10^1	10^2	10^3	10^4	10^5
km		SZA	$\leq$	90°			SZA	=	95°			SZA	$\geq$	100°	
90	+0.00	+0.00	+0.00	+0.00	+0.00	+0.00	+0.00	+0.00	+0.00	+0.00	+0.00	+0.00	+0.00	+0.00	+0.00
85	+0.00	+0.00	+0.00	+0.00	+0.00	+0.00	+0.00	+0.00	+0.00	+0.00	+0.00	+0.00	+0.00	+0.00	+0.00
80	+0.00	+0.00	+0.00	+0.00	+0.00	+0.00	+0.00	+0.00	+0.00	+0.00	+0.00	+0.00	+0.00	+0.00	+0.00
75	+0.00	+0.00	+0.00	+0.00	+0.01	+0.00	+0.00	+0.00	+0.02	+0.01	−0.00	−0.00	−0.00	+0.00	+0.01
70	+0.00	+0.00	+0.00	+0.02	+0.06	+0.00	+0.00	+0.01	+0.04	+0.06	−0.02	−0.02	−0.02	−0.01	+0.01
65	+0.01	+0.01	+0.01	+0.05	+0.15	+0.01	+0.00	+0.01	+0.07	+0.13	−0.10	−0.06	−0.07	−0.04	+0.01
60	+0.03	+0.02	+0.02	+0.08	+0.22	+0.01	+0.01	+0.01	+0.04	+0.17	−0.33	−0.19	−0.15	−0.15	−0.04
55	+0.04	+0.02	+0.02	+0.05	+0.19	−0.02	−0.01	−0.01	+0.00	+0.11	−0.59	−0.39	−0.27	−0.28	−0.16
50	−0.08	−0.04	−0.02	−0.01	+0.05	−0.15	−0.10	−0.06	−0.05	−0.02	−0.72	−0.55	−0.37	−0.36	−0.39
45	−0.55	−0.32	−0.16	−0.12	−0.10	−0.32	−0.26	−0.19	−0.16	−0.17	−0.74	−0.64	−0.47	−0.41	−0.49
40	−0.52	−0.45	−0.32	−0.23	−0.23	−0.45	−0.41	−0.33	−0.28	−0.32	−0.66	−0.61	−0.50	−0.44	−0.50
35	−0.39	−0.36	−0.32	−0.29	−0.31	−0.46	−0.43	−0.39	−0.36	−0.38	−0.62	−0.59	−0.53	−0.46	−0.49
30	−0.39	−0.37	−0.34	−0.29	−0.32	−0.48	−0.45	−0.40	−0.37	−0.38	−0.65	−0.62	−0.55	−0.45	−0.46
25	−0.47	−0.40	−0.28	−0.18	−0.18	−0.56	−0.50	−0.38	−0.25	−0.24	−0.65	−0.59	−0.46	−0.30	−0.30
20	−0.25	−0.19	−0.10	−0.05	−0.04	−0.34	−0.26	−0.15	−0.08	−0.07	−0.45	−0.37	−0.21	−0.12	−0.10

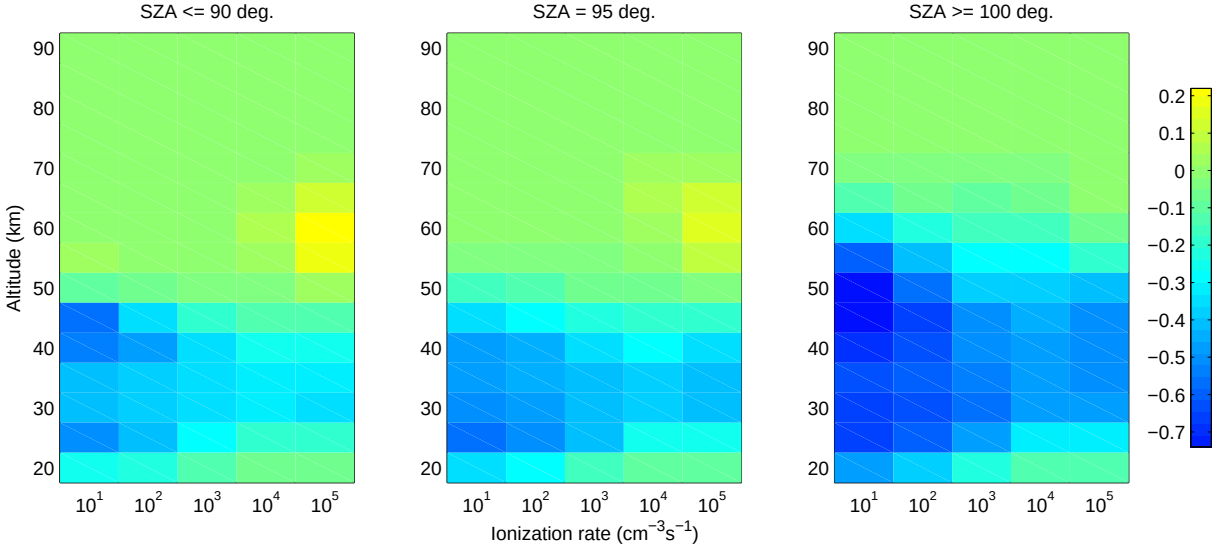

Fig. A30. P_{NO_2}/Q for October SH.

Table A31. P_{NO_3}/Q for October SH.

Q	10^1	10^2	10^3	10^4	10^5	10^1	10^2	10^3	10^4	10^5	10^1	10^2	10^3	10^4	10^5
km		SZA	$\leq$	90°			SZA	$=$	95°			SZA	$\geq$	100°	
90	+0.00	+0.00	+0.00	+0.00	+0.00	+0.00	+0.00	+0.00	+0.00	+0.00	+0.00	+0.00	+0.00	+0.00	+0.00
85	+0.00	+0.00	+0.00	+0.00	+0.00	+0.00	+0.00	+0.00	+0.00	+0.00	+0.00	+0.00	+0.00	+0.00	+0.00
80	+0.00	+0.00	+0.00	+0.00	+0.00	+0.00	+0.00	+0.00	+0.00	+0.00	+0.00	+0.00	+0.00	+0.01	+0.01
75	+0.00	+0.00	+0.00	+0.00	+0.01	+0.00	+0.00	+0.00	+0.00	+0.01	+0.01	+0.01	+0.01	+0.01	+0.02
70	+0.00	+0.00	+0.01	+0.01	+0.01	+0.01	+0.01	+0.01	+0.01	+0.02	+0.02	+0.01	+0.02	+0.02	+0.02
65	+0.01	+0.01	+0.02	+0.04	+0.03	+0.03	+0.02	+0.02	+0.02	+0.02	+0.02	+0.01	+0.01	+0.02	+0.03
60	+0.08	+0.05	+0.07	+0.10	+0.08	+0.08	+0.03	+0.03	+0.03	+0.03	+0.04	+0.02	+0.01	+0.02	+0.02
55	+0.32	+0.19	+0.14	+0.18	+0.14	+0.15	+0.05	+0.03	+0.02	+0.02	+0.07	+0.02	+0.01	+0.01	+0.02
50	+0.88	+0.46	+0.25	+0.21	+0.15	+0.18	+0.07	+0.02	+0.01	+0.01	+0.15	+0.06	+0.02	+0.01	+0.01
45	+1.47	+0.84	+0.38	+0.20	+0.12	+0.09	+0.09	+0.05	+0.03	+0.02	+0.10	+0.11	+0.06	+0.03	+0.03
40	+0.52	+0.44	+0.30	+0.16	+0.08	+0.02	+0.04	+0.07	+0.06	+0.05	+0.02	+0.05	+0.09	+0.08	+0.06
35	+0.05	+0.06	+0.07	+0.10	+0.08	+0.01	+0.01	+0.04	+0.08	+0.07	+0.01	+0.02	+0.05	+0.10	+0.09
30	+0.01	+0.01	+0.02	+0.04	+0.06	+0.00	+0.01	+0.02	+0.04	+0.06	+0.00	+0.01	+0.02	+0.05	+0.07
25	+0.01	+0.01	+0.02	+0.03	+0.04	+0.00	+0.01	+0.02	+0.03	+0.04	+0.00	+0.01	+0.02	+0.03	+0.05
20	+0.01	+0.01	+0.01	+0.01	+0.01	+0.01	+0.01	+0.01	+0.01	+0.02	+0.01	+0.01	+0.01	+0.01	+0.02

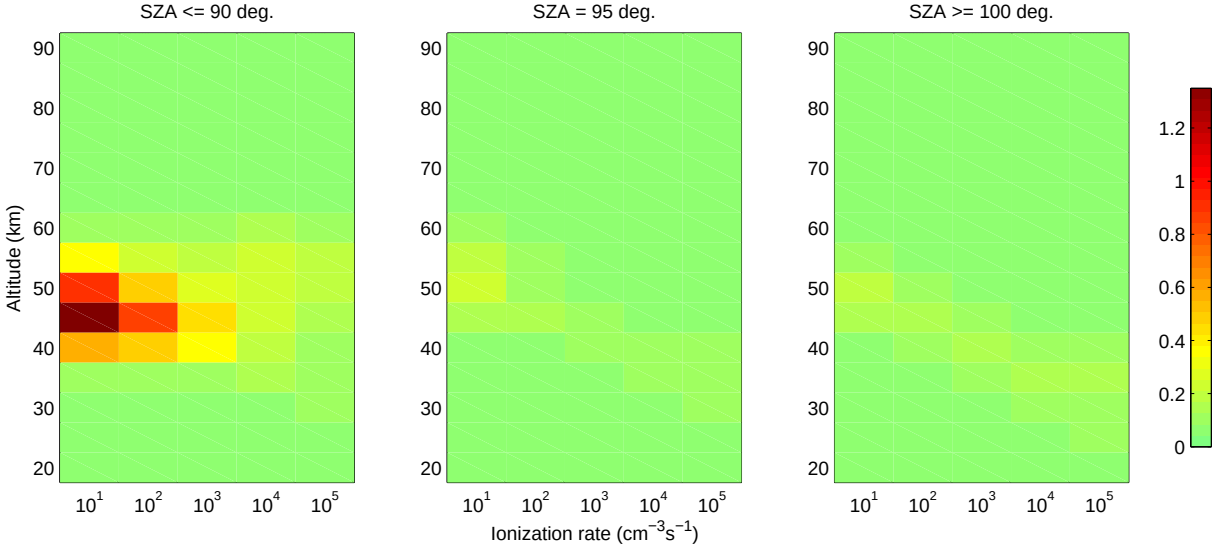

Fig. A31. P_{NO_3}/Q for October SH.

Table A32. $P_{N_2O_5}/Q$ for October SH.

Q	10^1	10^2	10^3	10^4	10^5	10^1	10^2	10^3	10^4	10^5	10^1	10^2	10^3	10^4	10^5
km		SZA	$\leq$	90°			SZA	$=$	95°			SZA	$\geq$	100°	
90	−0.00	−0.00	−0.00	−0.00	−0.00	−0.00	−0.00	−0.00	−0.00	−0.00	+0.00	−0.00	−0.00	−0.00	−0.00
85	−0.00	−0.00	−0.00	−0.00	−0.00	−0.00	−0.00	−0.00	−0.00	−0.00	−0.00	−0.00	−0.00	−0.00	−0.00
80	−0.00	−0.00	−0.00	−0.00	−0.00	−0.00	−0.00	−0.00	−0.00	−0.00	−0.00	−0.00	−0.00	−0.00	−0.00
75	−0.00	−0.00	−0.00	−0.00	−0.00	−0.00	−0.00	−0.00	−0.00	−0.00	−0.00	−0.00	−0.00	−0.00	−0.00
70	−0.00	−0.00	−0.00	−0.00	−0.00	−0.00	−0.00	−0.00	−0.00	−0.00	−0.00	−0.00	−0.00	−0.00	−0.00
65	−0.00	−0.00	−0.00	−0.00	−0.00	−0.00	−0.00	−0.00	−0.00	−0.00	−0.00	−0.00	−0.00	−0.00	−0.00
60	−0.00	−0.00	−0.00	−0.00	−0.00	−0.00	−0.00	−0.00	−0.00	−0.00	−0.00	−0.00	−0.00	−0.00	−0.00
55	−0.00	−0.00	−0.00	−0.00	−0.00	−0.00	−0.00	−0.00	−0.00	−0.00	−0.00	−0.00	−0.00	−0.00	−0.00
50	−0.00	−0.00	−0.00	−0.00	−0.00	−0.00	−0.00	−0.00	−0.00	−0.00	−0.00	−0.00	−0.00	−0.00	−0.00
45	−0.00	−0.00	−0.00	−0.00	−0.00	−0.01	−0.01	−0.00	−0.00	−0.00	−0.02	−0.01	−0.00	−0.00	−0.00
40	−0.03	−0.02	−0.01	−0.01	−0.01	−0.04	−0.03	−0.02	−0.01	−0.01	−0.08	−0.07	−0.05	−0.03	−0.03
35	−0.04	−0.04	−0.03	−0.02	−0.01	−0.05	−0.05	−0.04	−0.03	−0.03	−0.11	−0.10	−0.08	−0.07	−0.06
30	−0.04	−0.04	−0.03	−0.02	−0.01	−0.05	−0.05	−0.04	−0.03	−0.03	−0.09	−0.09	−0.07	−0.05	−0.04
25	−0.04	−0.04	−0.03	−0.02	−0.01	−0.05	−0.05	−0.03	−0.02	−0.02	−0.08	−0.08	−0.06	−0.04	−0.03
20	−0.05	−0.04	−0.02	−0.01	−0.01	−0.07	−0.06	−0.03	−0.01	−0.01	−0.09	−0.08	−0.05	−0.02	−0.02

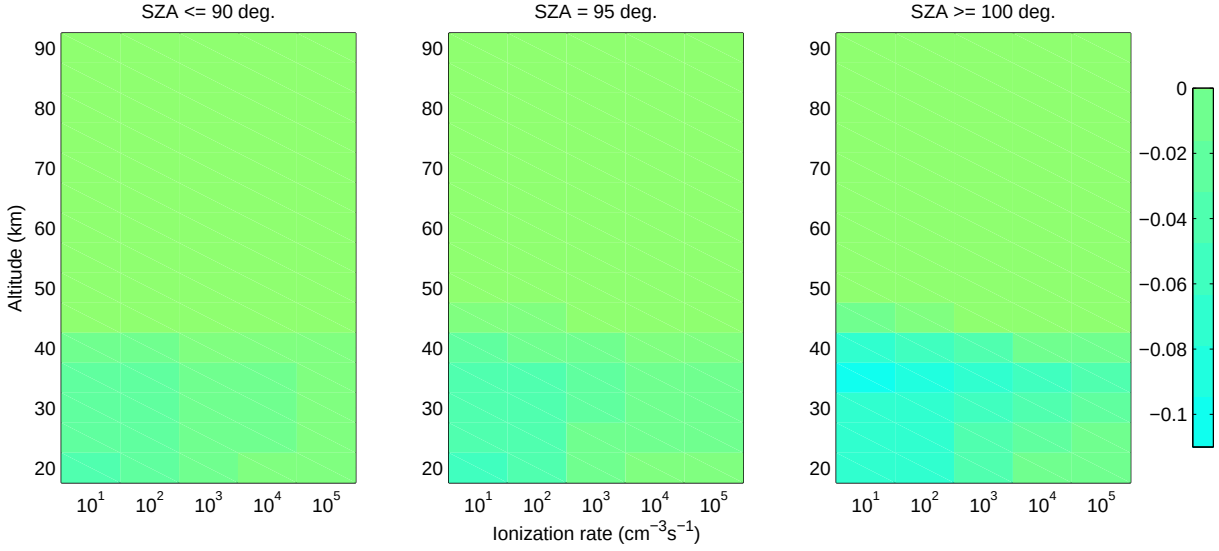

Fig. A32. $P_{N_2O_5}/Q$ for October SH.

Acknowledgements. The work of P. T. Verronen was supported by the Academy of Finland through the projects #136225 and #140888 (SPOC: Significance of Energetic Electron Precipitation to Odd Hydrogen, Ozone, and Climate).

Topical Editor K. Hosokawa thanks M. Friedrich and one anonymous referee for their help in evaluating this paper.

References

Aikin, A. C.: Production of stratospheric HNO_3 by different ion-molecule reaction mechanisms, J. Geophys. Res., 102, 12921–12926, 1997.

Arijs, E.: Stratospheric ion chemistry: Present understanding and outstanding problems, Planet. Space Sci., 40, 255–270, 1992.

Arijs, E., Nevejans, D., and Ingels, J.: Stratospheric positive ion composition measurements and acetonitrile detection: a consistent picture?, Int. J. Mass Spec. Ion Proc., 81, 15–31, 1987.

Crutzen, P. and Solomon, S.: Response of mesospheric ozone to particle precipitation, Planet. Space Sci., 28, 1147–1153, 1980.

Crutzen, P. J., Isaksen, I. S. A., and Reid, G. C.: Solar proton events: Stratospheric sources of nitric oxide, Science, 189, 457–458, 1975.

Damiani, A., Funke, B., Marsh, D. R., López-Puertas, M., Santee, M. L., Froidevaux, L., Wang, S., Jackman, C. H., von Clarmann, T., Gardini, A., Cordero, R. R., and Storini, M.: Impact of January 2005 solar proton events on chlorine species, Atmos. Chem. Phys., 12, 4159–4179, doi:10.5194/acp-12-4159-2012, 2012.

Funke, B., López-Puertas, M., Garcia-Comas, M., Stiller, G. P., von Clarmann, T., and Glatthor, N.: Mesospheric N_2O enhancements as observed by MIPAS on Envisat during the polar winters in 2002–2004, Atmos. Chem. Phys., 8, 5787–5800, doi:10.5194/acp-8-5787-2008, 2008.

Funke, B., Baumgaertner, A., Calisto, M., Egorova, T., Jackman, C. H., Kieser, J., Krivolutsky, A., López-Puertas, M., Marsh, D. R., Reddmann, T., Rozanov, E., Salmi, S.-M., Sinnhuber, M., Stiller, G. P., Verronen, P. T., Versick, S., von Clarmann, T., Vyushkova, T. Y., Wieters, N., and Wissing, J. M.: Composition changes after the "Halloween" solar proton event: the High Energy Particle Precipitation in the Atmosphere (HEPPA) model versus MIPAS data intercomparison study, Atmos. Chem. Phys., 11, 9089–9139, doi:10.5194/acp-11-9089-2011, 2011.

Grenfell, J. L., Lehmann, R., Mieth, P., Langematz, U., and Steil, B.: Chemical reaction pathways affecting stratospheric and mesospheric ozone, J. Geophys. Res., 111, D17311, doi:10.1029/2004JD005713, 2006.

Heaps, M. G.: The effect of a solar proton event on the minor neutral constituents of the summer polar mesosphere, Tech. Rep. ASL-TR0012, US Army Atmos. Sci. Lab., White Sands Missile Range, N. M., 1978.

Jackman, C. H. and McPeters, R. D.: The responce of ozone to solar proton events during solar cycle 21: A theoretical interpretation, J. Geophys. Res., 90, 7955–7966, 1985.

Jackman, C. H., McPeters, R. D., Labow, G. J., Fleming, E. L., Praderas, C. J., and Russel, J. M.: Northern hemisphere atmospheric effects due to the July 2000 solar proton events, Geophys. Res. Lett., 28, 2883–2886, 2001.

Jackman, C. H., Marsh, D. R., Vitt, F. M., Garcia, R. R., Fleming, E. L., Labow, G. J., Randall, C. E., López-Puertas, M., Funke, B., von Clarmann, T., and Stiller, G. P.: Short- and medium-term atmospheric constituent effects of very large solar proton events, Atmos. Chem. Phys., 8, 765–785, doi:10.5194/acp-8-765-2008, 2008.

Lehmann, R.: An algorithm for the determination of all significant pathways in chemical reaction systems, J. Atmos. Chem., 47, 45–78, 2004.

López-Puertas, M., Funke, B., Gil-López, S., von Clarmann, T., Stiller, G. P., Höpfner, M., Kellmann, S., Fischer, H., and Jackman, C. H.: Observation of NO_x enhancement and ozone depletion in the Northern and Southern Hemispheres after the October–November 2003 solar proton events, J. Geophys. Res., 110, A09S43, doi:10.1029/2005JA011050, 2005a.

López-Puertas, M., Funke, B., Gil-López, S., von Clarmann, T., Stiller, G. P., Höpfner, M., Kellmann, S., Mengistu Tsidu, G., Fischer, H., and Jackman, C. H.: HNO_3, N_2O_5 and $ClONO_2$ enchancements after the October–November 2003 solar proton events, J. Geophys. Res., 110, A09S44, doi:10.1029/2005JA011051, 2005b.

McPeters, R. D. and Jackman, C. H.: The response of ozone to solar proton events during solar cycle 21: The observations, J. Geophys. Res., 90, 7945–7954, 1985.

Orsolini, Y. J., Urban, J., and Murtagh, D. P.: Nitric acid in the stratosphere based on Odin observations from 2001 to 2009 – Part 2: High-altitude polar enhancements, Atmos. Chem. Phys., 9, 7045–7052, doi:10.5194/acp-9-7045-2009, 2009.

Porter, H. S., Jackman, C. H., and Green, A. E. S.: Efficiencies for production of atomic nitrogen and oxygen by relativistic proton impact in air, J. Chem. Phys., 65, 154–167, 1976.

Reid, G. C., Solomon, S., and Garcia, R. R.: Response of the middle atmosphere to the solar proton events of August–December, 1989, Geophys. Res. Lett., 18, 1019–1022, 1991.

Rusch, D. W., Gérard, J.-C., Solomon, S., Crutzen, P. J., and Reid, G. C.: The effect of particle precipitation events on the neutral and ion chemistry of the middle atmosphere – I. Odd nitrogen, Planet. Space Sci., 29, 767–774, 1981.

Seppälä, A., Verronen, P. T., Kyrölä, E., Hassinen, S., Backman, L., Hauchecorne, A., Bertaux, J. L., and Fussen, D.: Solar proton events of October–November 2003: Ozone depletion in the Northern Hemisphere polar winter as seen by GOMOS/Envisat, Geophys. Res. Lett., 31, L19107, doi:10.1029/2004GL021042, 2004.

Sinnhuber, M., Nieder, H., and Wieters, N.: Energetic particle precipitation and the chemistry of the mesosphere/lower thermosphere, Surv. Geophys., 33, 1281–1334, doi:10.1007/s10712-012-9201-3, 2012.

Solomon, S., Rusch, D. W., Gérard, J.-C., Reid, G. C., and Crutzen, P. J.: The effect of particle precipitation events on the neutral and ion chemistry of the middle atmosphere: II. Odd hydrogen, Planet. Space Sci., 8, 885–893, 1981.

Stock, J. W., Boxe, C. S., Lehmann, R., Grenfell, J. L., Patzer, A. B. C., Rauer, H., and Yung, Y. L.: Chemical pathway analysis of the Martian atmosphere: CO_2-formation pathways, Icarus, 219, 13–24, doi:10.1016/j.icarus.2012.02.010, 2012a.

Stock, J. W., Grenfell, J. L., Lehmann, R., Patzer, A. B. C., and Rauer, H.: Chemical pathway analysis of the lower Martian atmosphere: The CO_2 stability problem, Planet. Space Sci., 68, 18–24, doi:10.1016/j.pss.2011.03.002, 2012b.

Turunen, E., Verronen, P. T., Seppälä, A., Rodger, C. J., Clilverd, M. A., Tamminen, J., Enell, C.-F., and Ulich, T.: Impact of

different precipitation energies on NO_x generation during geomagnetic storms, J. Atmos. Sol.-Terr. Phys., 71, 1176–1189, doi:10.1016/j.jastp.2008.07.005, 2009.

Verronen, P. T.: Ionosphere-atmosphere interaction during solar proton events, Ph.D. thesis, University of Helsinki, available at http://urn.fi/URN:ISBN:952-10-3111-5, 2006.

Verronen, P. T., Seppälä, A., Clilverd, M. A., Rodger, C. J., Kyrölä, E., Enell, C.-F., Ulich, T., and Turunen, E.: Diurnal variation of ozone depletion during the October–November 2003 solar proton events, J. Geophys. Res., 110, A09S32, doi:10.1029/2004JA010932, 2005.

Verronen, P. T., Seppälä, A., Kyrölä, E., Tamminen, J., Pickett, H. M., and Turunen, E.: Production of odd hydrogen in the mesosphere during the January 2005 solar proton event, Geophys. Res. Lett., 33, L24811, doi:10.1029/2006GL028115, 2006.

Verronen, P. T., Rodger, C. J., Clilverd, M. A., Pickett, H. M., and Turunen, E.: Latitudinal extent of the January 2005 solar proton event in the Northern Hemisphere from satellite observations of hydroxyl, Ann. Geophys., 25, 2203–2215, doi:10.5194/angeo-25-2203-2007, 2007.

Verronen, P. T., Funke, B., López-Puertas, M., Stiller, G. P., von Clarmann, T., Glatthor, N., Enell, C.-F., Turunen, E., and Tamminen, J.: About the increase of HNO_3 in the stratopause region during the Halloween 2003 solar proton event, Geophys. Res. Lett., 35, L20809, doi:10.1029/2008GL035312, 2008.

Verronen, P. T., Santee, M. L., Manney, G. L., Lehmann, R., Salmi, S.-M., and Seppälä, A.: Nitric acid enhancements in the mesosphere during the January 2005 and December 2006 solar proton events, J. Geophys. Res., 116, D17301, doi:10.1029/2011JD016075, 2011.

von Clarmann, T., Glatthor, N., Höpfner, M., Kellmann, S., Ruhnke, R., Stiller, G. P., Fischer, H., Funke, B., Gil-López, and López-Puertas: Experimental evidence of perturbed odd hydrogen and chlorine chemistry after the October 2003 solar proton events, J. Geophys. Res., 110, A09S45, doi:10.1029/2005JA011053, 2005.

Winkler, H., Kazeminejad, S., Sinnhuber, M., Kallenrode, M.-B., and Notholt, J.: Conversion of mesospheric HCl into active chlorine during the solar proton event in July 2000 in the northern polar region, J. Geophys. Res., 114, D00I03, doi:10.1029/2008JD011587, 2009.

Winkler, H., Kazeminejad, S., Sinnhuber, M., Kallenrode, M.-B., and Notholt, J.: Correction to "Conversion of mesospheric HCl into active chlorine during the solar proton event in July 2000 in the northern polar region", J. Geophys. Res., 116, D17303, doi:10.1029/2011JD016274, 2011.

Winkler, H., von Savigny, C., Burrows, J. P., Wissing, J. M., Schwartz, M. J., Lambert, A., and García-Comas, M.: Impacts of the January 2005 solar particle event on noctilucent clouds and water at the polar summer mesopause, Atmos. Chem. Phys., 12, 5633–5646, doi:10.5194/acp-12-5633-2012, 2012.

Zipf, E. C., Espy, P. J., and Boyle, C. F.: The excitation and collisional deactivation of metastable $N(^2P)$ atoms in auroras, J. Geophys. Res., 85, 687–694, 1980.